UNIVERSITÀ DI PARMA

UNIVERSITÀ DEGLI STUDI DI PARMA

DOTTORATO DI RICERCA IN
"INGEGNERIA INDUSTRIALE"

CICLO XXXI

A study on the influence of laser ablation process configurations over the surface morphology and the mechanical behavior of aluminium bonded joints

Coordinatore:
Chiar.mo Prof. Gianny Royer Carfagni

Tutore:
Ing. Fabrizio Moroni

Dottorando: Francesco Musiari

Anni 2015/2018

Acknowledgements

I would like to sincerely acknowledge my tutor, Ing. Fabrizio Moroni, to whom my deepest gratitude goes and whose patience has been severely tested by my questions and insecurities for three years: your tangible example and your "maieutical" approach have certainly taught me more than many theoretical lessons did. Thank you for having invested in me.

A huge thanks goes also to Prof. Alessandro Pirondi, who firstly trusted in me and included me in his working team, in which I could tested my capabilities to address several "real life" engineering problems. Thank you for your helpfulness and for the time that you spent for me and my questions.

I would like to extend thanks to the people who shared part of their professional and private time with me during these three years: thanks to Claudio, Luca, Riccardo, Antonio and Pasquale, to Andrea Rossi for his kind availability and readiness in helping me with his work, to Tiziano and Corrado for their help in performing the SEM analysis and the contact angle measurements, to Prof. Luca Romoli and Adrian Lutey for their interest in my job and for helping me in untangling some nodes, to my "colleague" Teresa for aiding me in processing the optical microscope images, to Prof. Marco Alfano for having taken me on board in many interesting activities. Thank you also to the scientific committee of the MDA 2018 conference in Porto, with particular mention to Prof. Lucas da Silva and Prof. Robert Adams, whose appreciation of my work encouraged me more than they probably thought.

Thank you very much to my friends, my family, my grandparents and, last but not least, thank you to my parents, my first and most important supporters, to whom I owe everything.

Abstract

In this thesis, the effect of a pulsed-mode Yb-fiber laser ablation as a pre-treatment for AA6082-T6 aluminium alloy surfaces for adhesively bonding purposes is studied. Several laser configurations are tested, by varying the power and the scan speed, whose combination is summarized in an energy density representative index, as well as the hatch distance and the laser scanning direction. The laser induced changing over the ablated material is evaluated both in terms of the surface status and of the mechanical response of bonded joints. In particular, the surface morphology is assessed by measuring the surface roughness and the Pearson's first coefficient of skewness. The chemical modifications are evaluated through EDS measurements, by which an increase of the thick oxide layer with the energy density appears evident. Finally, contact angle measurements reveal that the wettability of the surface is complete when the energy density is risen beyond a specific value. The mechanical behavior is assessed by computing the critical value of the Mode I strain energy release rate with a campaign of quasi-static tests over laser pre-treated Double Cantilever Beam (DCB) joints. The fracture toughness increases with the energy density until a maximum, after which the tendency reverses. A diversification according to the hatch distance value is possible when it is higher than the nominal spot diameter, while, with respect to the laser scanning direction, the fracture toughness results similar both in the unidirectional and in the crossed textured joints. This is essentially due to the presence of air remained entrapped within the grooves when the energy density is quite high, which allows to find a direct correlation, statistically validated, between the fracture toughness and the coefficient of skewness, which appears to be a good indicator for the air entrapment phenomenon. Also the fatigue crack growth is tested on the same geometry, allowing a ranking of the laser configurations according to the crack growth rate which appears consistent with the results of the quasi-static tests. Finally, an accelerated aging cycle in control of temperature and relative humidity is applied to some specimens which then undergo quasi-static DCB tests. Even though a general lowering of the toughness is recorded on the aged joints with respect to the unconditioned ones, it is more marked in the grit blasted specimens, suggesting a benefit in using some specific laser ablation configurations instead of the traditional mechanical pre-treatment methods in presence of some critical environmental conditions.

Table of contents

List of figures

List of tables

Introduction

Adhesive bonding and laser technology are two topics which have become more and more relevant in the last decades.

The first is a widely employed technology of joining which is applied in many industrial fields where its properties dealing with the design flexibility, the effectiveness of production and often the improvement of the mechanical performance with respect to some traditional joining methods can be successfully exploited. The factors from which the achievement of a proper adhesion process mainly depends are dealing with the state of the surface on which the adhesive must be applied, from both a morphological and a chemical point of view. In fact it was extensively demonstrated how the surface roughness plays a key role in assuring or not the bond enhancement between the substrate and the adhesive layer because of the coupling effect of the so-called mechanical interlocking and of a changing in the amount of available load bearing area. Moreover, the chemical status of the surface can assume a crucial role in making the adhesion process correctly occur because of the nature of the adhesion mechanisms, which were explained in several theories, each one dedicated to a specific side among the ones concurring to the adhesion. The main discriminating factors for a good adhesion performance are the chemical compatibility of adhesive and substrate surface according to the property called wettability and the presence over the surface to be bonded of the so-called weak boundary layers, which can decrease the mechanical resistance of the adhesively bonded system. Therefore, the need for performing a prior treatment over the surface before the deposition of adhesive was found to be the bottleneck of the whole process, able to drive the success or the failure of the bonding application. To do this, several methods to pre-treat the surface were developed, with different levels of severity concerning the modifications acted over the original surface. These pre-treatment methods can be classified in chemical or mechanical according to the operating principles. The first usually are the most effective in improving the suitability of the surface to the adhesive bonding, but on one hand they do not allow a complete control over the induced surface topology and on the other they often imply high environmental hazards. The former feature is to be pursued because, as it was proven, due to the sensitivity exhibited by the achievement

of a good adhesion with respect to the surface morphology it is possible to exploit the surface roughness as a design parameter for the joints. As a consequence, given the application demands, several mechanical treatments, like the grit blasting, can be employed to tailor the surface roughness according to them.

The laser principle of working was theoretically formulated in the Twenties and the laser technology began to spread since the Sixties in very different fields of utilization, from the surgery to the telecommunications. With respect to the processing of materials for manufacturing purposes, it is widely applied for the cutting, the machining or the welding operations. An application which became more important in the last decades is dealing with the pre-treatment of surfaces aimed to be adhesively bonded, as a replacement of the traditional mechanical and chemical treatments. In fact, many works in the scientific literature testify that by using the laser ablation it is possible to achieve several benefits very useful for the improvement of the adhesive bonding functionality. Firstly, it allows the possibility to design specific textures over the surfaces and, once that the correlation existing between the laser process parameters (power, scan speed, line spacing, direction of scanning, etc) and the surface morphology relevant indexes (width and depth of the induced grooves, surface roughness, statistical distribution of the asperities over the surface with respect to the mean plane, etc) has been determined, it provides the capability to produce surfaces characterized by an high repeatability level which can be very easily adapted as the application demands change, which assures also high flexibility of the process. Moreover, the laser ablation is able to clean the surfaces from the weak boundary layers possibly present and promote the so-called surface activation, consisting in an enhancement of their free energies resulting finally in an improvement of the wettability. It results apparent however that the effectiveness of using the laser ablation as a pre-treatment strictly depends not only from the laser process parameters employed, bu also from the configuration resulted from a combination of them. As a consequence, many studies were dedicated to the study of the influence that using different laser parameters combinations has over the surface morphological and chemical status, as well as over the mechanical properties of adhesively bonded joints.

The aim of this thesis is to contribute to extend the knowledge about the useful ranges of employability of laser technology as a pre-treatment method integrated within the adhesive bonding process. In particular, the focus is placed over an AA6082-T6 aluminium alloy which belongs to the 6000 series, much employed in many industrial fields, including aerospace, architecture, food industry applications and generic welded structures. A pulsed-mode Yb-fiber laser is used to ablate the surfaces. Thick aluminium sheets are investigated with respect to the laser ablation capability to significantly modify their surface status and to improve the fracture toughness of adhesively bonded joints produced using them as substrates. To

do this, a wide experimental campaign is prepared, based upon the variation of the laser process parameters in order to explore as good as possible a design space with respect to the trend of several output indexes.The so-called energy density, defined as the energy provided to the ablated surface for unit area, is assumed as a driven parameter for the exploratory investigation. With refer to the aforementioned output indexes, the surface morphology is quantitatively assessed by means of measurements of the surface roughness and of the Pearson's first coefficient of skewness, while the chemical modifications induced over the surface are analyzed with EDS measurements. Even sessile drop tests are performed to evaluate the coupling effect of morphology and chemical changing. The mechanical response of the laser ablated joints is instead assessed by means of the computation of the critical value of Mode I strain energy release rate based on Double Cantilever Beam (DCB) tests data. Moreover, to enrich the quasi-static characterization with durability considerations related to the critical environmental conditions which the joints can address during their working life, even tests over specimens previously exposed to an accelerated aging cycle are conducted. Finally the specimens are fatigue tested, in order to verify the capability to preserve the laser induced modifications even when withstanding variable loads, which is a topic poorly touched by the existing literature with respect to the laser pre-treated joints.

The thesis is structured as follows. In Chapter 1, the general concepts related to the adhesive bonding technique, including a classification of adhesives, a description of the main theories of adhesion and mechanisms of failure, an overview of the most used surface pre-treatments and methods for the assessment of the surfaces, as well as a mention of the durability and fatigue performance of bonded joints and a presentation about the most employed specimens geometries, are proposed.

In Chapter 2, the basic concepts related to the operating principle of a laser instrument are given, along with a classification of the available marketed lasers, an overview of the main interaction phenomena between laser and processed materials and a review of many literature works dedicated to the employment of the laser ablation as a pre-treatment method for adhesively bonded joints.

Chapter 3 presents the materials properties, the details of the methods and the instrumentation employed in this work, as well as the type and range of parameters chosen to perform the laser ablation.

In Chapter 4, the results relative to the morphological and chemical analysis of the ablated surfaces are provided, moving from the presentation of the starting points of the work to the description of the surface roughness and coefficient of skewness measurements and of the findings dealing with the alterations of the atomic contents and of the contact angle induced by the laser process.

Finally, Chapter 5 is reserved for the illustration of the results concerning the mechanical response, in particular the findings of the quasi-static tests over the unaged specimens are provided, followed by the description of the identified fatigue behavior and by the presentation of the changing induced in the quasi-static response by the exposition to critical environmental conditions. Some concluding remarks are placed at the end of the dissertation.

Chapter 1

Fundamentals of adhesive bonding

1.1 General remarks about adhesive bonding

Adhesive bonding is a joining technique which is increasingly used in many fields of application, such as automotive, railway, aerospace, electrical, shoe industry and construction. The reason for the success of this method, which leads it to support or even replace the traditional joining methods (like riveting or welding), is to be found in the many advantages brought by the adhesive bonding to the structure in which it is employed, compared with the classic methods. For instance, the adhesive bonding technique can be exploited in those circumstances where factors as the weight saving of the structure, the strength with respect some kind of stresses, the economic convenience or the aesthetics features are crucial. Other benefits involving the use of the adhesive bonding method are:

- the curing temperature of most of adhesives is below 250°C, thus the thermal distortions which often occur after welding or brazing, as well as the residual stresses resulting in the bonded area, are avoided;

- the distribution of the stresses over the bonded area is uniform in a direction parallel to the one along which the adhesive takes action, while the stress gradient perpendicularly to the bonding direction is usually reduced with respect to the nailed or screwed surfaces which are affected by stress concentrations in correspondence of holes;

- the adhesive bonding does not result in a weakening of the substrates as instead occurs using nailing or screwing or, to a lesser extent, welding;

- the adhesive assures a near-perfect impermeability to liquids and gas;

- the high inner damping provided by the adhesive, due to its viscoelasticity properties, makes the adhesively bonded joint suitable for the acoustic and mechanical vibration insulation;
- in the case of a metal-to-metal heterogeneous joint, one substrate is segregated from the other by an adhesive layer, whose mechanical and electrical properties are such as to protect the less noble metal from the corrosion both with a mechanical effect of coverage and with the inhibition of the electrical currents generating in the contact zones between different metals.

At the same time, the use of adhesives as joining method presents also some critical issues, such as:

- due to the presence of the polymeric adhesive, the adhesively bonded joint is sensitive to static fatigue;
- the chemical and high temperature resistance is the one typical of polymers, which makes the adhesively bonded joints unsuitable for the most of the mechanical applications requiring the presence of high temperature;
- the adhesively bonded joint requires an adequate preparation of the substrates, involving mechanical machining (if the joint must be shaped) and an appropriate surface preparation: in particular, the surface must be usually cleaned, degreased and sandblasted in order to remove every oxide or impurity or trace of lubricant which are bond inhibitors;
- the hardening time of adhesives is higher with respect to the times required by other joining techniques;
- the adhesion is a complex phenomenon and the resistance and strength of the adhesively bonded joints is affected by a multitude of variables, resulting in a difficult capability by the laboratory tests to comprehensively replicate the real work conditions of the joint. Therefore, the available data for the adhesively bonded joints are only indicative of the adhesive behavior in the different environmental and loading conditions and are related only to the tested configurations, resulting in the need for an adequate experimental activity to overstep the uncertainty over the behavior of the joints, as well as the need for the adoption of high safety factors.

The classic and well known definition offered by Kinloch [1] to describe what an adhesive is reads: "An adhesive may be defined as a material which when applied to surfaces of

materials can join them together and resist separation". Although the provided definition is referred to generic materials without further specifications, which involves even materials not usually considered adhesives (like mortar and solder [2]), until recent times the adhesive bonding technique was considered restricted only for wood structures. Only the advent of the polymeric resin based adhesives made the development of the so called "structural adhesives" possible. An adhesive is usually called structural when its high strength is the crucial factor for the survival of the structure to which is applied. A structural adhesive is typically formed by an organic polymer (single component adhesive), or two compound (hardener and basic resin) able to chemically react together when in contact in order to produce a polymer (two component adhesive). The adhesion occurs in two distinct phases: in the first, the adhesive, in the liquid state, creates molecular bonds with the surface of the substrates over which it is laid, then the hardening occurs. Usually the single component adhesives harden in presence of high temperature (for instance, for epoxy adhesive it is higher than 120°C), while for the two component adhesives the hardening starts even at room temperature, as soon as the hardener and the basic resin come in direct contact.

It is possible to carry out a classification of the marketed structural adhesives according to different criteria. One of this is the chemical characteristics of the polymer, even if this criterion presents some classifying problem with respect to the existence of several blends of some types of adhesives, used to enhance their effectiveness. A brief overview of the main families of adhesives is offered hereinafter.

- Phenolic-vinyl based adhesives: they present a good shear and peel strength, the vinyl phase works as a plasticizer and enhances the fatigue resistance; the hardening occurs at 160-170°C and under the application of a pressure in order to avoid the generation of gas bubbles within the adhesive.

- Phenolic-nitrile based adhesives: they offer an high stability below 160°C and a high resistance to chemical aggression; the hardening occurs at high temperature and under pressure.

- Phenolic-chloroprene based adhesives: they present high resistance to vibrations and to low temperatures (until -50°C), but they are very sensitive to chemical agents.

- Polyacrylic adhesives: they are usually single component anaerobic adhesives, the hardening occurs at room temperature in absence of air; they present low resistance to chemical aggression and are typically employed as thread-lockers and for cylindric coupling subjected to tight tolerance.

- Cyanoacrylate adhesives: they are single component adhesives, without solvents, characterized by a fast hardening at room temperature and by a good shear strength, but they are sensitive to impact, chemical aggression and high temperatures.
- Polyurethane adhesives: they present good peel strength and resistance to low temperatures, the shear strength is not as good as the one exhibited by the previously described adhesives.
- Polyamide adhesives: they are used when a work temperature ranging from 150-200°C to 300°C is required.

A slighter wide space is dedicated to present one of the most important families of adhesives, which is the one of the epoxies. These adhesives offer an excellent mechanical performance and are available both in the single component and in the two component version. They are usually employed in addiction with other polymers, in particular:

- epoxy-nylon adhesives: they are used in the aerospace industry due to their good peel resistance and to low temperatures (-50°C);
- epoxy-polyamide adhesives: they present excellent flexibility but the hardening at room temperature is very slow;
- epoxy-polysulphide adhesives: they offer a good flexibility and are used typically for joining materials subjected to several levels of temperatures;
- epoxy-phenolic adhesives: the phenolic phase provides a good stability at high temperature (below to 200°C), but the peel strength is low; the hardening occurs at high temperature (170°C) and under pressure.

It is worth mentioning the toughened adhesives, which are acrylic and epoxy adhesives in which elastomeric particles are dispersed with the intent to segregate the crack propagation: while using a conventional adhesive a fracture would occur, in the toughened adhesive layer the stresses are re-distributed from the sides to the center when the loading increases, therefore the joint failure does not occur in an abrupt and catastrophic mode, but after distortions which alert about the forthcoming collapse and allow to take suitable retaliatory measures.

Another criterion according to which it is possible to classify the structural adhesives is the way in which the hardening occurs, that can be by loss of water, loss of solvent, cooling or chemical reaction. A class of adhesives omitted by this classification is the pressure-sensitive adhesives, which do not harden but remain permanently sticky.

1.2 Theories of adhesion

Because of the complexity of the adhesion phenomenon, there are several theories which are intended to describe the mechanisms occurring during the joining between adhesive and adherent and each of them achieves to accurately explain some aspects of the bonded joints behavior but results deficient with respect to other ones. The most important theories of adhesion are:

1. Physical adsorption theory
2. Chemical bonding theory
3. Mechanical interlocking theory
4. Diffusion theory
5. Electrostatic theory
6. Weak boundary layer theory

1.2.1 Physical adsorption theory

The wide range of the intermolecular forces which can arise between the adhesive layer and the surface substrate is summarized in Tab. 1.1.

Table 1.1 A summary of intermolecular forces acting between adhesive and adherent [3]

Bond type	Bond energy [kJ mol^{-1}]	Equilibrium length [nm]
Primary		
Ionic	600-1200	0.2-0.4
Covalent	60-80	0.07-0.3
Secondary		
Hydrogen	~50	0.3
Dipole interaction	~20	0.4
London dispersion (Van der Waals)	~40	<1

The formation of primary interfacial bonding will be addressed separately in Par. 1.2.2. In this paragraph, only the contribution given by the secondary interfacial bonding is considered. According to the physical adsorption theory, the adhesion phenomenon is driven by the intermolecular attraction forces, known as secondary or Van der Waals forces, developing as a consequence of the adsorption of adhesive molecules into the adherent. Although the

Van der Waals forces are the weakest among the inter-molecular forces group, they are sufficient to assure the strength required for the joining at the interface, provided that the distance between overlooking surfaces is adequate. In particular, it has been proven that the distance between overlooking surfaces becomes crucial, being the potential energies associated to the attraction forces proportional to r^{-6}, where r is the distance of separation [2]. The presence of the secondary bonding forces was detected in many works. In [4] the so called JKR equation was formulated in order to propose a correction to the Hertz equation for the case of two rubber spheres coming in contact as a result of the application of a load. The found deviation in the value of the diameter of the contact zone when the load is low was ascribed to the presence of the work of adhesion generated by the attraction forces between the surfaces in contact. Huntsberger [5] analytically evaluated the secondary bonding forces involved in the attraction between two bulk phases, finding that a a distance of separation equal to 1 nm would result in an intermolecular force corresponding to approximately 100 MPa, which goes well beyond the expected strength of a typical adhesively bonded joint. The disagreement between analytical and experimental results is mainly due to the fact that the analytical evaluation did not take into account the presence of inclusions and voids which reduce the amount of material affected by the presence of the secondary bonding forces and act as stress concentration points after the bonding, making the failure of the joint occur at a significantly lower load than the one predicted by the theoretical calculations. Anyway, the relevance of the secondary bonding forces in determining the strength of the adhesively bonded joints was demonstrated.

As a direct consequence of these observations, an intimate contact between adhesive and substrates, able to minimize or erase the interfacial discontinuities which act as stress concentration points, is needed. To achieve this, the capability of the adhesive to spread over the surface in such a way to establish a continuous contact with the substrate surface becomes crucial. This property is called wettability. To define it, it is necessary to introduce the so called surface free energy, which is defined as the energy associated with the intermolecular forces at the interface between two substances and is evaluated as shown in Eq. 1.1 and 1.2, valid for a surface in solid (S) or liquid (L) state, respectively:

$$\gamma_S = \gamma_S{}^d + \gamma_S{}^p \tag{1.1}$$

$$\gamma_L = \gamma_L{}^d + \gamma_L{}^p \tag{1.2}$$

where the apexes "d" and "p" point out the dispersion and the polar components of the surface free energy, respectively. Assuming the presence of a three phases system as the one

illustrated in Fig. 1.1, where a drop of a fluid liquid (L) is in contact with a solid substrate (S) in presence of the fluid vapor (V), the Young equation 1.3 drives the equilibrium of the three phases:

$$\gamma_{LV}\cos\Theta = \gamma_{SV} - \gamma_{SL} \tag{1.3}$$

where γ_{LV} is the surface free energy or interfacial tension of the liquid phase in equilibrium with its vapor, γ_{SV} is the interfacial tension of the solid phase in equilibrium with the fluid vapor, γ_{SL} is the interfacial tension of the solid phase in equilibrium with the fluid liquid and finally Θ is the equilibrium contact angle.

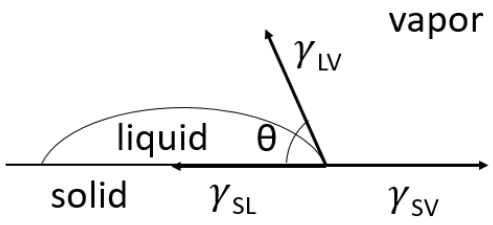

Fig. 1.1 Three phases system for the evaluation of the equilibrium conditions by means of the Young equation

The Duprè equation 1.4 provides the thermodynamic work of adhesion per unit area between two liquid substances A and B separated in dry air:

$$W_A = \gamma_A + \gamma_B - \gamma_{AB} \tag{1.4}$$

where γ_A and γ_B are the surface free energies of the phase A and the phase B, respectively, and γ_{AB} is the surface free energy of the interface between the two phases, which can be evaluated using the Fowkes equation 1.5 [6]

$$\gamma_{AB} = \gamma_A + \gamma_B - 2(\gamma_A{}^d\gamma_B{}^d)^{\frac{1}{2}} - 2(\gamma_A{}^p\gamma_B{}^p)^{\frac{1}{2}} \tag{1.5}$$

Assuming, as some researchers did [7], that the Duprè equation is successfully applicable even to a solid adhesive/substrate interface, combining the Eq. 1.3 and the Eq. 1.4 and considering γ_A as the interface tension of the substrate and γ_B as the interface tension of the adhesive, it results that:

$$W_A = \gamma_B(1+\cos\Theta) \tag{1.6}$$

Therefore, a contact angle Θ as close as possible to 0° or slightly higher assures the existence of a positive work of adhesion between adhesive and substrate, while values of Θ higher than 90°make the cohesive work of the adhesive prevail, resulting in the incapability by the adhesive to spontaneously spread over the surface and thus adequately wet the substrate surface. With refer to the Young equation 1.3, this means that the wetting is facilitated when:

$$S = \gamma_{SV} - \gamma_{SL} - \gamma_{LV} > 0 \tag{1.7}$$

where S is called the spreading coefficient.

Just because the wettability is a property referred to a couple of substances, it is possible that an adhesive presents different equilibrium contact angles with respect to different materials or, viceversa, that a material is wetted in a different way by two different adhesives. Usually, an adhesive whose wettability with respect to metals is quite good does not reach to wet just as well glass or paper surfaces, characterized by a low surface free energy. The problem is thus transferred to the compatibility between materials and to the sensitivity of an adhesive to a certain substrate material, resulting in the need to carefully choose proper couplings and to adequately prepare and pre-treat the substrates surfaces with the intent of enhancing their surface free energy with respect to the adhesive one.

1.2.2 Chemical bonding theory

The part played by primary interaction forces in the adhesive bonding mechanism is briefly discussed in this paragraph. Both the ionic and the covalent bonds, as well as the hydrogen bonds and the Lewis acid-base interactions, have been proven [8] to be the main kind of bonding forces acting across the interface in certain circumstances. Both the ionic and the covalent bonds present extremely higher strength than the Van der Waals forces. Just the high strength exhibited by the Si-O covalent bond (whose strength energy is approximately equal to 368 kJ mol^{-1} [2]) through the substrate is the cause of the wide diffusion of the silane-based primers as adhesion promoters, as found by Koenig and Shih [9] by means of the Laser-Raman spectroscopy and by Chiang [10] employing the Fourier transform infrared spectroscopy. Although the presence of the primary interaction forces was rarely detected in a direct way, many researchers addressed the phenomenon, finding evidence of the presence of the primary bonds between adhesive and substrates: Klein [11] used the infrared method to find the occurrence of primary bonds between a polyurethane adhesive and an epoxy-based primer, Chu et al [12] studied the ionic bonds ($COO^{-}Al^{+}$) generating interfacially from 4-hydroxybenzoic and 4-aminobenzoic to aluminium oxide, Zhou and Frazier [13] studied

the urethane linkages forming as a reaction of hydroxile groups with cellulose or lignine when an adhesive containing isocyanate is applied on wood.

1.2.3 Mechanical interlocking theory

The mechanical interlocking theory states that the main cause of the adhesion is the so called interlocking or mechanical keying, consisting in the indentation of the adhesive within the asperities of the surface over which it is laid. This theory does not agree with the fact that adhesion has been proven to successfully occur even in presence of perfectly smoothed surfaces [14] [4]. Nevertheless, the possibility to get an improvement of the joint strength by means of increasing the bonding surface roughness is documented in literature: Jennings [15] studied some aluminum and stainless steel butt bonded joints, comparing the strength results obtained depending on the topography of the substrates surfaces, which were previously polished or abrading (or sandblasting) in order to make them smooth or rough, respectively. His conclusions are summarized in Tab. 1.2.

Table 1.2 Joint strength in function of surface roughness as a result of some tests over aluminium and stainless steel specimens [15]

Surface condition	Butt joint strength [MPa]	Coefficient of variation [%]
Aluminium alloy 6061		
Polished 1 μm diamond past	28.8	24.4
Abraded through 600 SiC paper	30.9	24.9
Abraded through 280 SiC paper	39.0	17.5
Abraded through 180 SiC paper	36.7	20.4
Sandblasted with 40 to 50 mesh SiO_2 grit	48.5	14.4
Stainless steel 304		
Polished 1 μm diamond past	27.8	20.8
Regular machined grooves	35.2	20.0
Sandblasted with 40 to 50 mesh SiO_2 grit	53.4	10.8

As the Tab. 1.2 shows, the strength of the joints seemed to increase with the roughness. However, an explanation for this trend was offered, rather than ascribing it to the mechanical interlocking, by noticing that a high macroscopic random roughness as the one obtainable through sandblasting can prevent the crack propagation along an interfacial weak line formed by the alignment of flaws and small cracks, avoided by the random distribution of the irregularities over the surface. This behavior is expected to be reduced for more ductile adhesives, which is in line with the experimental observations dealing with the reduction

of the differences in the strength values between smooth and rough surfaces when the temperature is risen significantly up. Even Evans and Packam [16] did not ascribe the recorded increase of peel strength of the joint between polyethilene and various metal substrates with the roughness to the mechanical interlocking effect, but to the corresponding increase of the volume of adhesive undergoing viscoelastic energy dissipation during the failure of the joint. The behavior of the irregularities of the surface as a barrier to the propagation of the crack, forced to follow a more tortuous path and to dissipate an higher amount of energy to produce the failure of the joint at the interface, is illustrated by the Fig. 1.2, taken from [17], where the two cases of joints with macroscopically rough and smooth bonding surfaces, respecitvely, loaded with a wedge inserted into the edge of a narrow interface are juxtaposed.

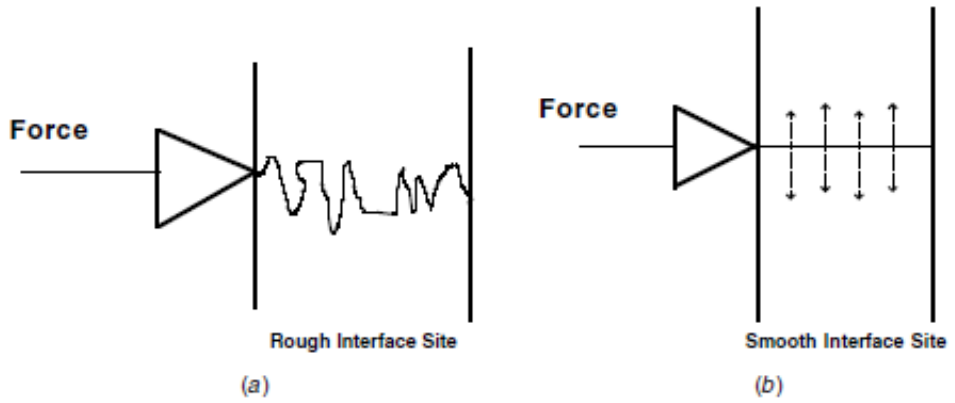

Fig. 1.2 Schematic representation of adhesively bonded joints with a rough (a) and a smooth (b) interface surface, respectively, under a wedge loading [17]

With refer to the strength of the joint, the influence of the mechanical interlocking is still topic of debate. Sargent [18] identified an increasing trend of the peel strength of aluminium alloy bonded joints consistent with the simultaneous increase of the surface roughness without finding any correlation between peel strength and chemical properties of the interfacial surface. An analogue result was achieved by Shahid and Hashim [19] which focused on the influence that the increase of the contact area has over the strength in cleavage joints. On the other hand, no detectable change in the joint strength with the surface roughness was noticed by other researchers like Critchlow and Brewis [20] or Thery et al [21]. The work of Kim et al [22] dealt with micro-patterns realized over a steel substrate in order to induce a regular surface topography: their findings prove that there is no any apparent correlation between the surface roughness and the interfacial fracture toughness of the joint, but the increase of roughness brings a benefit when it goes towards an increase of the ratio between the width of the excavated line, where the failure occurs within the adhesive,

and the preserved line width. This behavior was attributed to the mechanical interlocking. Other works [23] addressed the relation between the macro-roughness and the depth and the width of the surface grooves and the increase of the lap shear strength of bonding joints was found to be very sensitive to the features of the grooves rather than to the macro-roughness [24], in particular the mechanical interlocking provides a poor contribute to the adhesion if the grooves are too deep or too wide [25]. Even Gude et al [26] found that, while the shear strength of unidirectional carbon fibre/epoxy laminates lap joints decreases as the surface roughness grows up, the Mode I adhesive fracture energy receives a benefit from the increase of the mean summit curvature and the density of the summities of the surface, identifying in the mechanical interlock the predominant mechanism of adhesion with refer to mode I loading conditions. In other works [27] the influence of the roughness was evaluated with respect to the load conditions (tensile, shear and peel tests), resulting in the identification of an optimal value of roughness in the tensile strength of the adhesion, while for the shear and the peel strength the relation with the surface roughness is not clear.

The effect of the roughness over the wettability was incidentally studied by Wenzel [28] and Cassie and Baxter [29] considering the change of the apparent contact angle induced by the presence of a rough substrate. Wenzel proposed a model which describes the behavior of a liquid drop over a homogeneous rough surface under the main assumption that the wettability properties are influenced more by the amount of the actual surface area interacting with the liquid rather than by the texture features of the surface. Eq. 1.8 is the formulation that he provided for the correction of the contact angle

$$\cos\Theta_r = r_f \cos\Theta_s \tag{1.8}$$

where Θ_r is the apparent contact angle measured over a rough homogeneous surface, Θ_s is the contact angle measured over a smooth surface and r_f is the so called roughness factor, which represents the ratio between the actual load bearing area and the nominal area of the substrate surface. According to this model, an increase of the surface roughness always leads to a magnification of the current wettability regime, which means that increasing the roughness of an hydrophilic or a hydrophobic surface will result in a surface even more hydrophilic or hydrophobic, respectively.

Instead, the model proposed by Cassie and Baxter is based on the assumption that the drop is in contact with an heterogeneous substrate surface, where more than one substance is present, according to Eq. 1.9

$$\cos\Theta_r = r_f f \cos\Theta_{sy} + f - 1 \tag{1.9}$$

where Θ_{sy} is the contact angle that would be measured over a smooth surface of the pure solid substance designated with "y", r_f is the roughness factor of the wet surface area and f is the fraction of solid surface area wet by the liquid drop.

Fig. 1.3 illustrates the two alternative models.

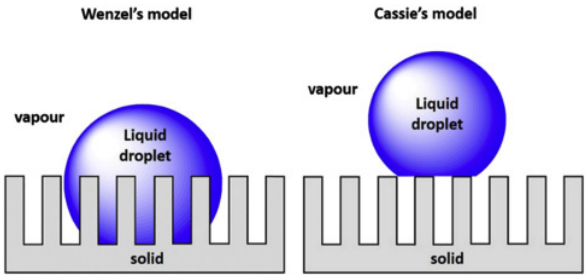

Fig. 1.3 Illustration of the models of Wenzel and Cassie-Baxter, respectively [30]

The Cassie-Baxter model is applicable to the circumstance where the adhesive drop is placed over the top of the asperities and several air pockets lie below it, resulting in a hydrophobic condition which prevents the spontaneous spreading of the drop.

The results of more recent studies [31] [32] have proven that the wettability which seems to increase with the surface roughness undergoes a lowering when the roughness oversteps a threshold, probably because of the restriction given to the spreading of the adhesive due to the fact that the asperities behave as a barrier with respect to the spreading of the drop, which makes the transition from the Wenzel's model to the Cassie-Baxter's model happen.

1.2.4 Diffusion theory

The diffusion theory is based upon the assumption that the adhesion is mainly promoted by the diffusion of molecules in the adhesive and in the substrate. As a consequence, the theory is applicable only to homogeneous polymeric systems, because the molecules must possess high mutual solubility and high capability of movement.

The main application in which the diffusion can play a crucial role is the solvent or heat welding of thermoplastics substrates and it provides also a valid explanation for the adhesion between cured primer and adhesive resins.

The arguments and experimental findings related to this topic are mainly due to the work of Voyutskii [33].

1.2.5 Electrostatic theory

The electrostatic theory does not play a central role comparable with the physical adsorption, chemical bonding and mechanical interlocking in driving the adhesion phenomenon. Nevertheless, there are some specific application cases in which it seems one of the prevalent mechanisms acting, for instance in the documented case of zirconium-coated gold spheres of cadmium sulphide single crystal substrates [34]. The theory states that a double layer of electrical charge is generated at the interface between adhesive and adherent and that the electrostatic forces contribute to the joint strength. The work of Derjaguin [35] in particular was dedicated to this topic and considered the substrate/adhesive system as a capacitor: when the failure occurs at the interface, a separation of charge takes place promoting an increasing potential difference which finally produces an electrical discharge. Just the fact that electical discharges were detected during the peeling of an adhesive from a substrate is taken as a proof of the validity of the theory. Therefore, the work of adhesion was evaluated by Derjaguin assuming that it was equal to the electrical energy stored in the system, not considering the fact that the failure can occur within the adhesive and not always at the interface.

1.2.6 Weak boundary layer theory

The weak boundary layer theory due to Bikerman [36] states that when the joint failure occurs at the interface often it does not involve the adhesive layer but it is actually a cohesive failure of a so called weak boundary layer placed between adhesive and adherent. A weak boundary layer is constituted by whatever substance acting as an inhibitor with respect to the adhesion phenomenon. A list of examples of weak boundary layers may include low molecular weight species (like plasticizers or other processing additives included into the chemical formulation of the adhesive and migrating to the adhesive layer surface), metallic oxides, air-borne contamination, traces of lubricants. The weak boundary layers can arise during all the process phases of bonding and also during the working life. Before the deposition of the adhesive, at the liquid state, over the substrate surface, the first and most common weak boundary layer that must be removed is the air. Other examples of weak boundary layers which can be developed during this phase are the low molecular weight constituent distributed in the polyethilene substrates and weak oxides as the copper ones. During the cure or the solidification of the adhesive, other weak boundary layers can be generated by the chemical reaction between determined metal substrates like titanium and some hardeners present in the adhesive composition, or by the adsorption of water or low molecular weight species over the substrate surface. Finally, even during the service life of the joint some weak boundary layers can appear: it is the case of the hydration of the

aluminium oxides by water diffused through the adhesive, the migration of low molecular weight components towards the adhesive surface (like for the plasticized polyvinyl chloride in which the migration of plasticizers added to the adhesive formulation occurs with time), the corrosion of the substrate at the interface, the liberation of moisture due to the exposure to moderately high temperatures, as in the case of the under-cured phenolic substrates.

Some criticisms about this theory were raised, mainly due to the simplifying assumptions on which the Bikerman's theory was based and by experimentally proving the existence of a pure interfacial failure [5], especially by means of Auger and X-ray Photoelectron Spectroscopy.

1.3 Mechanisms of bond failure

Some terms as "cohesive failure" or "interfacial failure" have been incidentally mentioned in the previous section, but a general definition explaining what exactly that terminology means has not been provided yet. In this section the main mechanisms of bond failure usually considered are described.

A failure in an adhesively bonded joint is defined "cohesive" when the crack propagation occurs within the adhesive bulk, while a so called "adhesive failure" or "interfacial failure" is a failure which involves the adhesion forces between adhesive and substrate and which occurs when the crack propagates at the interface. A third typical failure mode, given by the combination of the two aforementioned modes and called "mixed cohesive/adhesive failure", is very common. Fig. 1.4 provides a schematic illustration of the main presented failure modes.

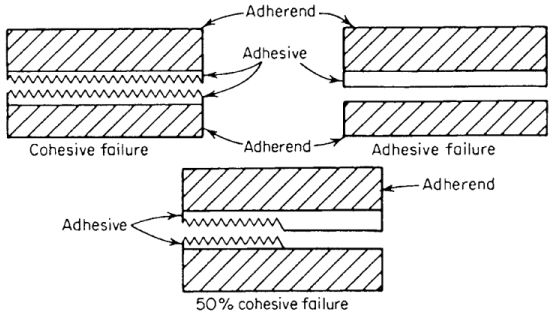

Fig. 1.4 Schematic illustration of cohesive, adhesive and mixed failure [17]

A cohesive failure is usually considered more desirable during an experimental test because it means that the interfacial strength of the joint is higher than the bulk adhesive strength, resulting in a successful performance of the adhesion. Since the bulk adhesive

strength is also, in this case, the joint strength it will be sufficient to select the proper adhesive according to its capability to withstand the service load or to try to improve the adhesive strength by modifying the chemical formulation or the process conditions. It is worth noting, however, that any changes is presumed to affect also the interfacial properties.

Viceversa, when an interfacial failure occurs, it is useless to try to enhance the cohesive strength of the adhesive, because the weakest point of the joint is to be investigated at the interface surface. The problem dealing with the accurate and exact identification of the cause of an adhesive failure is still open, because the factors able to result in it are several. The main reasons for a premature interfacial failure are usually the presence of a weak boundary layer (see Par. 1.2.6), an inadequate preliminary surface preparation, the incapability of the adhesive to properly wet the substrate surface, the generation of internal stresses due to different physical properties of adhesive and adherent as, for instance, the coefficients of thermal expansion, the kind of stress and its orientation with respect to the bonding surface, the rate of loading.

1.4 Surface pre-treatments overview

As it has been mentioned in the previous section, the need for properly preparing the surfaces aimed to be bonded is crucial for the success of the adhesion. The main benefits achievable by performing a pre-treatment over the surface before the deposition of the liquid adhesive are the removal of any weak boundary layers possibly present at the interface, the inhibition of the formation of new weak boundary layers during each phase of the bonding and of the service life of the joint, the possibility to increase the surface free energy of the substrate so as to encourage the wettability between adhesive and substrate, the capability to match the substrate crystal structure and the adhesive molecular structure and the possibility to adequately drive and control the surface roughness.

The available process for the pre-treatments of the substrate surfaces are disparate. They are generically classified according to the nature of their driven mechanism into chemical and mechanical ones, but they were developed also depending to the materials which are needed for. In particular, plastic and elastomeric adherents are very sensitive to some specific pre-treatments, such as:

- oxidation by means of chemical or flame treatment
- electrical corona discharge
- ionized inert gas treatment

- metal-ion treatment
- application of primers and adhesion promoters

Since the present work is focused over the pre-treatment of aluminium substrates to improve the quality of the adhesively bonded joints, it is not worth going deeper in the description of every pre-treatment for other materials. Therefore, the next subsection will be dedicated to carry out an overview of the most common pre-treatments used for aluminium.

1.4.1 Pre-treatments for aluminium

The wide range of pre-treatments usually employed for aluminium alloys substrates surfaces was meticulously analyzed by Critchlow and Brewis [24].

Chemical pre-treatments

The main chemical methods used to pre-treat the aluminium substrate surfaces for bonding purposes are reviewed and discussed hereinafter.

- *Degreasing* - The degreasing is usually employed as the basic stage of multiple-stage pre-treatments, often coupled with the alkaline cleaning with the aim of removing the oxide already present over the surface. The achievable increase of bond strength is small, but no significant surface modification is induced by this treatment. With refer to the durability performance, the degreased joints behave worse than the FPL (Forest Products Laboratory) etched joints [37]
- *Acid paste treatment* - No information about the surface modification induced by this treatment is available while it is well known the high sensitivity of acid paste treated joint to environmental attack with respect to the FPL etched joints [38]
- *Acid etchings* - The most used acid ethcings used to pre-treat the surfaces are chromic based, often all incorrectly designated as FPL, which is the most common and extensively used treatment for aluminium alloys. It is documented both as a classic preliminary treatment to bonding [39] and as a pre-treatment to be applied before anodising [40]. The FPL etch consists in a dichromate-sulphuric acid pickle which was reported to be the most effective in providing a high initial joint strength and in improving the durability behavior. The structure generating over the surface is reported [40] to be a matrix of ~5 nm diameter fibrils extending ~40 nm from the surface, beneath which a relatively thin oxide layer about 5 nm thick is placed. A chromic-free,

sulphuric acid-ferric sulphate based etch is the P2, which has been demonstrated to provide a similar surface topography than the one produced by the FPL etch [41] and to improve the durability with respect to the use of FPL on 6061-T6 alloy [42]

- *Conversion coating* - The durability performance exhibited by Zirconium-based coatings has been proven to be comparable with the one given by FPL etch [43]. Also the chromate or chromate-phosphate coatings have been extensively studied: even if on a macro-scale the topography after the treatment is the same of the untreated surface, on a micro-scale it is possible to notice the presence of spherical particles agglomerate which form a highly structured porous oxide often thicker than 1 μm [44]. More recently, the effect of of $Mg(OH)_2$ and Bohemite conversion coatings, respectively, over the shear strengths of magnesium and aluminium alloys was studied in [45].

- *STAB 1, 2 and 3* - They are non-acid and non-chromate chemical treatments. STAB 1 is based upon an ultrasonic degreasing after which the subsequent steps of rinsing and immersion in tap or deionised water added with K_2CO_3 for 10 minutes at 80°C are performed. STAB 2 consists in a degreasing followed by a room temperature soak in an ammonium hydroxide solution containing a commercial cleaner. STAB 3 is a treatment based on the immersion in a concentrated NaOH solution for 3-10 minutes and then on a hard spray rinse. The results are quite variable, even if the STAB 3 treatment has been documented to give better durability results than the FPL etch.

- *Chromic acid anodising* - Chromic acid anodising (commonly abbreviated in CAA) is the most adopted treatment by the European aeroplane manufacturers. The result of the pre-treatment is a thick, porous and highly structured oxide. Even if the hydration of the surface has been detected, the oxide offers a good resistance to the moisture and even the durability results show an improvement with respect to the FPL treated joints.

- *Phosphoric acid anodising* - Phosphoric acid anodising (commonly abbreviated in PAA) is the most adopted treatment by Boeing Aerospace Co. Even in this case, the oxide is porous and presents wall thinner than the ones of the CAA oxide. Although the presence of the phosphate which is supposed to confer high moisture resistance properties to the surface, the hydration of the surface was documented after an ageing at a temperature of 50°C and a relative humidity of 100% for 72 h [46]. The durability performance provided by the PAA treatment is considered the best achievable, even if in some cases it has been proven to be comparable or less effective than the one given by CAA treatment [47] [48].

- *Other acid anodising* - Several anodising methods are available for the pre-treatment of the surface of bonded joints, in particular the following are documented even if for the most of them a limited amount of data have been collected: sulphuric acid anodising, sealed sulphuric acid anodising, sulphuric acid anodising plus phosphoric acid dip treatment, boric acid anodising, tartaric acid anodising, ammonium tartrate anodising, oxalic acid anodising.

- *Primers* - The main two benefits achievable by using primers to pre-treat high surface free energy substrates before deposing the adhesive are the enhancement of the performance of the joint by means of several different mechanisms (lowering of the viscosity of the adhesive and subsequent improvement of the wettability, strengthening of the interfacial forces between adhesive and adherent, protection from the environmental attack, increase of the peel strength) and the increase of the production flexibility due to the fact that the primers behave as a barrier with respect to the adsorption of contaminants by the pre-treated surfaces, so that the application of the adhesive can be delayed without removing the effects of the pre-treatments [1].

Mechanical treatments

This subsection is dedicated to summarize the main mechanical methods used as a pre-treatment for aluminium surfaces aimed to be bonded.

- *Grit blasting* - The grit blasting is the most used mechanical pre-treatment for bonding purposes and its effectiveness has been extensively documented even in recent works [49]. It is performed typically with graded alumina or silica and, often combined with degreasing, produces an high roughness over the treated surface, promoting the occurring of the mechanical interlocking effect. With respect to the durability, it provides variable results. In particular, it either improved or decreased the performance with respect to the FPL etch treated surfaces in presence of high temperature and high relative humidity [50]. It has been tested after a sea environmental exposure, giving better results than various chemical treatments [38]. Investigations concerning the changes in the adhesion properties of grit blasted mild steel and aluminium alloys substrates conclude that they are not dependent exclusively on the surface roughness, but also on the physical and chemical changes [31]. Other remarks about the influence of the grit blasting treatment over the fatigue and the durability performance of bonded joints are postponed to the apposite sections.

- *Mechanical abrasion by Scotchbrite, belt-sand or wire wool* - Even in this case the result of the treatment is a highly rough surface, but is it possible that residual debris

remain over the surface, contributing to the failure of the bonding process. A poor wettability is achievable by using Scotchbrite and even the durability performance which is possible to obtain with it is low compared with the one given by FPL or grit blasted surface joints [51]. Instead, a good resistance to the environmental aggression is showed by the belt-sanded joints.

- *Machining* - The machining with or without polishing plus the immersion in either distilled or tap water at 10°C is reported to result in variable joint durability depending on the type of treatment employed, due to the variation in oxide composition and stability [52].

- *Liquid and vapour degreasing* - Both these treatments are used to remove traces of lubricants and contaminants from a mill-finished bonded surface. In detail, the liquid degreasing regards the rinse or wipe with acetone, methyl ethyl ketone or carbon tethrachloride while the vapour degreasing is constituted by the use of perchloroethylene, trichloroethylene or 1,1,1-trichloroethane. Toxic fumes can be generated by the chlorinated solvents upon the aluminium surfaces. The degreased surfaces present a good initial bond strength but a low durability when exposed to aggressive environments [53].

- *Corona discharge treatment* - This treatment is able to produce the increase of the surface free energy and therefore of the wettability, but fails in providing a good durability performance with respect to the abrated surface, due to the oxide generated after treatment and behaving as a weak boundary layer.

- *Plasma-spray coating* - 99.5% pure alumina powder can be sprayed into a previously roughened surface by means of mechanical treatments in order to promote the adhesion between glass reinforced epoxy composites and aluminium [54].

1.5 Methods for the assessment of the surfaces

Since the surface on which the adhesion happens plays a key role in determining the final joint strength and in influencing the failure mechanism occurring within a bonded joint, several methods are currently available in order to assess the status of the surface from both chemical and morphological point of views. The main needs for the application of techniques to assess the surface are fundamentally two: firstly, it is important to characterize the surface in the "virgin" conditions to acquire knowledge, for instance, about the possible presence of weak boundary layers; on the other hand it is very useful to inspect the changes induced by

the application of a pre-treatment, in order to verify its effectiveness, applicability and the quality of the bonding.

The X-ray Photoelectron Spectroscopy (XPS), even called Electron Spectroscopy for Chemical Analysis (ESCA), is a technique consisting in bombarding the joint surface with mono-energetic X-rays (usually AlKα or MgKα) in ultrahigh vacuum (<10^{-5} Pa) [55]. The spectrum in terms of electron intensity vs. the binding energy to the atom of photo-excited electrons subsequently being ejected from the surface is acquired by means of pulse-counting techniques, giving therefore the possibility to acquire information about the chemical composition of the surface [56]. This is a method very sensitive to the surface, because only electrons very near to the surface (in a range comprised from about 1.5 to 9 nm) maintain high the probability to departure from the surface keeping intact their energy. The main advantage presented by the XPS technique with respect to other methods (as the AES that will be presented in the next lines) lies in the possibility to minimize the charging effects and in the readiness of the analysis of the surfaces of insulators.

According to the aforementioned AES method (acronym standing for Auger Electron Spectroscopy) a small diameter (from 0.1 to 50 μm) electron beam is used to excite the Auger electrons in the apical surface regions, achieving to obtain a good spatial resolution, higher than the one gained with XPS method. Nevertheless, due the using of a primary electron beam, is is possible to applicate it only over metallic substrates [1] [57].

Other tools successfully employed for the chemical characterization are the Secondary Ion Mass Spectroscopy (SIMS) [58] [59] and the Ion Scattering Spectroscopy (ISS).

The most used method to assess the surface compatibility in order to get a good wettability level is the measure of the contact angle by means of the sessile drop or the captive-bubble tests. They consist in the measure of the profile of a sessile drop of liquid or a bubble, respectively [60] [61], placed upon a perfectly smooth (from a macroscopic point of view) and rigid solid surface and allowed free to flow until an equilibrium position with the surface is achieved. It is possible to carry out the measure directly (with a telescope fitted with a protractor eyepiece) or indirectly (by measuring the angle at which light from a point source is reflected from the surface of a liquid drop at its point of contact with the solid or by means of the measurement of drop dimension [62] or by using the interference microscopy [63]). With regard to the measurement of drop dimensions, it can be executed evaluating the contact angle starting from the height and the base diameter of the drop, considering negligible the gravitational distortion, which seems reasonable only for small drops. The interference microscopy method, indeed, is especially used for the evaluation of contact angles lower than 10°, which can be scarcely measured with the tangent techniques. Due to the fact that is very infrequent that solid surfaces are perfectly smooth and chemically homogeneous, the contact

angle undergoes an hysteresis phenomenon which is to be taken into account when using this method to assess the wettability. It is reported that the alternative technique of inverse gas chromatography was employed, for instance, by Papirer [64].

Other common methods useful to evaluate the capability of the adhesive to properly wet the surface are the water break test, which is essentially a test to verify the cleanliness of the surface, and the use of dyne test markers, based on the application of pens containing inks of specific and known surface tension, used typically to ensure the effectiveness of a pre-treatment in enhancing the wettability features of a surface.

Finally, the surface morphology is another typical element able to enhance or weaken the adhesion over the surface and therefore it is of interest for investigations. The most common method to take awareness of the surface topology is using the Scanning Electron Microscopy (SEM), based on the interaction between the surface and a focused electron beam scanning the surface itself [65]. The result is a high magnification image of the surface. The reasons for the preference usually given to SEM to the detriment of optical microscopy lie in both the lack of magnification offered by the optical technique with respect to the one provided by SEM and poor depth of field and depth of focus of the optical microscopy. It is worth noting in fact that the effects of some pre-treatments act at a micro-scale, so that only the high resolution offered by SEM can reveal, as in the case of the acid anodized aluminium surfaces discussed in [66]. As it will be showed in the next sections, SEM is often used also to inspect the fracture surfaces in order to help to identify the failure mode and its main causes. The principle of operation of SEM, in fact, involves the possibility to quite clearly distinguish the traces of adhesive, which is an insulant material and therefore producing a darker contrast around it due to the amount of electric charge over it, from the conductive metal substrates, allowing to deeply investigate concerning the occurrence of a cohesive or an interfacial failure. For the specific attributes of this method, the polymeric substrates are not so easy to be assessed with it because for the aforementioned reasons they produce blurred images, so they have previously to be coated with a thin alloy of gold or carbon to prevent electrostatic charging, which makes other techniques like Atomic Force Microscopy (AFM) preferred to SEM.

The use of profilometry is crucial in the attempt to translate the qualitative remarks based upon the fracture surfaces as they appear in SEM images into a quantitative characterization based on the evaluation of the surface roughness. The classic approach of the profilometry is the one prescribing the use of a stylus profilometer in which a diamond stylus is used to scan the surface following the profile and graphically describing the trend of peaks and valleys, directly (by means of the deflection of the stylus) or indirectly (by means of an interferometric approach) [67]. Some disadvantages of this technique are detectable: the ones

related to the difficulty in measuring the narrowest grooves and the fact that the roughness evaluation does not provide any information regarding the distribution of the peaks and the valleys over the surface will be addressed later, in explaining the methodology employed in this work. Another problem lies in the fact that the vertical data related to the height of the profile are much more magnified than the horizontal data related to the measured length. An alternative approach is represented by the use of a non-contact optical profilometer.

The Scanning Probe Microscopy (SPM) is based on two different techniques called Scanning Tunnelling Microscopy (STM) and Atomic (or Scanning) Force Microscopy (AFM or SFM). An electron beam tunnels between a probe and the conductive surface placed over a piezoelectric scanner. Even if it is not wide used for the adhesion science, the complementarity of this method with respect to SEM was discussed in [68], while in [69] the effectiveness for the application of AFM to the study of surfaces aimed to be bonded was demonstrated.

1.6 Durability performance

With respect to the durability, a ranking of the pre-treatments based upon their capability to improve it was attempted by Chritchlow [24]. From a literature review, he found that the untreated or simply degreased surfaces present a bad performance through time, while the grit blasted specimens are relatively durable. In general, however, when the exposure to high temperature and strict moisture conditions is unavoidable, the primacy of the chemical treatments is documented. Nevertheless, given the wide range of parameters available for the chemical treatments, the inconsistency of the inner ranking between different chemical treatments is not surprising. In particular, the results obtainable with chromic acid etchings like the FPL one are reported to be both worse and better than the performances given by CAA or chromate-phosphate conversion coating. Even the PAA is demonstrated to provide equal or better results, depending on the circumstances, with respect to the CAA ones.

The failure mode is extremely influenced by the durability. Kinloch [70] reported that in adhesively bonded joints presenting cohesive failure when tested just after the production the locus of failure tends to switch to the interface after an environmental exposure, even if whether the failure path is truly at the interface or in an oxide layer or finally in a thin boundary layer of the adhesive is still matter of debate. However this is a behavior well known in literature and many other examples would be presentable, even in recent works like [71].

To simulate the environmental effect, suitable accelerated ageing cycle including the presence of strong variations in temperature and relative humidity, as well as optionally

the presence of an aggressive atmosphere like the one gained with salt spray, have been developed. The main damaging mechanism in these conditions is represented by the effect of water, which can either be diffused through the adhesive or migrate through cracks in the adhesive or voids at the interface [51]. The main effects of the water diffusion through the adhesive from an exposed edge are essentially three, as found by Brewis [72] and Bowditch [73].

1. The water diffusion induces the plasticization of the adhesive, which initially leads to an improvement of the strength given by the relief of the shrinkage stresses generated during the curing cycle but with the passing of time has a bad influence over the mechanical properties of the adhesive (the effect however is documented to be reversible by means of drying); alternative methods for evaluating the pattern of distribution of water in a bonded joint were developed by some researchers including Comyn [74].

2. The adsorption of water can cause the displacement of the adhesive at the interface, therefore disrupting the interfacial bonds, if it modifies the equilibrium status between adhesive and adherent. In particular, as reported by Adams [75], if the adherent is constituted by a high energy substrate (as, for instance, a metal oxide) and the amount of adsorbed water oversteps a threshold, to assure the reaching of an equilibrium position between adhesive, adherent and water the creation of a thin film of water at the interface is needed. This film constitutes, of course, a weak boundary layer lowering the joint strength. In order to explain this phenomenon, Kinloch [1] proposed a variation of the formulation of the work of adhesion, reported in Eq. 1.6, when a liquid is present, as it is shown in Eq. 1.10:

$$W_A = \gamma_{AL} + \gamma_{BL} - \gamma_{AB} \tag{1.10}$$

where γ_{AB} is the interfacial surface free energy between the substances A and B (the adhesive and the substrate, respectively) while γ_{AL} and γ_{BL} are the interfacial surface free energies between the adhesive and the liquid and between the substrate and the liquid, respectively. Where this goes towards a change in the work of adhesion from a positive to a negative values, then it means that the stability of the interface is lost because of the presence of the liquid and a new equilibrium position is pursued, leading to the displacement of the adhesive. This approach is revealing of the difficulty in bonding the high energy substrates, like metals, with respect to the assurance of the desired service life in a high humidity environment.

When a primary coat is applied, it remains bonded to the substrate after the water adsorption, but a separation of the adhesive from the coat can occur due to the moisture, which is an uncommon behavior but has been documented in circumstances involving structural bonding joints pre-treated with a phenol-formaldehyde coating. While the separation between adhesive and primary coat appears to be a reversible phenomenon with drying, the displacement of the adhesive from the adherent is not such and it is often followed by the creation of a band of corrosion at the interface which goes reducing the load bearing area until failure.

3. The moisture finally leads to the hydration or corrosion of the metallic substrates, in particular in the considered case of aluminium alloy adherents the hydrated oxide becomes a weak boundary layer (joint failures associate to this mode are widely documented in literature, for instance in [76])

With refer to aluminium joints, several studies in literature documented how substrate surfaces whose service conditions require the exposition to an high humidity environment are to be preferentially pre-treated with a chromic-sulphuric acid etch and the simply degreasing alone must be avoided, as shown in Fig. 1.5 derived from [77].

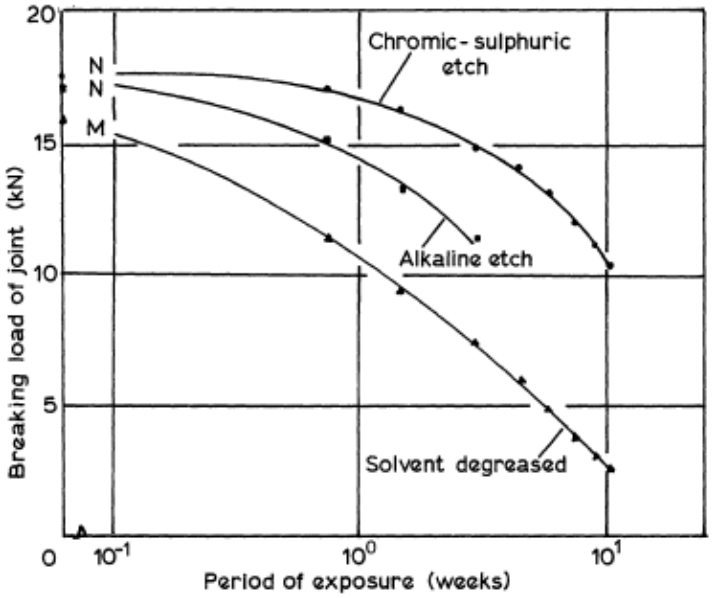

Fig. 1.5 Aluminium/epoxy-polyamide FM 1000 adhesively bonding joint strength after the exposure to a temperature T=43°C and a relative humidity RH 97% (taken from [77] and adapted by Adams [75])

In a work of Costa *et al* [78] the effect of moisture over the mechanical behavior of some AA6082-T6 aluminium joints, bonded with either a ductile (XNR 6852-1 supplied by Nagase Chemtex) or a brittle (SikaPower 4720 supplied by Sika) adhesive to test the sensitivity from the adhesive response with respect to the possibility of yielding and reaching to higher strain levels, was studied. Both adhesive and adherents bulk specimens, as well as Double Cantilever Beam (DCB) joints, were produced and immersed in distilled water at 32°C. Fig. 1.6 shows the variation in the stress-strain response of tensile bulk specimens realized with the brittle (a) and the ductile (b) adhesive, respectively, in function of the exposure time.

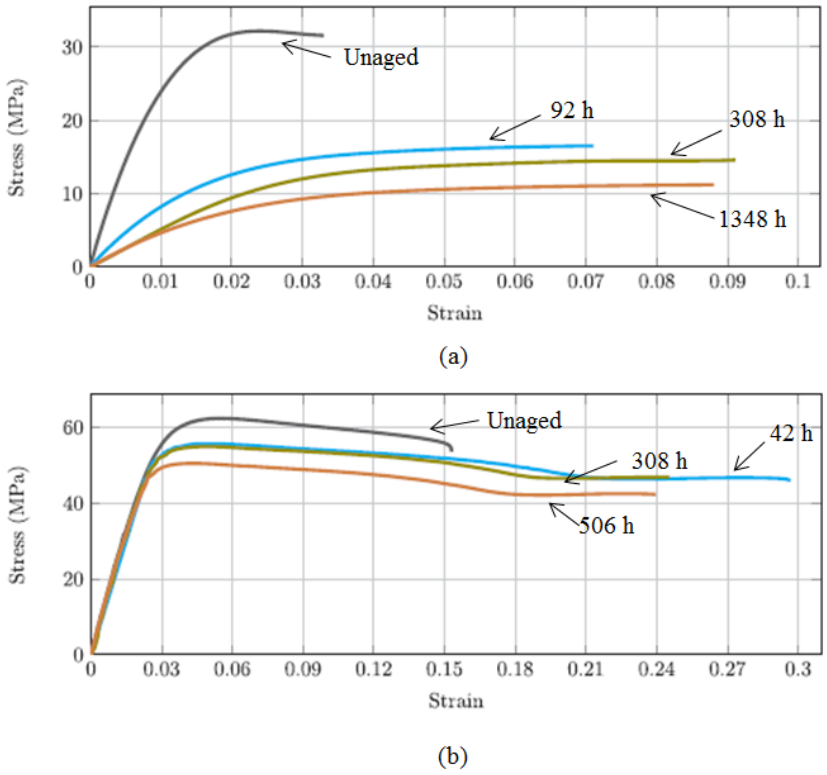

Fig. 1.6 Sress-strain curves in the unconditioned and three different aged stages for SikaPower 4720 (a) and XNR 6852-1 (b) [78]

The SikaPower adhesive presents a marked decrease of the tensile strength and Young's modulus in the conditioned specimens with respect to the unaged one, while the sensitivity of the tensile strength of XNR 6852-1 to the water adsorption is lower and its Young's modulus does not seem to be affected by the aging. Moreover, a significant increase of the elongation at break in both cases, due to the improvement of the ductility of the adhesives caused by the water, occurs.

Measures of the fracture toughness by means of DCB tests show that a slight but progressive decrease of the fracture toughness is exhibited by the SikaPower adhesive because of the

lowering of the maximum bearable load caused by the water adsorption. Instead, Nagase XNR 6852-1, which was interested by a lower water adsorption with respect to the other adhesive, keeps substantially constant the bearable load but increases the elongation at break, resulting in an higher fracture toughness of the corresponding DCB joints with respect to the unaged conditions. Nevertheless, after a level of relative humidity equal to 25%, the trend of the fracture toughness with the water adsorption becomes similar to the one showed by the joints bonded with SikaPower. These last results are offered in Fig. 1.7, where even analytical curves obtained by a proposed predictive equation are plotted.

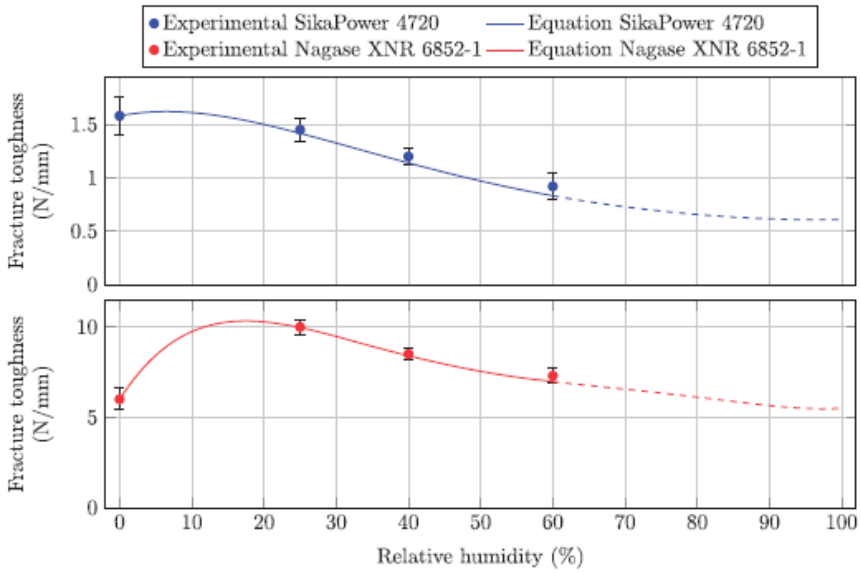

Fig. 1.7 Experimental and analytically predicted trends of fracture toughness in function of the relative humidity for both the tested adhesives [78]

The same two adhesive systems were studied by Viana *et al* [79] with refer to the variations induced by the moisture over some bulk material properties, including the glass transition temperature. Two aging environments were used to condition the specimens: distilled water and a saturated solution of NaCl. The assessment of the changing in the adhesive properties was conduced at three different temperatures: -40°C, 23°C and 80°C. By means of Dynamic Mechanical Analysis (DMA), a decrease of the Tg value as the moisture uptake increases was recorded. The results, showed in Fig. 1.8, confirm the distilled water as the most aggressive environment. The Tg of SikaPower 4720 adhesive is more sensitive to the aging environment, presenting a lowering below the room temperature when subjected to immersion in distilled water (which has a severe effect over the tensile strength of the material, especially at high temperature), while the XNR 6852-1 adhesive exhibits a 15°C drop moving from the unaged to the distilled water aged conditions. The same authors

performed also a detailed review of the main results obtained within the topic of the damage induced by temperature and moisture in the adhesive materials [80].

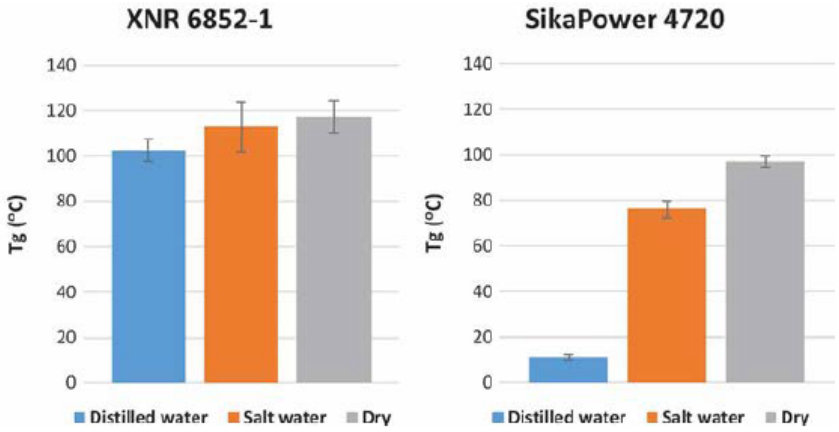

Fig. 1.8 Glass transition temperature ox XNR 6852-1 and SikaPower 4720 adhesives in function of the aging environment [79]

It is worth noting that very often the accelerated ageing cycles require the exposure of the joints to high temperatures, which are promoters of water adsorption by the adhesive, but since these temperatures are never (during the normal outdoor ageing) or scarcely (in specific applications) reached, the risk of obtaining failure mechanisms far from the real ones and not representative of the actual damage occurring in a bonded joint during its service life is not unusual.

1.7 Fatigue

An extensive review of the existing literature concerning the fatigue behavior of adhesively bonded joints is performed in [81].

In general, the adhesives own a good dynamic fatigue properties with respect to the behavior exhibited by other traditional joint methods (like rivets, fasteners and welding), because of the more uniform distribution of stresses in the adhesive joints. First of all, the usual gap between the fatigue service conditions, often complicated by the effect brought by many different parameters (including stress conditions, geometry and environmental variables), and the simulated experimental tests is to be underlined.

With refer to the frequency employed, Hart-Smith [61] documented that single lap-shear joints bonded with a rubber-toughened epoxy adhesive are able to keep their structural integrity for more than 10^7 cycles when tested at a frequency of 30 Hz, but fail in a few hundred cycles when the frequency is lowered to 10^{-4} Hz. This is mainly due to the effect

of the stress concentrations: in the single lap joint the length of the overlap is usually low, therefore the stresses and the strains generating throughout the length of the bonded area are high, resulting in the occurrence of the creep phenomenon when the frequency is low, while an high frequency does not let to the specimen the time to creep before the load is removed.

The most wide attempt to extend the concepts of fracture mechanics to the description of a crack growth in an adhesively bonded joint undergoing dynamic fatigue is due to Mostovoy and Ripling [63]. Their work was based upon the use of the aluminium Tapered Double Cantilever Beam (TDCB) joint geometry bonded with an epoxy resin. In Fig. 1.9 a typical example of the results obtained, plotted in terms of crack growth rate, da/dN, in function of the adhesive fracture energy, ΔG, is showed, revealing that the central range of experimental crack growth rate data is quite according to the Paris' law (which will be presented in Chapter 5).

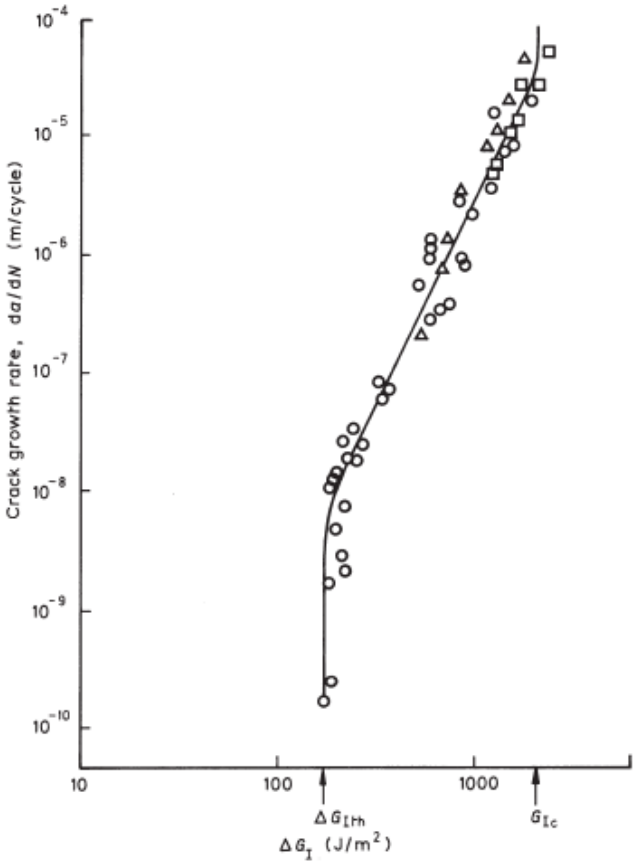

Fig. 1.9 Crack growth rate vs adhesion fracture energy for an aluminium TDCB bonded with an epoxy adhesive and fatigue tested under different frequencies [63]

The data showed in Fig. 1.9 also point out the substantial independence of the trend from the frequency employed (even if in other circumstances a decrease of the crack growth

rate with the frequency, due to the occurrence of a localized heating at high frequencies able to blunt the crack tip, has been recorded) and the existence of two significant values of the adhesive fracture energy, in the graph called ΔG_{Ith} and G_{Ic}, which are respectively the threshold value under which the crack growth does not occur and the typical critical value for crack growth under short-term monotonic loading conditions. Other works, like [82], point out the significant effect that the mean load has over the fatigue behavior of adhesively bonded joints.

With respect to the topic of the possibility to enhance the fatigue performance of bonded joints by means of some of the available pre-treatments previously discussed, a comparison between mechanical blasting methods [83] over the surfaces of some steel Thick Adherent Shear Test (TAST) and End Notched Flexure (ENF) joints bonded with an epoxy adhesive results in the recognition of the crucial role played by the surface roughness upon the fatigue life and of the higher influence that the application of a pre-treatment has on the fatigue performance than on the quasi-static features. On this point, a recent study [84] illustrates the relation between the adhesive fracture energy fatigue threshold and the surface roughness in aluminium bonded joints subjected to a mixed-mode cyclic loading, finding that the lower values of the toughness threshold are reached both for very low and very high values of roughness. Even da Silva [85] found that some aluminum specimens with an induced patterned and structured surface morphology present an higher fatigue strength than the ones without pattern.

The coupled effect of dynamic fatigue and the environmental conditions has been extensiveley studied too, for instance in [86] three surface pre-treatments (grit blasting plus degreasing, PAA and finally PAA plus the application of an anti-corrosion primer) have been ranked with respect to the fatigue response of some aluminiun bonded joints immersed in liquid water and in 55% RH, finding that the lowest adhesive fracture energy threshold belongs to the grit blasted joints, in which the failure occurs in a predominantly adhesive mode.

An extensive review of the environmental effect over the fatigue behavior of adhesively bonded joints is offered in a work by Costa *et al* [87]. They concluded that the tendencies are not univocal: many works [88] [89] [90] demonstrated a decrease of the threshold fracture toughness with the moisture, but even exceptions to this trend are present [91] [92] [93]. Similar inconsistent trends are detectable with refer to the slope of the Paris' law.

1.8 Influence of joint geometry

The independence of the adhesive fracture energy, G_{Ic}, and the fracture toughness, K_{Ic}, for joints bonded with brittle epoxy adhesives whose locus of failure is within the adhesive, from the joint geometry employed has been demonstrated in many works [94] [95] [96], as well as their equivalence to the strain energy release rate and the fracture toughness, respectively, of the adhesive [97]. In other works [98] [63], even the independence of G_{Ic} from the thickness of the bondline in similar joints, if it is within the common range usually employed (0.08-2 mm), has been proven. The only exception to these experimental observations is constituted by the case in which the adhesive layer in the joint is very thin and the crack tip micro-mechanisms are affected by the presence of high stiffness and high yield strength substrates (e.g. flexible peel joints).

A general and brief overview of the main used typologies of specimen geometries for the adhesively bonded joints characterization is offered in the next lines, with major focus over the Double Cantilever Beam (DCB) joints which are selected for the experimental tests reported in this work.

The most wide used geometry for testing adhesive joint strengths is the Single Lap-shear Joints (SLJ), schematically represented in Fig. 1.10 with the main variants derived from SLJ.

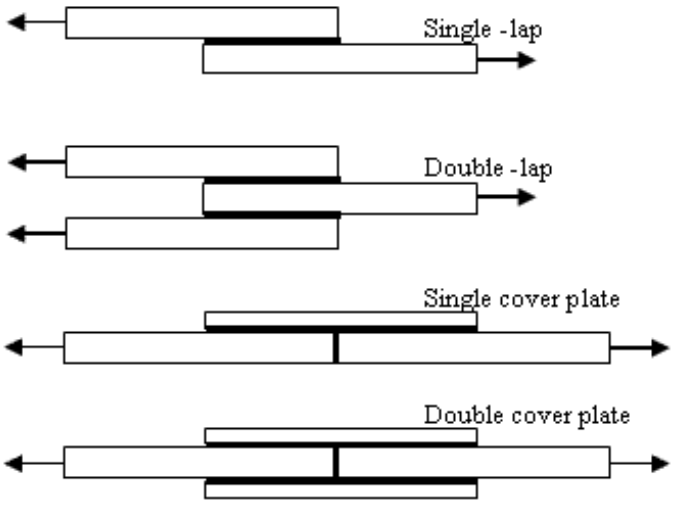

Fig. 1.10 Schematic examples of Single Lap-shear Joints and its main variants

With refer to Fig. 1.10, the Single Lap-shear Joints present a load asymmetry with respect to the mean plane of the joint, which can induce peel stresses if the stiffness of the substrates is not high. The stress distribution perpendicularly to the bondline, showed in Fig. 1.11, is not even, being withstood almost entirely by the boundary zones of the overlap area.

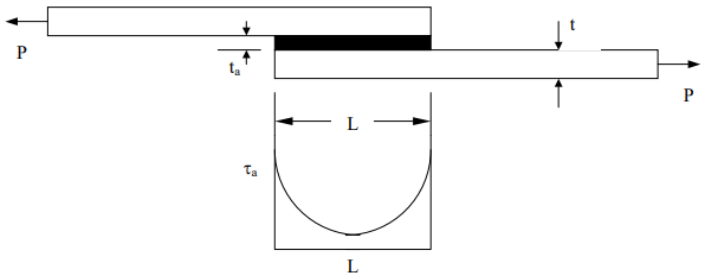

Fig. 1.11 Distribution of the shear stress along the overlap length of a SLJ

The Double Lap Joints represent one of the various attempts to reduce the risk of the generation of peel stresses due to the loading misalignment present in the SLJ test, although the bending of the outer adherents is unavoidable because of the fact that even in this case the load is transmitted to the substrates through the adhesive, away from the neutral axis.

The joints with cover plates are a mix between butt joints and SLJ, in particular the specimens with the double cover plate allow to avoid the risk of peel stresses insurgence and they can be realized in such a way to optimize also the shear stress distribution in the bondline.

The scarf joints exploit the geometry showed in Fig. 1.12 to erase the problem dealing with the stress concentrations at the ends of the bonded length. The draft angle value is depended on the adherents material, the adhesive and the loading direction, but usually it is optimized when it is about 4.5°. The variant constituted by the stepped lap joints considerably simplifies the assembling operations.

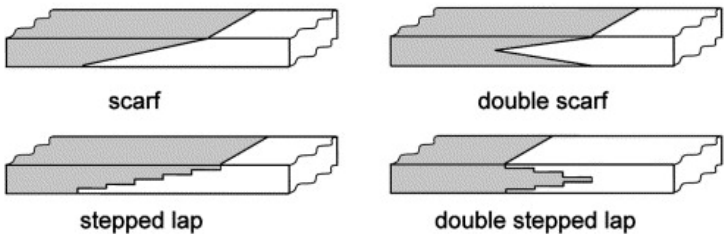

Fig. 1.12 Schematic representation of bonded scarf joints and stepped joints [98]

If the draft angle in a simple scarf joint is equal to 90°, the specimen assumes the name of butt joint and it is used to characterize the tensile stress or the torsional shear stress. Often they are realized with a cylindrical geometry. They are very sensitive to bending effects and to possible non-uniformity of the adhesive thickness. Moreover, the bonding area is usually small, so the joint strength is strictly depending on the adhesive strength, typically lower than

the one of the adherent, resulting in a general suggestion to avoid butt joints in real bonding applications.

Another geometry very used to bond them tubes or rods together is the tubular joint, which is schematically represented in Fig. 1.13. Many variants of this geometry are available, including for instance the presence of tapering corners for keeping constant as much as possible the stress distribution in the adhesive or the butt joints when a variation of the tube diameter is to be avoided.

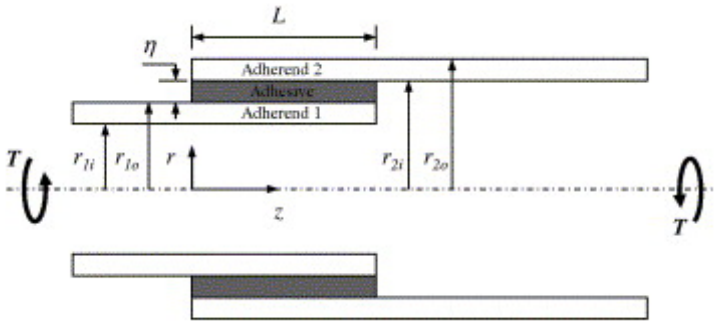

Fig. 1.13 Schematic representation of one of the typical tubular bonded joints geometry bonded scarf joints and stepped joints [99]

Another alternative geometry to the conventional SLJ is the Thick Adherent Shear Test (TAST) joint, which exploits the increase of substrates thickness and stiffness with respect to the SLJ samples to segregate as much as possible the pure adhesive shear stress from the other contributes derived from the complicated state of stress to which the adhesive is subjected in a SLJ. In Fig. 1.14 the typical geometry of a TAST joint is proposed.

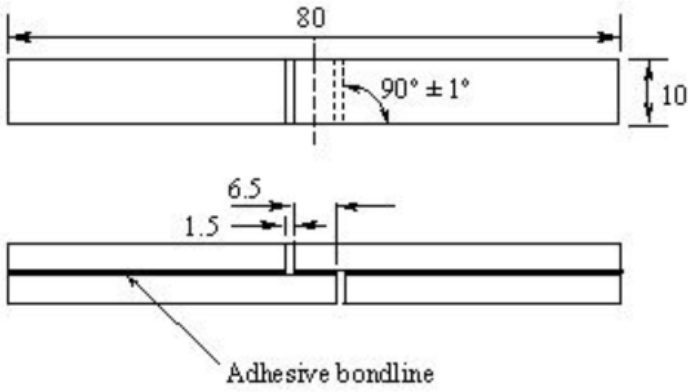

Fig. 1.14 Schematic representation of a typical TAST joint geometry (all dimensions in mm)

For the application of a linear elastic fracture mechanics (LEFM) approach to the evaluation of the fracture process within adhesively bonded joints, the fracture toughness is needed. The most of the available data in literature regards the Mode I fracture toughness assessed by means of the Double Cantilever Beam (DCB) tests, which will be discussed later. For the evaluation of the fracture toughness associated to Mode II loading there are several employable tests, the main of which is the End Notched Flexure (ENF) which essentially consists in a three-point bending test over a pre-cracked bonded joint in which, therefore, the adhesive is loaded by shear stresses. Fig. 1.15 provides an illustration of a typical ENF joint.

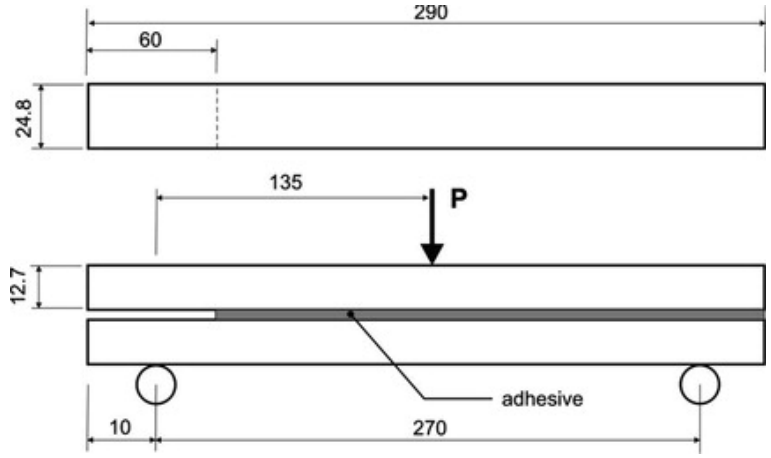

Fig. 1.15 Schematic representation of a typical ENF joint geometry (all dimensions in mm) [100]

With refer to the determination of the peel strength of the adhesive bonding joints with flexible substrates, the main geometry used for performing the test is the T-peel joint, showed in Fig. 1.16.

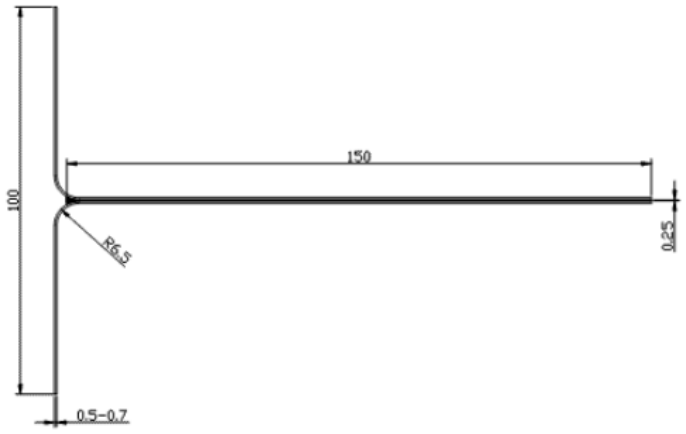

Fig. 1.16 Schematic representation of a typical T-peel joint geometry (all dimensions in mm)

The resistance of the adhesive to the cleavage loading, which together with peel stresses is the most dangerous form of loading to which an adhesively bonded joint can be subjected, is measured with some tests like the wedge cleavage test (Fig. 1.17), in which also the sensitivity to the environmental moisture is tested, and the compact tension test (Fig. 1.18), suitable to test the cleavage strength of metal-to-metal bonded joints.

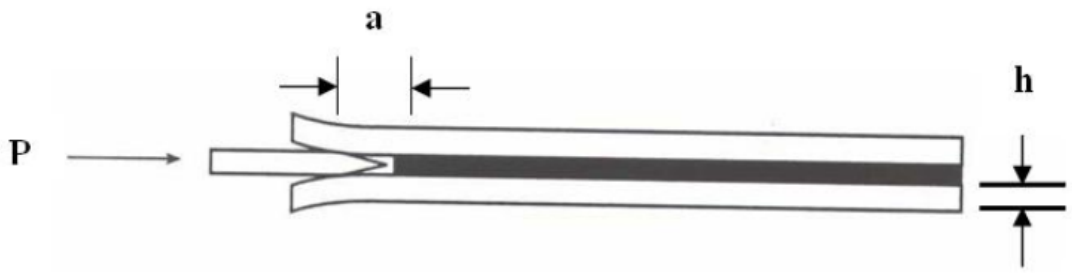

Fig. 1.17 Schematic representation of a typical wedge cleavage joint geometry

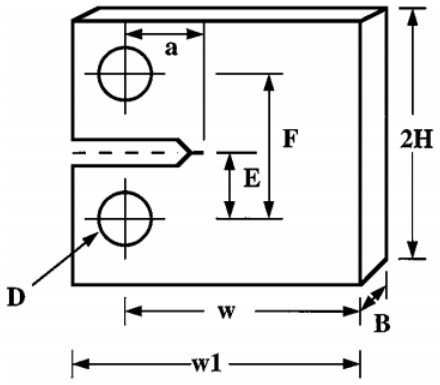

Fig. 1.18 Schematic representation of a typical compact tension joint [101]

1.8.1 Double Cantilever Beam test joint

The Mode I fracture toughness is usually evaluated by means of the Double Cantilever Beam (DCB) test, which is standardized in ASTM D3433 [102]. Fig. 1.19 shows the geometry and the dimensions prescribed in aforementioned standard for a flat adherent specimen.

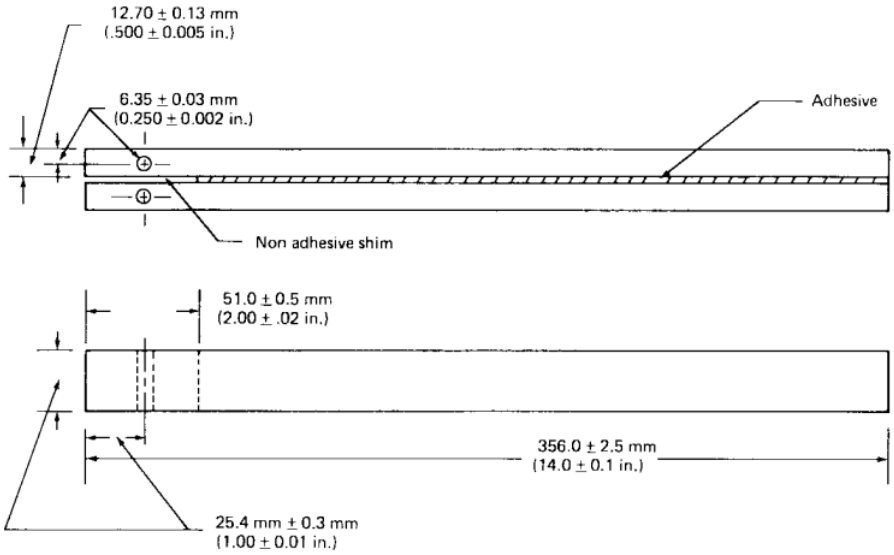

Fig. 1.19 Flat adherent DCB specimen [102]

The test is performed by pulling apart the two adherents at a specific rate, resulting in an increasing deflection of the substrates with the load. When the load oversteps a threshold, the crack (pre-induced during the production by means of the insertion of a non-stick material piece) starts propagating within the adhesive (in the case of a cohesive failure mode) or at the interface (adhesive failure mode) towards the length of the specimen, leading to a drop of the load due to the loss of stiffness.

According to [102], the fracture toughness associated to the opening mode (or Mode I) from the load needed for the start of the crack propagation is evaluated as in Eq. 1.11

$$G_{Ic} = \frac{4P_{MAX}^2(3a^2+h^2)}{EB^2h^3} \tag{1.11}$$

where P_{MAX} is the load required to start crack, E is the Young's modulus of the adherents, B is the specimen width, a is the crack length measured as the distance between the crack tip and the pin hole centers and h is the thickness of the adherent in a normal direction to the bonding plane. This equation is based upon elastic stress analysis and its validity is influenced by the establishment of a sharp-crack condition in the bondline, which means that the state of stress near the crack front is assumed to approach tritensile plane strain and the crack-tip plastic region is small with respect to the crack size and the specimen dimensions in the constraint direction.

If the compliance of the adhesive is not neglectable, its properties (e.g. crack tip deflections or rotations) can not be ignored in evaluating the fracture toughness of the joint, which can be assessed by means of the compliance method, as it is shown in Eq. 1.12

$$G_{Ic} = \frac{P^2}{2B}\frac{dC}{da} \tag{1.12}$$

where P is the applied load and C is the compliance of the joint.

There are several formulations relating the compliance to actual crack length and thus allowing the evaluation of the term dC/da, as documented in [103]. The most employed are the Euler-Bernoulli and the Timoshenko beam theories, which however do not take into account the flexibility of the adhesive and the rotation of the adhesive at the crack tip due to its flexibility and to the distortion of the substrates. According to the Timoshenko theory, the compliance is given by Eq. 1.13

$$C = \frac{\Delta}{P} = \frac{2a^3}{3EI} + \frac{h^2 a}{4GI} \tag{1.13}$$

where Δ is the displacement of the loading point, $I = bh^3/12$ is the second moment of area of the beam section and G is the shear modulus of the substrates. The Euler-Bernoulli theory is based upon the same Eq. 1.13 deprived of the second term, resulting in the following formulation of the Mode I fracture toughness, Eq. 1.14

$$G_{Ic} = \frac{P^2 a^2}{BEI} = \frac{12P^2 a^2}{B^2 h^3 E} \tag{1.14}$$

The corresponding formulation according to the Timoshenko theory, assuming a Poisson's ratio ν=0.33, is provided by Eq. 1.15

$$G_{Ic} = \frac{12P^2 a^2}{B^2 h^3 E}\left[1 + \frac{1}{12}\left(\frac{h}{a}\right)^2\right] \tag{1.15}$$

To take into account the contributions for the rotation of the crack tip and the flexibility of the adhesive, a correction δ has been introduced [104], therefore the compliance formulation becomes the one proposed in Eq. 1.16

$$C = \frac{8}{Eb}\frac{(a+|\delta|)^3}{h^3} \tag{1.16}$$

The corrected versions of the Euler-Bernoulli and Timoshenko formulations of the Mode I fracture toughness are reported in Eq. 1.17 and 1.18, respectively

$$G_{Ic} = \frac{3P\Delta}{2B(a+|\delta|)} \tag{1.17}$$

$$G_{Ic} = \frac{4P^2}{EB^2}\left[\frac{3(a+|\delta|)^2}{h^3} + \frac{1}{h}\right] \tag{1.18}$$

From experiments, in [105] the correction length δ is found equal to about $h/3$.

In this work, the Krenk model [106] is used because it automatically takes into account, without the need for experimental correction, the contributions given by the flexibility of the adhesive and the rotation occurring at the crack tip. The mathematical formulation of the compliance and the Mode I strain energy release rate evaluated with this approach will be reported in Chapter 3.

Chapter 2

Laser ablation surface pre-treatment

The effectiveness of the chemical pre-treatments in making the substrates surfaces suitable for the bonding, by increasing their surface free energy or by altering the surface morphology in such a way to promote the interlocking effect, has been discussed in Chapter 1. In many works [107] [108] [109], however, the high environmental hazards and the risks for the operator innate in the chemical pre-treatments are underlined. Some strategies were developed in order to reduce the dangerous materials or phases of the work, as attempted for instance by Critchlow et al [110] with respect to the topic of the replacement of chromic acid anodizing, but the fact that often these alternatives are not always cost-effective must not be underestimated. On the other hand, the grit blasting is rather easy to be performed and brings some enhancement in the surface morphology, although it does not reach to achieve the performance levels provided by the most of the chemical and electro-chemical treatments for adhesively bonding purposes.

A valid alternative to the grit blasting which has been more and more studied in the last years is the laser ablation. It presents many benefits related to the flexibility of the process and the repeatability of the results. Moreover, it assures the possibility to circumvent the poor control over the resulting surface morphology obtainable by means of the traditional chemical and mechanical pre-treatments [111] [112].

In this Chapter the main characteristics of the laser ablation process will be touched, as well as the main documented goals which is possible to achieve with respect to the adhesion quality and to the bonded joint strength will be discussed.

2.1 Basic concepts about laser ablation

Laser is an acronym which stands for Light Amplification by Stimulated Emission of Radiation. The laser apparatus consists in a laser gain medium, an external source of

energy (called pump) and a series of mirrors usually referred to as the optical resonator or, erroneously, optical cavity. According to [113], a laser is definable as a coherent, convergent and monochromatic beam of electromagnetic radiation with wavelength ranging from ultraviolet to infrared.

The classical theory dealing with electromagnetic radiation considers it as a wave propagating in a perpendicular direction to the ones associated to the oscillations of the electric and the magnetic fields, respectively. For a plane polarized light, the oscillation of the electric field is not randomly directed but is is strictly confined to a specific plane. The so-called intensity of radiation is the energy per unit area perpendicular to the propagation direction. By dividing the frequency by the energy, the characteristic wavelength of the radiation is available, whose value is the discriminative element which divides the electromagnetic spectrum into several ranges, each one corresponding to a different type of radiation (e.g. radio waves, micro-waves, infrared radiations, visible light, ultraviolet radiations, x-rays, gamma-rays).

To better explain the occurrence of some events, an alternative approach called quantum theory was developed, according to which the electromagnetic radiation is considered as composed by particles referred to as photons, each one possessing a specific amount of energy.

The three main mechanisms through which a laser works are the population inversion, the stimulated emission and the amplification. The first one, called pumping, is the process which leads the electrons from lower to higher states of energy, therefore perturbing the thermal equilibrium of a material by "inverting the population" in terms of typical distribution of electrons. The main mechanisms involved in the population inversion for a typical lasing system with three and four levels of energy, respectively, are shown in Fig. 2.1.

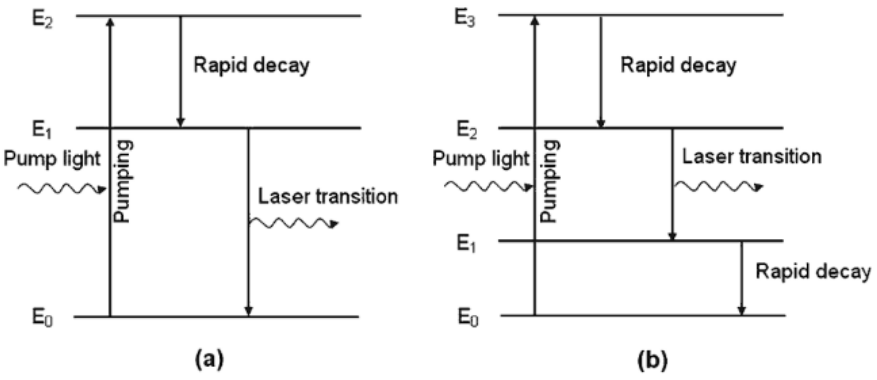

Fig. 2.1 Schematic representation of the population inversion phenomenon in a laser system employing three (a) and four (b) levels of energy,respectively [113]

Basically, the adsorption of an electromagnetic radiation from an external source triggers the pumping phenomenon, leading the electrons from the low state of energy E_0 to an higher lever (E_2 in the three levels case, E_3 in the four levels case), from which they undergo a rapid radiationless decay to a lower level of energy (E_1 in the three levels case, E_2 in the four levels case). The subsequent decay towards a further lower state of energy (the original E_0 in the three levels case, the level E_1 in the four levels case) is accompanied by the emission of a laser radiation, provided that the pumping intensity is beyond the so-called laser threshold. In solid-state lasers (e.g.: Nd:YAG) the population inversion is performed by means of gas-filled flashlamps or by using diode-lasers as pumping source. In the gas lasers, indeed, the pumping occurs electrically.

The stimulated emission is the phenomenon associated to the interaction of a photon and the excited atom of the laser medium whose electrons, submitted to population inversion, are going to decay from a high to a low state of energy, as it is exemplified by Fig. 2.2.

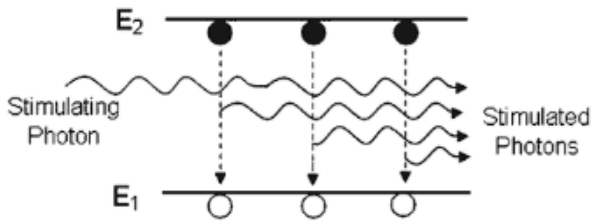

Fig. 2.2 Schematic representation of the stimulated emission [113]

When the stimulated photons are in the same phase and state of polarization, they are able to increase the amplitude of an incoming photon, resulting in an amplification of the light. This is performed in the so-called optical cavity, at whose ends a set of mirrors is adequately placed. The laser medium is positioned between the mirrors and typically one mirror is completely reflecting (in order to boost the amplification) while the other one is partially transmitter. In Fig. 2.3 an amplification phenomenon from the reflective mirror (on the left) to the partially transmitter one (on the right) is shown.

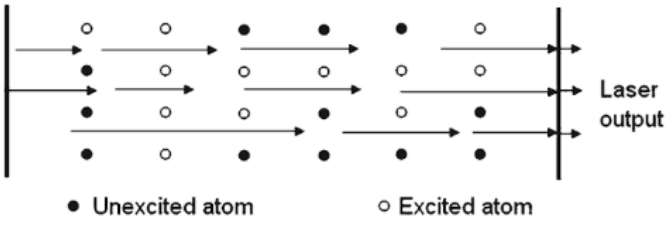

Fig. 2.3 Schematic representation of the amplification phenomenon [113]

The main properties of the laser beams are listed and defined below.

- *Monochromaticity*: property related to the narrow bandwidth of the lasing light.
- *Collimation*: property depending on the capability of the beam to focus on small areas even at high distance.
- *Coherence*: the degree of orderliness of waves, which measures the correlation between the light waves in two different points at two different times.
- *Radiance or brightness*: the amount of power emitted per unit area per unit solid angle by the laser beam.
- *Focal spot size* - the distance between the beam axis and a point at which the intensity drops to $1/e^2$ from its value at the center of the beam (as defined in [114]), on which the property called irradiance of the beam strictly depends.
- *Transverse modes*: specific spatial profiles apparent from the observation of a cross section of the laser beam and represented as electromagnetic modes. Fig. 2.4 graphically depicts the concept.

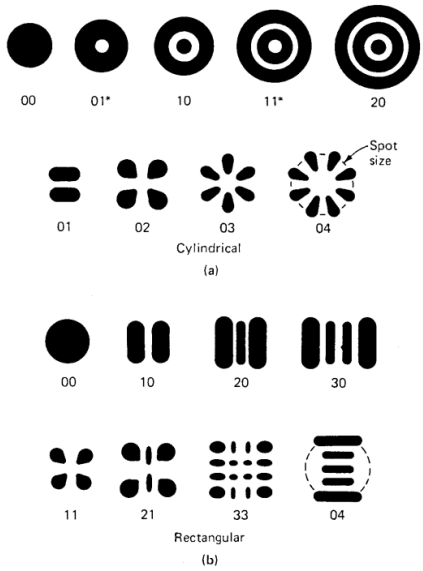

Fig. 2.4 Examples of cylindrical (panel a, where the two subscripts point out the number of dark rings and the number of dark bars across the pattern, respectively) and rectangular (panel b, where the two subscripts point out the number of dark bars in the x- and y-directions, respectively) transverse mode patterns [115]

The relation ratio between the beam diameter d_s and its value associated to the fundamental mode d_0 is expressed by a factor M, and the same relation is valid for the ratio between the multimode divergence ϕ_s and the fundamental mode parameter ϕ_0.

Since it is possible to reduce the divergence by means of a telescope, according to the brightness theorem reported in Eq. 2.1:

$$\phi_s d_s = M^2 \phi_0 d_0 \tag{2.1}$$

where M^2 is called beam quality factor. The beam quality factor characterizing a laser operating in the fundamental mode, whose intensity distribution is therefore described by a Gaussian profile, is M^2=1 and its typical beam-parameter product is expressed by Eq. 2.2

$$\phi_0 d_0 = \frac{4\lambda}{\pi} \tag{2.2}$$

where λ is the wavelength of the radiation

- *Temporal mode*: mode of operation of a laser beam with time: it can be pulsed mode or continuous; in the former in turn the pulsing can be performed mainly according to three different ways: normal pulsing, Q-switching, mode locking.
- *Frequency multiplication*: operation consisting in using frequency multiplier materials (e.g. potassium dihydrogen phosphate or lithium niobate), characterized by a non-linear behavior of the laser beam with respect to the electric field, in order to double or triple the frequency of the beam.

2.2 Classification of industrial lasers

Among the hundreds of materials which have been proven to have the capability to work as laser mediums, only a few have become important from the point of view related to the industrial applications. The several types of industrial lasers currently available can be grouped in the four families of solid-state lasers, gas lasers, semiconductor lasers and finally dye lasers. The table 2.1 listed the main examples of lasers for every group.

In solid-state lasers the population inversion involves impurity ions doped in a crystalline or glass material. The pumping is typically optical, by means of other laser sources or lamps. Two important laser types belong to this class, namely the ruby one, which is the first laser of history invented by Theodore Harold Maiman in 1960, and the Nd:YAG one, which gets its name by the nomenclature of the solid-state host (Yttrium Aluminum Garnet, $Y_3Al_5O_{12}$) and of the doping ions (neodymium, Nd^{3+}) and which is the most widely employed laser. The applications in which it is involved range from the welding of heavy metals, to surgery, to the

Table 2.1 Main typologies of industrial lasers with the typical wavelengths (data from [113])

Laser type	Wavelength [nm]
Solid-state lasers	
Nd:YAG	1064
Ruby	694
Nd:glass	1062
Alexandrite	700-820
Ti-sapphire	700-1100
Er:YAG	2940
Nd:YLF	1047
Gas lasers	
HeNe	632.8
Argon	488, 514.5
Krypton	520-676
HeCd	441.5, 325
CO_2	10600
ArF	191
KrF	249
XeCl	308
XeF	351
Copper vapor	510.6, 578.2
Gold vapor	628
Semiconductor lasers	
InGaAs	980
AlGaInP	630-680
InGaAsP	1150-1650
AlGaAs	780-880
Liquid dye lasers	
Rhodamine 6G	570-640
Coumarin 102	460-515
Stilbene	403-428

recording of spectroscopic measurements or to the acquisition of a topography profile [116]. It consists in a four level energy laser system (see Fig. 2.1b) in which it is rather simple to achieve the population inversion even with simple lamps and low pumping energy.

In gas lasers, an electrical discharge crosses a gas whose atoms, excited to higher energy levels, collimate with neutral atoms in the ground state. The resulting transfer of energy and electron transition in the neutral atoms is the main responsible phenomenon for the laser emission. One peculiar member of this group is the excimer laser. An excimer laser, where

"excimer" stands for "excited dimer", is based upon provoking an electrical discharge in a highly inert gas mixture and therefore generating a molecule with two atoms that can exist only in the excited state. The decay of the molecule to the instable ground state provokes the dissociation of this molecule into two unbound atoms, generating therefore a population inversion between the two states and provoking the stimulated emission of a photon.

The semiconductor lasers are usually called LEDs (acronym for Light Emitting Diodes) and exploit the lasing phenomenon which can occur in a semiconductor (used as laser medium) when the pumping current, electrically induced, oversteps a threshold and subsequently the population inversion becomes adequately high.

The dye lasers use liquid solutions composed by organic dyes in a solvent as laser medium. Due to the characteristics of the dyes, it is possible to make the laser work over a wide range of wavelengths (0.2-1.0 μm) [113].

A mention of the laser system used in this work is finally offered. The simplest version of a single-clad fiber laser consists in a doped core immersed in a cladding with a lower refractive index. The stimulated emission occurs in the core supporting a single propagation mode for a given wavelength [117]. The inconvenience of this system is the need for a pumping source providing a radiation with the same high beam quality of the laser output and therefore the need for expensive low-power pumping sources. A solution may be offered from the multi-mode fibers, characterized by a larger core diameter and generating a lower quality beam. The problem however can be circumvented by the implementation of the double-clad fiber laser, whose typical structure is shown in Fig. 2.5.

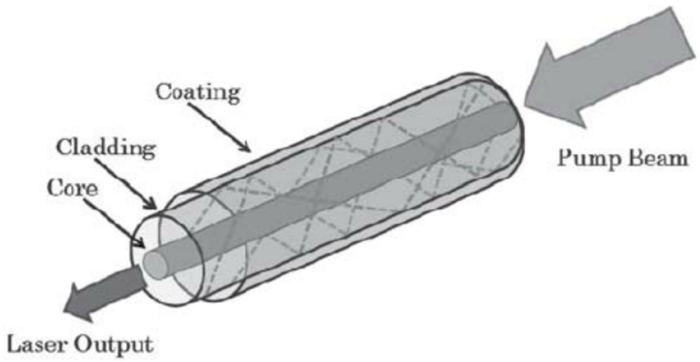

Fig. 2.5 Illustration of the structure of a double-clad fiber laser [118]

With refer to Fig. 2.5, the working principle of a double-clad fiber laser is based upon the fact that the materials constituting the core, the cladding and the coating are characterized by different values of the refractive index, which decreases moving from the first to the last. The core is doped with the aim of working as laser medium and providing for the stimulated emission of light, while the pump light propagates guided by the reflection occurring within

the inner cladding. The absorption of a progressively increasing amount of reflecting pumping energy leads to the amplification of the light signal confined into the core. The fact that this system supports the propagation of light at different wavelengths enables the adoption of high power diode lasers as pumping sources.

2.3 Laser processing of materials

The interaction between the laser beam and the materials can result in a series of numerous and different phenomena. Among these, the most relevant for the purpose of processing the impacted surface appears the absorption of the laser radiation by the material. In fact, this is the main mechanism which causes processes like heating, melting, vaporization or plasma formation [119]. The amount of effectiveness of the laser processing of materials is obviously strictly dependent from both the laser parameters and the properties of material. In particular, the main laser beam parameters on which it is possible to act to drive the process are the intensity, the wavelength, the coherence (both spatial and temporal), the angle of incidence on the surface, the polarization, the illumination time, while the material can influence the absorption by means of its absorptivity, thermal conductivity, specific heat, density, latent heat.

The Beer-Lambert law, reported in Eq. 2.3 [119], is used to express the relation between the intensity of the absorbed beam I and the depth z at which it is evaluated within the material

$$I(z) = I_0 e^{-\mu z} \tag{2.3}$$

where I_0 is the incident intensity and μ is the absorption coefficient.

The absorptivity of an opaque material at normal incident is defined as

$$A = \frac{4n}{(n+1)^2 + k^2} \tag{2.4}$$

where n is the refractive index and k is the extinction coefficient, which are strongly dependent from the wavelength of the radiation and from the temperature, which explains the influence exercised by these parameters over the absorption capability of the material [114]. The dependence of the reflectivity (and thus of the absorptivity) from the wavelength of several metal materials is shown in Fig. 2.6, from which the increase of the absorptivity when the wavelength radiation is short is apparent.

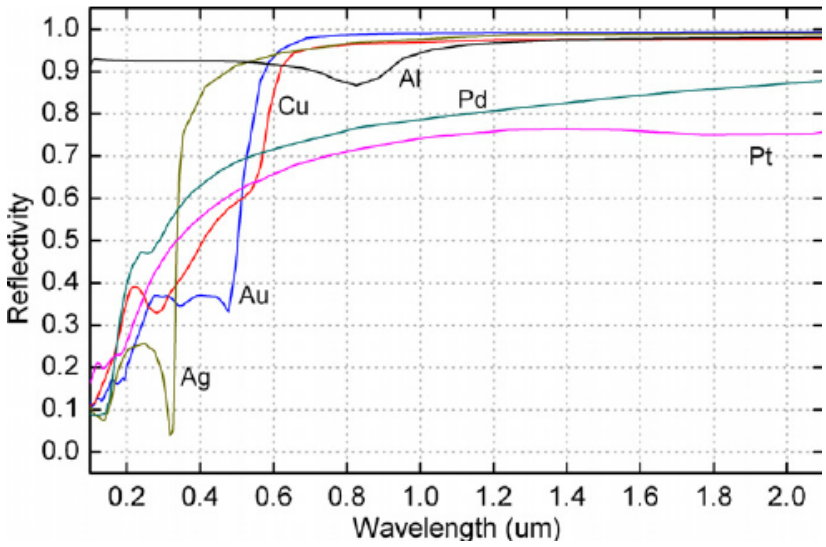

Fig. 2.6 Reflectivity vs wavelength in some common metallic materials [120]

With respect to the dependence from the temperature, the absorptivity rises when the temperature grows up, which is particularly noticeable since the laser processing of the materials has the effect to increase significantly the material temperature. In fact, the primary excitation energy of the radiation absorbed within the material degrades and is converted into heat, resulting in the typical aforementioned macroscopic effects associated to the laser processing of materials, presented in Fig. 2.7.

The arising of a specific effect rather than the others is depending from the combinations of laser intensity and time of interaction with the material. With refer to the general phenomenon of the heating of the material, Fig. 2.8 depicts how the temperature varies in function of the time and of the depth z (the example concerns the case of copper irradiated for 1 μs with a laser power density equal to 10^{10} W/m^2). The main trend which is worth noting by Fig. 2.8 is the one exhibited by the time at which the maximum temperature occurs in function of the depth: higher the depth, higher the range between the time corresponding to the maximum temperature and the time pulse, at which the maximum temperature on the surface (z=0) is achieved [121].

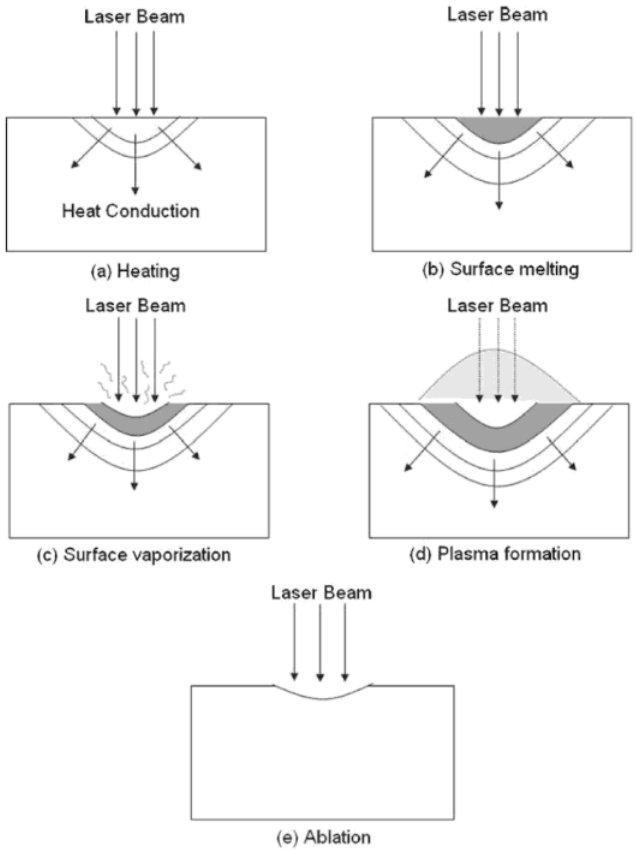

Fig. 2.7 Schematic representation of the main effects induced by the heat generation following the absorption of a laser radiation within the material [113]

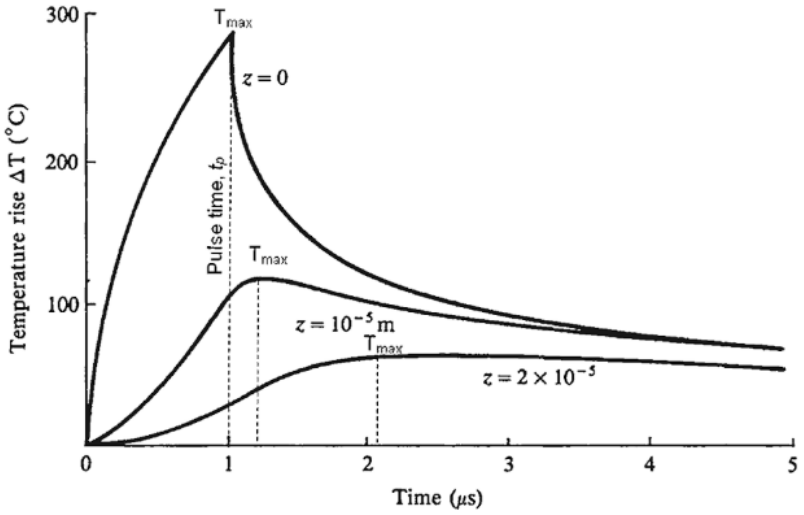

Fig. 2.8 Variation of temperature in function of time and depth in the case of copper irradiated for 1 μs with a laser power density equal to 10^{10} W/m^2 [121]

When the laser power density oversteps a value, approximately equal to 10^5 W/cm^2, besides the heating of the material even the melting point of the material can be reached by the temperature, which is why that intensity value is often called melting threshold. In [113] Fig. 2.9 is offered to analyze the temporal evolution of the depth of melting during laser irradiation of a surface.

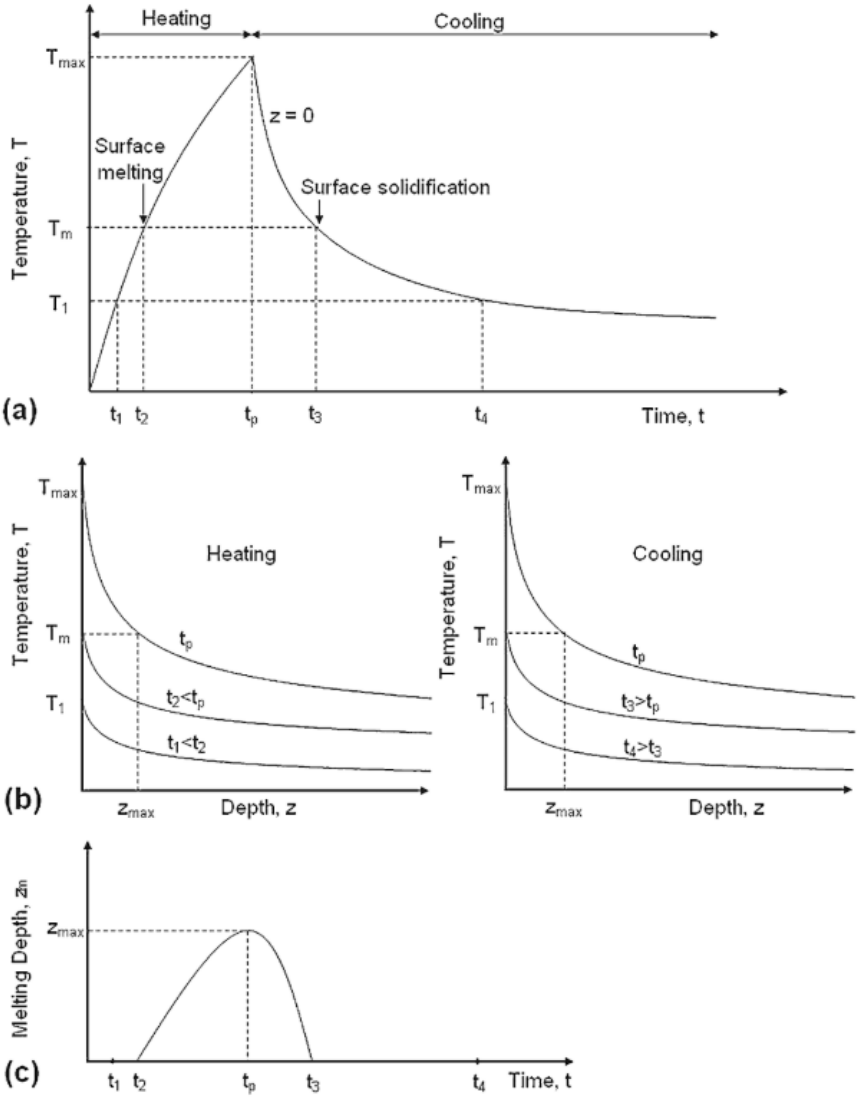

Fig. 2.9 Temporal evolution of depth of melting: (a) surface temperature vs time, (b) temperature vs depth below the surface during heating and cooling, (c) depth of melting vs time [113]

Keeping constant the value of time, the plot of the temperature in function of the depth below the surface during heating and cooling (Fig. 2.9, panel (b)) can provide information about the position of the solid-liquid interface: in the example, the maximum depth of it (z_{max})

is reached at the time t_p. Finally, plotting the identified positions of the liquid-solid interface in function of time, it is possible to evaluate the temporal range in which the absorption of a laser radiation provokes the melting of the material. In the example of Fig. 2.9, panel (c), before t_2 only the material without phase change is present, at t_2 the liquid-solid interface is on the surface, from t_2 to t_p the extension of the melting depth increases from the surface to z_{max}, from t_p to t_3 finally the cooling takes over, bringing back the liquid-solid interface position to the surface at time t_3. In Fig. 2.10 the increase of the depth of melting with the intensity and the pulse time, respectively and keeping one parameter fixed while varying the other, is shown.

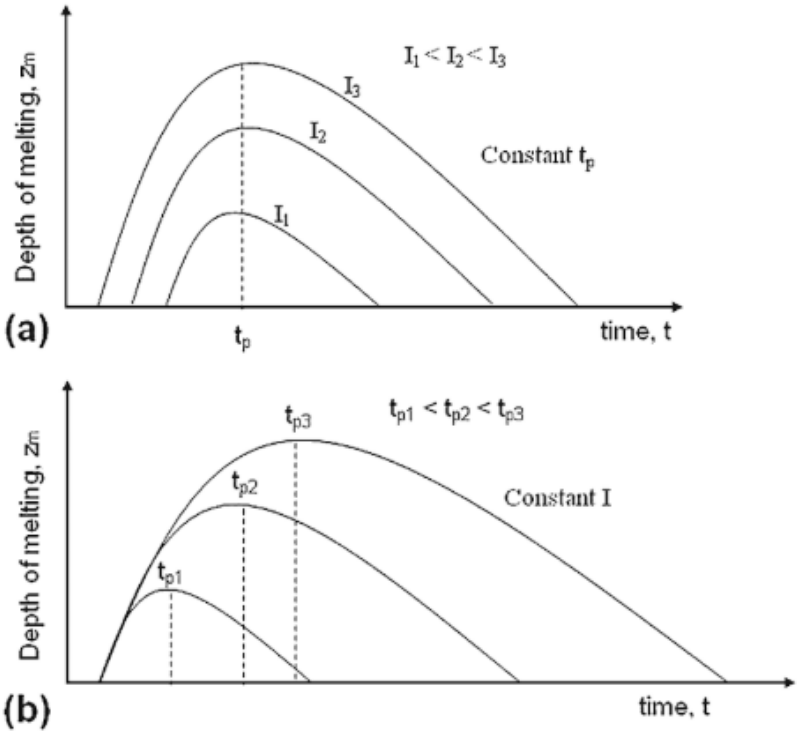

Fig. 2.10 Trend of depth of melting in function of the laser intensity at constant pulse time (a) and in function of the pulse time keeping the laser intensity fixed (b) [113]

When the surface temperature overcomes the boiling point of the material, the initiation of the surface evaporation takes place. Once the depth of melting reaches z_{max} and the surface evaporation initiates, further increases of laser intensity or pulse time do not result in a further shift of the liquid-solid interface position but only in a removal of a certain amount of material from the surface by evaporation.

After the initiation of the surface evaporation, the subsequent interaction between evaporated material and the laser beam results in the important phenomenon of the ionization of

vapor. The alternative mechanisms of formation of this ionized vapor (usually called plasma) are essentially the cascade ionization and the multiphoton absorption. Given the laser power density I_p at which the ionization occurs, when the laser intensity is just above I_p the plasma forms near the surface and remained there confined, phenomenon usually referred to as plasma coupling. This one can significantly improve the absorptivity of laser radiation by the material when its reflection is high and in presence of long wavelength laser radiation. When the laser intensity becomes considerably higher than I_p, the expansion of plasma moves it away from the surface, interrupting the energy transfer and making the laser radiation being absorbed in the plasma instead in the dense material. This behavior is called plasma shielding [122].

Finally, the ablation process can be caused by a photo-termal or photo-chemical interaction between laser radiation and material and results in the formation of visible craters and grooves over the surface. When the former mechanism takes place, the process is called thermal ablation and consists in the removal of the surface material by means of the onset of thermal stresses or vaporization induced by the increase of the temperature [122]. The photo-chemical induced ablation, referred to as photoablation, mainly involves the organic materials and arises when the energy of the photon is responsible for the breaking of the bond in the molecular chains, resulting in the molecular fragmentation of the material [113]. Often, the actual mechanism leading to the ablation of the absorbing material results from the simultaneous effect of thermal ablation and photoablation. To encourage the occurrence of this last kind of ablation, which minimizes the thermal damage, the energy of the photon should be greater than the one of the bond (even if for ultraviolet radiation with longer wavelengths this problem is surpassed by means of multiphoton mechanism) and the pulse time should be shorter than the thermal relaxation time, defined in Eq. 2.5

$$\tau = \frac{d^2}{4\alpha} \tag{2.5}$$

where d is the absorption depth and α is the thermal diffusivity of the material. Therefore, the most effective laser ablation processes are the ones in which the laser radiation is characterized by short wavelengths and works with micro-second pulses mode. As in the cases of melting and vaporization, even in the case of ablation the word "threshold" is employed to point out the ablation level defined as the minimum energy required for the ablation to take place: if the absorbed energy is below the ablation threshold energy only the heating effects are present, while when the threshold is overcome the ablation is promoted by the bond breaking. When this last circumstance happens, the depth of ablation has been predicted to increase with the energy of the laser beam, even if it can be affected by other phenomena like the possibility of the existence of a plasma shielding effect or the variation

of the material absorption coefficient induced by the radiation, as reported in [123]. Moving to consider which are the main parameters influencing the ablation rate, an increase of the ablation rate, beyond the ablation energy threshold, occurs in agreement with the trend of the laser fluence F, which is defined in Eq. 2.6 as the optical energy provided per unit area

$$F = \frac{P_m}{f_r A_0} \tag{2.6}$$

where P_m is the laser nominal average power, f_r is the pulse repetition rate and A_0 is the area of a cross section of an ideal Gaussian beam. The energy provided with a single pulse is represented by the hatched area in Fig. 2.11 showing the evolution of the laser power with time during a multipulse irradiation working mode and it is provided by Eq. 2.7

$$\frac{P_m}{f_r} = \int_0^{t_p} P dt \tag{2.7}$$

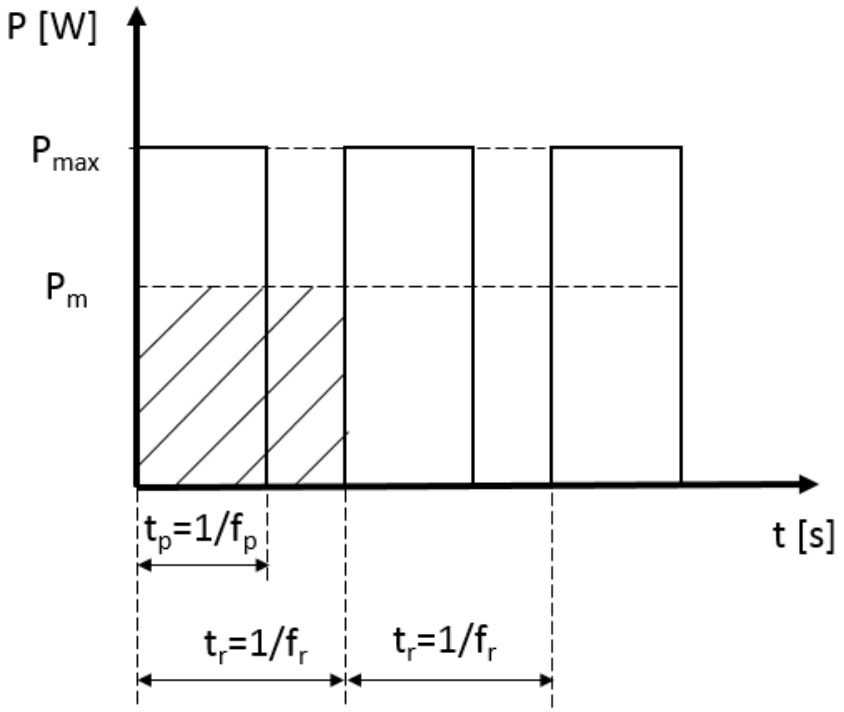

Fig. 2.11 Temporal evolution of laser power during a multipulse irradiation working mode

An experimental evidence of the existence of a threshold value for the fluence under which no ablation apparently takes place has been found [124]. In this regard, as it is

described in [125], the variation of ablation rate a_r with the fluence F when this last one overcomes the fluence threshold F_{th} is expressed by the Beer law, reported in Eq. 2.8

$$a_r = \frac{1}{\mu} ln\left(\frac{F}{F_{th}}\right) \tag{2.8}$$

Moreover, keeping the fluence fixed, an increase of the ablation rate with the pulse repetition frequency f_p was experimentally recorded [124].

Many works in literature dealt with the characterization of the effect of laser ablation over the surfaces. Some examples are provided in the following lines.

Since in a work by Preuss *et al* [126] the metal ablation in air was found to be significantly less effective than in the vacuum because of the shielding effect and the re-deposition of the ablated material, Umm-i-Kalssom *et al* [127] investigated the effect of the laser fluence and of the environmental conditions over the micro- and nano-structuring of stainless steel after a pre-treatment with an excimer laser. The main result of their analysis was the observation of laser-induced periodic structures over the surface (LIPSS, in this case called ripples) due to both the re-deposition of the ablated material and the Kelvin-Helmholtz instability, which are more pronounced when the ablation is carried out in the vacuum rather than in oxygen (probably because of the shielding effect offered by the gas).

Byskov-Nielsen and Balling [128] analyzed the variations of surface morphology induced by a nanosecond laser ablation over six different types of steel. They observed how the ablated material re-deposits over the surface blocking the drilled hole, which could be exploited, for instance, to trigger a micro-mechanical interlocking effect for adhesively bonding purposes. Keeping the average power of the laser fixed and reducing the pulse energy, which means to increase the pulse repetition frequency and therefore the number of pulses per unit of time, the phenomenon is amplified, resulting that an efficient micro-mechanical interlocking can be achieved using a pulse repetion frequency below a specific threshold. Another way to elude the blocking of the holes consists in allowing the cooling of the material between subsequent laser pulses by moving the laser ablation over another hole and periodically returning to each hole to shoot a pulse rather than performing all the pulses in a single run.

2.4 Laser based surface pre-treatments for bonding

The industrial applications of the laser technology are numerous, especially for manufacturing processes like drilling, cutting, machining or welding. With respect to the fundamental problem of joining, in the last decades the laser has carved out a role more and more relevant with respect to the possibility to be employed as a pre-treatment of surfaces for adhesively

bonding purposes instead of some traditional chemical and mechanical processes. This results from the several benefits achievable by using the laser ablation in that way: the cleaning of the surface from the natural oxides and weak boundary layers, the improvement of the surface free energy and thus of the wettability, the capability to drive the surface morphology in such a way to increase the surface roughness, and therefore the available load bearing area, of the desired quantity.

A brief overview of the main findings with respect to both the modifications of the surface morphology and the effects over the mechanical properties of the bonded joints realized with various materials is proposed, in order to testify the wide effectiveness of the process. Finally a focus over the aluminium joints will be proposed.

Benard *et al* [129] studied the effectiveness of using an excimer laser to pre-treat glass/epoxy and carbon/epoxy composites in order to selectively remove the organic matrix without degrading the fibrous reinforcements, with the aim of improving the adhesion quality of these materials by bonding them directly on the fibers rather than on the polymeric matrix. The surface roughness was assessed by means of the parameter S_a instead of the classic R_a according to ISO 25178-2 [130], which is a strategy adopted also for the present work. They found that, to effectively perform the treatment and at the same time to prevent the damage incurring over the fibrous phase, the working fluence of the laser radiation has to be set between the ablation threshold of the polymeric matrix material and the ablation threshold of the fibres. An ESCA (Electron Spectroscopy for Chemical Analysis) investigation revealed also that no chemical modification is induced over the surface, but the treatment carries out a surface cleaning which is responsible for the strong improvement of the wettability measured with sessile drop tests even after a single pulse.

The excimer laser is the topic even of the aforementioned work of Laurens *et al* [125], where its effect over the adhesion properties of PEEK (polyether-etherketone) was assessed, by varying the fluence, the number of pulses and the gas in which the tested material specimens are immersed. SEM analysis revealed that when the fluence is risen above a small value (definitely lower than the ablation threshold) some spherolite formations previously observed over the surface disappear which means that the surface amorphization due to the thermal effects occurs. When the fluence, indeed, overcomes the threshold value, the formation of the typical conical structures associated to the ablation phenomenon leads to a strong increase of the surface roughness. The progressive modifications of the surface as the fluence increases resulting from SEM observations are offered in Fig. 2.12.

With refer to the mechanical effect provided by the laser treatment, it was evaluated by means of DCB tests over specimens realized as in Fig. 2.13 and an increase of the fracture energy in the ablated joints was recorded with respect to the untreated ones, while the fracture

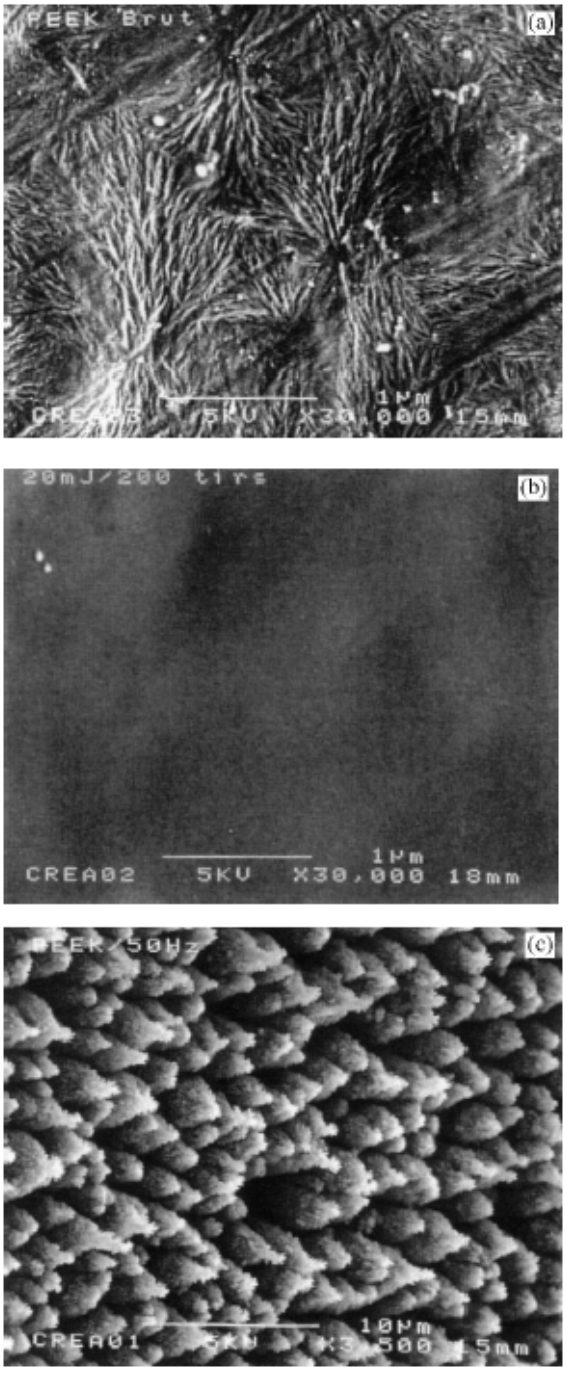

Fig. 2.12 SEM images of the PEEK surface: (a) untreated surface (b) after treatment performed below the ablation threshold, (c) after treatment in the ablation regime [125]

mode tends to move from adhesive to cohesive (within either the adhesive or the PEEK film shown in Fig. 2.13).

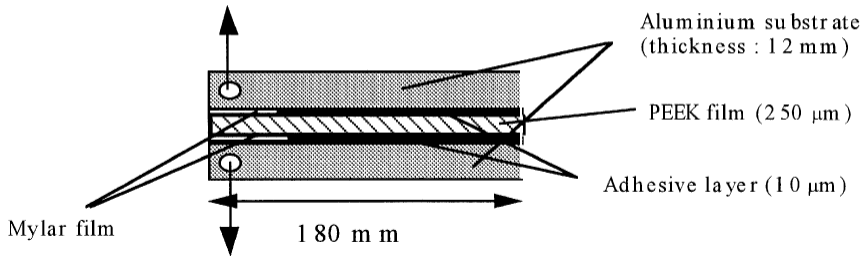

Fig. 2.13 Schematic representation of the DCB geometry and configuration employed in [125]

The increase of the joint strength was found to be uncorrelated with the increase of the surface free energy, because the treated surface with the lowest value of the work of adhesion was also the one presenting the highest fracture energy. The reasons for the toughening of the joints were therefore searched in what happens during the surface amorphization, in particular the role of the polar groups created on the surface, whose increase in concentration by oxidizing treatments promotes the wettability but probably induces a degradation of the mechanical performance of the oxidized surface, was taken into account.

The work of Baburaj *et al* [111] dealing with the improvement brought to the strength of titanium bonded joints by the development of Micro-Column Arrays (MCA) over the surface by means of laser pre-treatment is briefly discussed. In particular, the benefits of the MCA generation are the increase of the interlocking effect which induces an increase of the mechanical strength, the increase of the load bearing area by a factor significantly higher than the one achievable with traditional processing, the increase of the stability of the joint due to the capability of the MCA structures to deform under the stress due to the different thermal expansion coefficients between substrates and adhesive, the changes in the chemical state of the surface able to induce an improvement to the wettability properties. To study these effects, the authors carried out in open air (due to make the process easy to be replicated in an industrial application) the laser ablation, while the adhesive was deposed under vacuum for circumventing the troubles possibly arising from the presence of air bubbles within the adhesive or between adhesive and substrates. From SEM observations, the presence of porous structures caused by the vaporization, subsequent re-deposition, solidification and finally oxidation of the irradiated material was recognized. The wettability of the titanium surface was proved to increase because of both physical (like the large cavities generated between the micro-columns or the small porous and oxidized structures generated over the micro-columns) and chemical alterations (like the oxidation of the surface). Single-lap joints

realized using both thin and thick epoxy adhesive layers, respectively, were tested. When the adhesive layer is thin, an increase of the fracture strength of the MCA-structured joints higher by more than four times with respect to the untreated case was recorded and it apparently seems to increase with the thickness of the bondline. With regard to this last one trend, the opposite occurs in the thick adhesive layer joints.

Fischer *et al* [131] studied the employment of Carbon Fiber-Reinforced Plastics (CFRP) along with adhesively bonding technology for lightweight construction and addressed the two main problems of these applications: the need for an effective removal of surface contaminants without damaging the fibers and the will of having the fibers exposed to allow the direct introduction of the load into them rather than transfer it through the surface, which can be affected by the presence of weak boundary layers. They found, among the others, that, even if the use of an excimer laser ablation to circumvent them can improve the strength to the desired value, the employment of unsuitable laser parameters can heighten the risk of a failure occurring in the adhesive mode or of delamination.

In the work of Molitor and Young [132] alternative effective techniques to perform the adhesive bonding of Glass Fiber-Reinforced Plastics (GFRP) and titanium alloy were assessed. Among the tested pre-treatement methods, even the excimer laser was used both to modify and to only clean the surface. According to the average peel strength, the pre-treatments involving the use of laser ablation are better than the anodisation with sodium hydroxide. Nevertheless, the durability exhibited by some single lap joints undergoing surface cleaning by excimer laser when tested after being immersed in hot water at 70°C for 30 days is very low.

The work of Demir *et al* [133] offered some examples of Q-switched fibre laser texturing for several applications, including the adhesion. This one was investigated by texturing three different structures (grid, chaotic and dimpling) over the surface of Ti6Al4V alloy sheets, as it is visible in Fig. 2.14.

The grid texture was conceived with the aim to improve the contact area between adhesive and substrate and to develop an interlocking effect between the two phases. It is worth noting that due to the width of the channels, increased so to enlarge the section of the adhesive which has to withstand the load, a stress concentration might be induced where the adhesive failure occurs. The chaotic texture was generated by the re-melting of the metallic material. The same characteristics of the previous described texture have been detected. Finally, the dimpling texture presents the main disadvantages of the capillarity of the microholes, which can inhibit the flow of the adhesive, and the absence of undercuts, which means that no constraint is opposed to the displacement of the adhesive in a direction parallel to the surface normal.

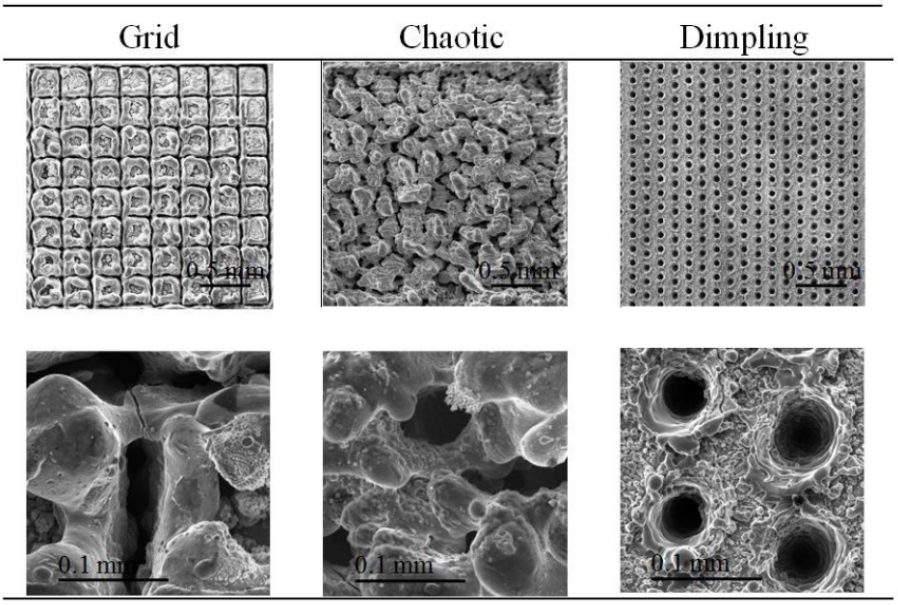

Fig. 2.14 Laser induced texture patterns to improve the adhesion of Ti6Al4V [133]

Moving to consider the applications of the laser technology to the improvement of the adhesion properties of aluminium substrates, the works dealing with this topic are numerous.

Wong *et al* [134] started from the work of Matsunawa [135] about the cracking of the melt pools produced by the laser ablation of a metallic substrate and resulting from their fast cooling. This phenomenon and the presence of concentric rings within the melt pools appear to be among the most critical factors affecting, for instance, the fatigue strength of the joints produced after the surface treatment. These two peculiar characteristics were then studied by means of Nd:YAG laser texturing of 6016 aluminium alloy and 1100 series (containing 99% pure) aluminium substrates. The concentric rings were found to be caused by the wave motion of the melted material and an increase of the probability to generate this kind of motion before the re-solidification as the laser intensity grows up was assumed. With respect to the cracking of the melt pools, it was ascribed to a dual motivation: the first responsible for it in 6016 alloy is the dissolution of the Mg_2Si precipitates, which has a bad influence over the strength and the hardness of the melt pool, and secondly the overcome of the deformation capability of the material by the shrinkage extension during the solidification, along with a high cooling rate, induces the generation of thermal stresses (which is why this kind of cracking is also known as "hot cracking") which finally encourages the cracking sensitivity, as stated also in [136]. The tests over the 1100 aluminium found that none of the melt pools contain cracks, which testifies the influence over the hot cracking by the dissolution

of alloying elements. In Fig. 2.15 a view of the concentric rings within a melt pool in 1100 aluminium alloy is offered.

Fig. 2.15 Magnified view of concentric rings within a melt pool in 1100 aluminium alloy [134]

The work of Alfano *et al* [137] is very interesting for the purposes of the present work, since they focused over the effect of the laser irradiation on the damage sensitivity of aluminium/epoxy joints, taking into account the combination of the same laser type (Yb fiber laser operating in a pulsed mode) and the same substrate material (AA6082-T6) to the one employed in this work. They carried out a selection of the most suitable combination of laser process parameters based upon SEM observations of the induced surface morphology and the measurement of the contact angle by means of sessile drop tests to evaluate the wettability. The process parameters tested are summarized in Tab. 2.2.

A comparison between SEM images of the laser treated surfaces, shown in Fig. 2.16 with the untreated and the grit blasted surfaces, proofs that, by keeping the line spacing constant at 150 μm and the scan speed at 1000 mm/s, an increase of the average power from 40 (panel c) to 100 W (panel f) induces a strong modification of the surface morphology. Instead, an increase of the line spacing value from 50 (panel d) to 150 μm (panel e), being fixed all the other process parameters, results in the fact that both the laser scans and the asperities and the oxide particles (due to the condensation of the vaporized gas during the solidification) become recognizable, while finally a variation in the scan speed from 500 (panel e) to 1000

Table 2.2 Laser process parameters employed for the irradiation of AA6082-T6 aluminium alloy in [137]

Process parameter	Value
Laser radiation wavelength	1064 nm
Pulse repetition frequency	100 kHz
Pulse width	150 ns
Pulse energy	1 mJ
Average power (P)	40/100W
Scan speed (v)	500/750/1000 mm/s
Programmed line spacing (LS)	50/100/150 μm

mm/s (panel f) while the line spacing is set to 150 μm produces a lowering of the depth of the grooves.

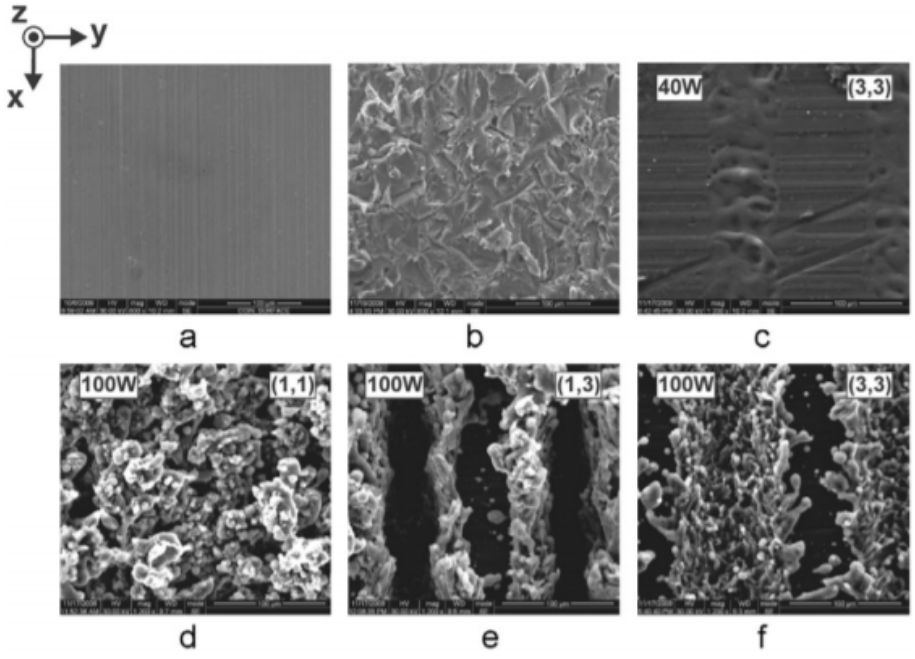

Fig. 2.16 SEM observations of AA6082-T6 surfaces: (a) untreated; (b) grit blasted; (c) laser treated with P=40 W, LS=150 μm, v=1000 mm/s; (d) laser treated with P=100 W, LS=50 μm, v=500 mm/s; (e) laser treated with P=100 W, LS=150 μm, v=500 mm/s; (f) laser treated with P=100 W, LS=150 μm, v=1000 mm/s. The laser beam is moved in the x-direction [137]

The results of the sessile drop tests conduced over the laser treated surfaces in function of the different process parameters are summarized in Fig. 2.17, where panel (a) is referred to the contact angle in the side (S) direction while panel (b) reports the values measured in the front (F) direction (the distinction was applied because of the elongation which the liquid drop can undergo in the direction of the laser scan, phenomenon known as anisotropic wetting).

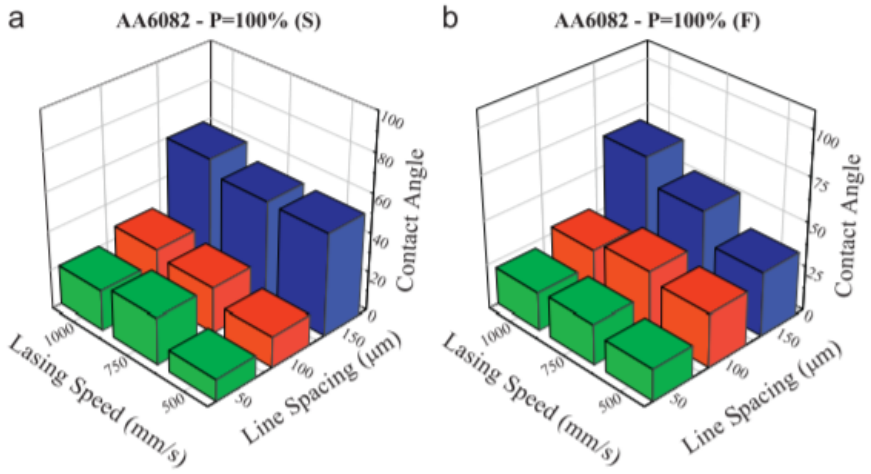

Fig. 2.17 Variation of contact angle in function of the laser process parameters evaluated with sessile drop tests performed with glycerol liquid over AA6082-T6 surfaces. The measurements were taken along both the side (a) and the front (b) direction [137]

Considering that the measured contact angle for an untreated surface was found equal to 83°, the trend of the contact angle of the laser treated surfaces seems quite consistent with the Wenzel's model, recording a general decrease, less marked in the case of the highest line spacing value where a mixed state wetting regime (between the Wenzel and the Cassie-Baxter one) is probably acting.

Finally, T-peel joints were produced with a process parameters configuration consisting in P=100 W, LS=50 μm and v=750 mm/s and tested, along with some grit blasted samples. The results testified a sensible increase of the maximum load and elongation at failure in the laser treated specimens with respect to the grit blasted ones, while subsequent SEM observations of the fracture surfaces revealed how the locus of failure switched from the interface (in the grit blasted case) to the adhesive (in the laser treated joints).

Another work by Alfano *et al* [138] was dedicated to a study upon two families of substrates realized in AISI 304 stainless steel and in a very similar material (AA6082-T4 aluminium) to the one used in this work, respectively, and using the same laser apparatus employed in the analysis explained in the following chapters. With refer to the results

concerning the aluminium surfaces, some XPS measurements were performed and the results of the as-produced and some laser treated samples are given in Tab. 2.3 and in Fig. 2.18.

Table 2.3 Elemental composition of as produced and laser treated AA6082-T4 aluminium substrates obtained by XPS measurements [138]

Substrate	Al [%]	O [%]	C [%]	W [%]	F [%]
As produced	29.2	17.5	49.6	1.5	2.2
Laser ablated (P=8 W)	29.7	19.3	47.6	1.3	2.1
Laser ablated (P=18 W)	39.8	12.4	47.8	ND	ND

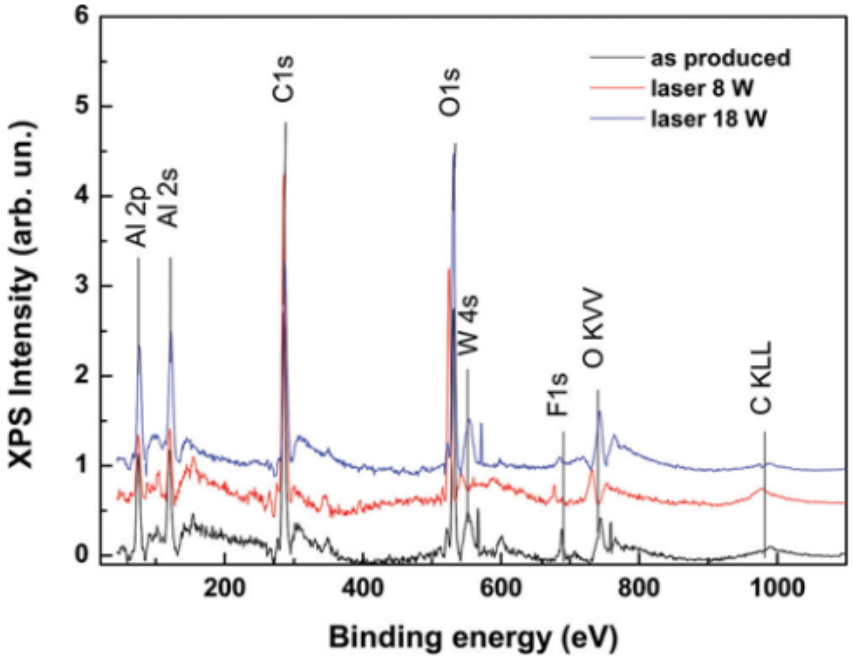

Fig. 2.18 XPS results from as produced and laser treated AA6082-T4 aluminium surfaces [138]

Firstly, a certain level of contamination is appreciable over the laser ablated samples due to the surface carbonization which is the main responsible for the formation of a thin CO_2 layer. The surface composition is slightly modified by the ablation carried out at a power level equal to 8 W. A threshold equal to 12 W was identified, based on an increasing drop of the average surface roughness recorded on a surface ablated with that laser power by means of stylus profilometry conduced over surfaces treated at various level of power. When that threshold is overstepped, a strong increase in the aluminium atomic content is accompanied

by a decrease of the oxygen atomic percentage. A shift in the Al 2p line peak detected from 75.6 eV to 76.6 eV in correspondence of laser powers higher than 12 W made the authors conclude that the original Al_2O_3 layer is replaced by an AlO oxide layer for high laser power treatments.

Consistently with these results, contact angle measurements performed with the sessile drop test using water did not find any significant difference between the as produced and the laser treated surface with a level of power lower than the threshold. When this last one is exceeded, a dramatic increase of the contact angle was recorded and a behavior according to the Wenzel's model was detected: the surface, which even in the initial as-produced state is hydrophobic, becomes more hydrophobic with the increase of surface roughness. The trend of the contact angle with the laser power is offered in Fig. 2.19.

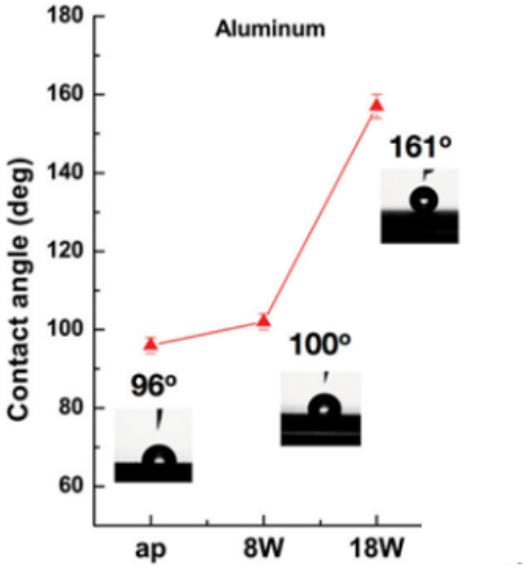

Fig. 2.19 Trend of static water contact angle on the as produced and some laser treated AA6082-T4 aluminium surfaces [138]

Some SLJ realized bonding together two laser ablated AA6082-T4 aluminium substrates (pre-treated with the following parameters: power P=18 W, line spacing LS=60 μm and scan speed v=5 mm/s) with Loctite Hysol 6466 epoxy adhesive and compared with some reference specimens (simply degreased and grit-blasted) revealed an increase of the average shear stress of about 100% in the laser ablated joints with respect to the simply degreased ones, probably because of the improvement of the adhesion due to the modified surface oxide layer. On the other hand, the fact that the oxide particles are weakly bonded to to the substrates and it is possible to make them be detached during the loading can justify the

lowering of the average shear stress with respect to the grit blasted specimens. These results are plotted in Fig. 2.20.

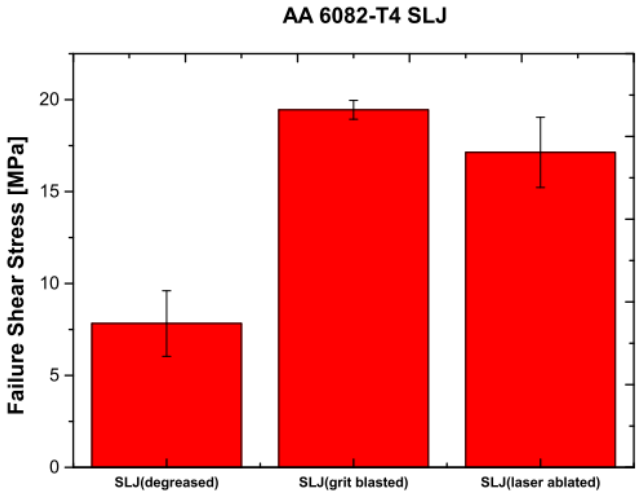

Fig. 2.20 Failure shear stress for AA6082-T4 aluminium/epoxy SLJ, compared with the simply degreased and the grit blasted specimens [138]

In order to segregate the effects due to the adherents plasticity over the increase of the peeling strains from the shear stress evaluation, in another work [139] Chiodo *et al* carried out a series of experimental tests over TAST joints realized with the same aluminium and adhesive and comparing the same types of surface treatments. The results are provided in Fig. 2.21. In this set, the increase of shear strength of the laser ablated joints with respect to the simply degreased samples is in the order of 20%.

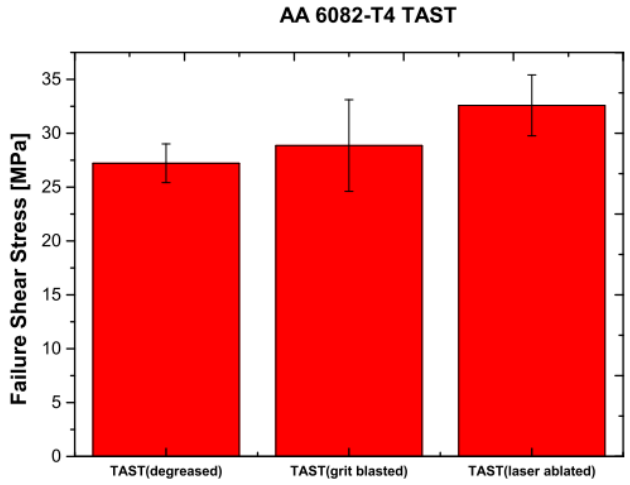

Fig. 2.21 Failure shear stress for AA6082-T4 aluminium/epoxy TAST joints, compared with the simply degreased and the grit blasted specimens [139]

Futher SEM investigations over the fracture surfaces focusing over an area in which the failure path switched from one interface to other, showed in Fig. 2.22(a), revealed that in the transition region where the failure occurred in a cohesive mode, apparent in Fig. 2.22(b), the concurrent presence of inelastic shear deformations of the adhesive was recorded. These deformations are highlighted in Fig. 2.22(c) and are substantially to be ascribed to the interlocking mechanical effect, much evident in Fig. 2.22(d), which was not detected during the SLJ tests reported in [138].

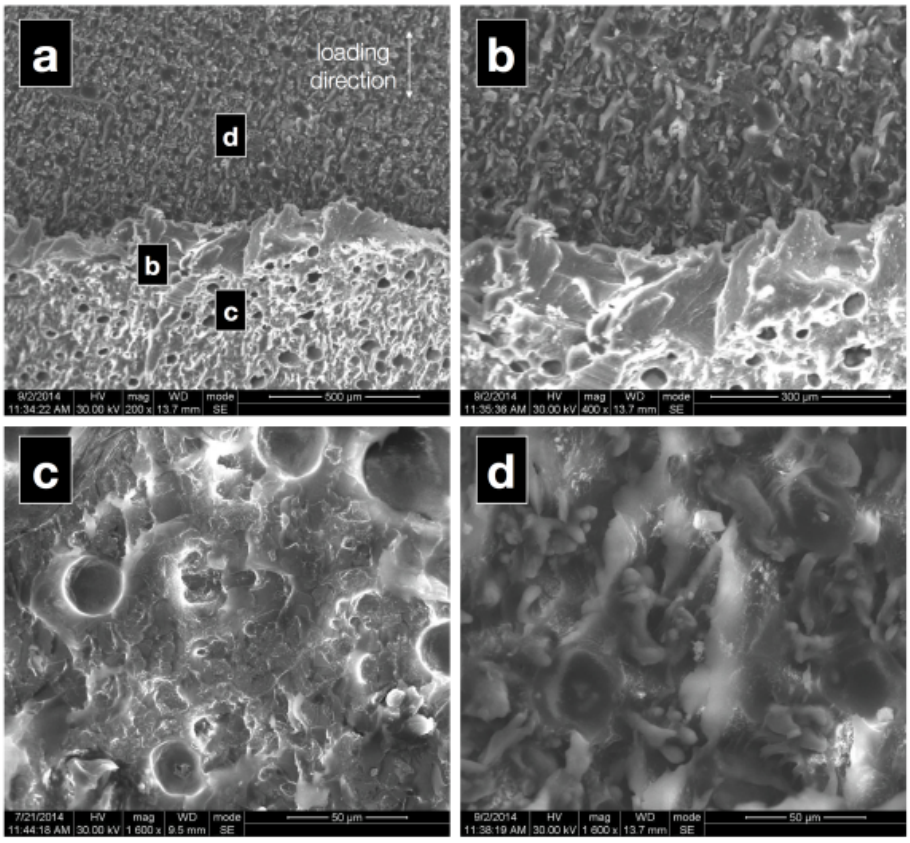

Fig. 2.22 SEM images of fracture surfaces of TAST joints: (a) overview of the fracture surface in the transition region where the failure path drifts from an interface to the other; (b) close-up image of the transition region where the adhesive fails in a cohesive mode; (c) adhesive side of failure revealing the presence of inelastic shear deformations and air voids; (d) failure surface where the occurrence of the interlocking effect is quite apparent [139]

In the same work, Chiodo tested some DCB configurations, whose critical mode I strain energy release rate results are reported in Fig. 2.23.

Even in this case, the typical whitening associated to the inelastic deformations of the adhesive was identified in the laser ablated joints, which exhibited an increase of the fracture toughness by a factor of almost 3 with respect to the simply degreased specimens.

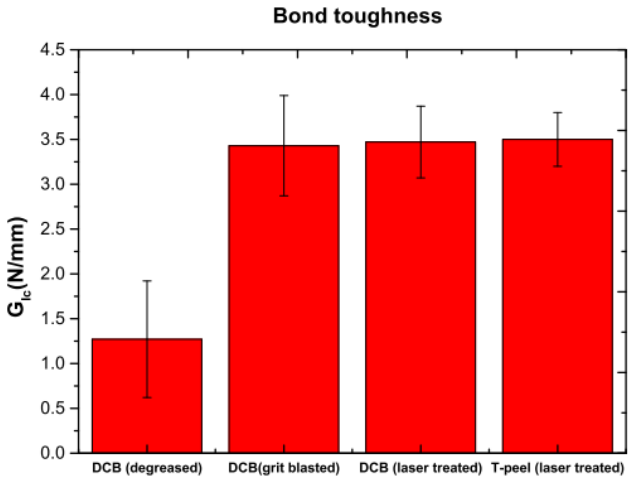

Fig. 2.23 Fracture toughness for AA6082-T4 aluminium/epoxy DCB joints, compared with the simply degreased and with some T-peel results [139]. The T-peel data were taken from [140]

Consistently, the locus of failure switched from the interface, in the degreased joints, to the adhesive, in the laser ablated and the grit blasted joints, which presented analogue values of G_{Ic}.

Rechner *et al* [141] started considering the beneficent influence exercised over the aluminium adhesively bonded joints strength by the oxide layer, which due to its porosity allows the adhesive to flow within it, as already noticed by Rider [142]. They investigated the modifications induced by the laser pre-treatment over the oxide layer generating in $AlMg_3$ and the interaction between its properties and the changing of laser fluence. A comparison between EDX spectra measurements performed over PAA and laser treated surfaces, respectively, showed that over anodized surfaces a thicker oxide layer is generated with respect to the laser treated surfaces, where however the oxygen content progressively increases with the laser fluence. This behaviour was supposed to be correlated to the high sensitivity of the aluminium oxide layer growth rate to the increase of temperature.

Mandolfino *et al* [143] developed a Design Of Experiments (DOE) to investigate which are the process parameters which affect more the efficiency of aluminium adhesively bonded joints pre-treated with either plasma or laser cleaning. The laser equipment employed was a Q-switched pulsed Yb-fiber laser, while the material used to produce the substrates was AA6061-T6 aluminium alloy. A 2^2 full factorial design was implemented, using the pulse power and the grid dimension (namely, the nominal distance between the centres of adjacent laser induced dimples) as control factors. The laser ablation configurations resulting from the mutual combinations of values of the two chosen control factors are showed in Tab. 2.4.

Table 2.4 Experimental design matrix for laser treatment [143]

Std. order	Pulse peak power [kW]	Grid dimension [μm]
1	5	50
2	15	50
3	5	100
4	15	100
5	10	75

The Single Lap Joint geometry was chosen to assess the mechanical response, bonding the aluminium substrates with a two-component epoxy adhesive. The results of the mechanical tests performed over laser ablated, plasma treated and reference specimens (untreated and degreased with acetone) in terms of shear stress, represented in Tab. 2.5, clearly pointed out that the laser treatment provided the highest values of ultimate shear stress, both when evaluating the maximum and the minimum and finally the average value.

Table 2.5 Ultimate shear stress values measured after pre-treated the bonding surface with several methods [143]

Value	Untreated	Cleaned (acetone)	Plasma (Ar)	Plasma (O_2)	Laser
Max	6.45	9.63	17.91	19.18	24.36
Min	5.12	7.38	10.51	10.39	12.28
Average	5.77	8.42	14.39	15.13	19.35
St. Dev.	0.55	1.02	2.14	2.57	2.95

Consistently with the shear stress values, the observation of the fracture surfaces allowed to verify that, except in the case of the untreated specimens in which the crack propagated at the adhesive-substrate interface, all the employed treatments produced a cohesive failure. A deeper investigation, by means of the ANOVA method, on the statistical significance of the main effects and the two-factor interactions for the ultimate shear stress clarified that, as expected, the value of τ_{max} increases when the pulse power increases and the grid dimension decreases. The detrimental effect of the increase of the grid dimension and therefore of the untreated area was reduced when the pulse power is such to produce a large dimple, as it happened in the case of the fifth configuration listed in Tab. 2.4 (pulse power=10 kW and grid dimension=75 μm) which was able to induce an higher value of shear strength than the

ones reached by the specimens treated with the "corner" configurations, namely the ones obtained by combining the extreme values of the explored ranges of the tested parameters. This remark justified the fact that the ANOVA test highlighted also the interaction between the two control factors as statistically significant.

Buchman *et al* [144] dedicated their efforts to a detailed analysis about the effect of Nd:YAG laser treatment over the strength of several types of adhesively bonded joints. The methods employed included SEM observations, XPS analysis, contact angle measurements, FTIR/ATR scans, mechanical tests on single lap and butt joints to measure, respectively, the shear and the tensile strength. Among the numerous substrate materials tested, the focus is here placed over the results concerning 2024-T3 aluminium. First of all, the laser treatment was proven to effectively clean the surface from weak oxides and corrosion products (see Fig. 2.24) and to induce the formation of small globules within the grooves, which can behave as anchoring points to the adhesive. Moreover, the XPS analysis revealed that the Nd:YAG laser treatment chemically activates the surface, promoting the formation of new oxidized elements (Al_2O_3, MgO, ZnO), as it resulted from the XPS analysis which documented an increase of the oxygen content from 13.5% to more than 32% by means of the laser treatment.

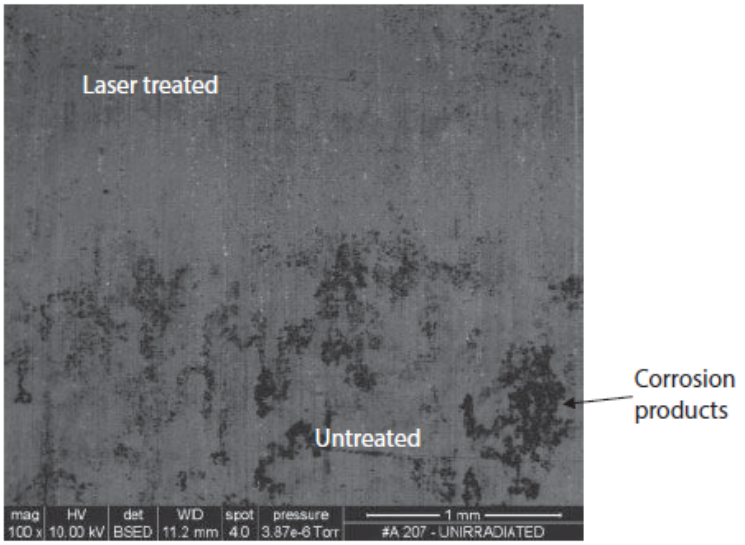

Fig. 2.24 SEM image comparing untreated and Nd:YAG laser treated Al surface [144]

Sessile drop tests showed that, unexpectedly, an increase of the contact angle was induced by the laser pre-treament, probably because of the different concentrations and combinations of oxides. Nevertheless, as the data presented in Tables 2.6 and 2.7 comparing the laser treated results with the ones obtained by untreated and chromic acid anodized specimens testify, the shear and tensile strengths of laser ablated aluminium/epoxy joints are enhanced,

consistently with the switch of the locus of failure from the interface to the adhesive (apparent in Fig. 2.25 for the SLJ), with respect to the untreated or the abraded joint, respectively.

Table 2.6 Shear strength of aluminium SLJ bonded with the epoxy adhesive SW9323-2. The laser parameters employed were: wavelength=1046 nm, scan speed=1.1 mm/s, intensity=950 mJ/cm^2, energy=360 mJ/pulse. [144]

Surface treatment	Shear strength [kg/cm^2]	Failure mode
No treatment	140±10	Interfacial
Anodized	252±11	Cohesive
Laser treated (line spacing=2 mm)	276±6	Cohesive
Laser treated (line spacing=4 mm)	284±1	Cohesive

Table 2.7 Tensile strength of aluminium butt joints bonded with the epoxy adhesive SW9323-2. The laser parameters employed were: wavelength=1064 nm, scan speed=1.1 mm/s, intensity=780 mJ/cm^2, energy=500 mJ/pulse. [144]

Surface treatment	Tensile strength [kg/cm^2]	Failure mode
Abrasive Al_2O_3	375±5	Cohesive
Anodized	381±3	Cohesive
Laser treated (line spacing=2 mm)	395±7	Cohesive
Laser treated (line spacing=4 mm)	407±6	Cohesive

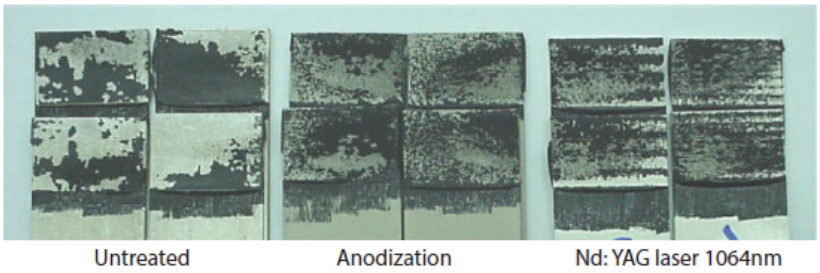

Fig. 2.25 Comparison between fracture surfaces of untreated, anodized and laser treated SLJ [144]

It is worth moreover mentioning the works by Guo *et al*, in which the shear strength and the fracture toughness of SLJ and DCB, respectively, realized with Yb-pulsed laser pre-treated AA7075-T6 aluminium substrates bonded together with Dow Betamate 1486 adhesive

were evaluated in function of the surface roughness and of a new parameter proposed by the authors, E_{TU}, which is defined by Eq. 2.9

$$E_{TU} = \frac{E_T S}{D_{ET}^2 \left(1 - \frac{C}{100}\right)^2} \tag{2.9}$$

where E_T is the total energy contained in each laser pulse, S is the area of the beam spot on the substrate during laser ablation, D_{ET} is the nominal crater diameter and C is the overlapping or separation coefficient, defined as

$$C(\%) = \left(1 - \frac{\delta}{D_{ET}}\right) x100 \tag{2.10}$$

where δ is the crater center-to-center distance.

With refer to the trend of the shear strength τ_M and the Mode I fracture toughness G_{Ic} in function of the surface roughness, it was possible to identify in S_a=2 μm the threshold value which segregates the region in which τ_M and G_{Ic} grow up with the surface roughness S_a from the region in which a lowering of τ_M and G_{Ic} occurs as S_a further increases. The plots of τ_M and G_{Ic} in function of S_a and E_{TU} are offered in Fig. 2.26.

A complete and fully-comprehensive review of the existing literature concerning the topic of the use of laser ablation for the pre-treatment of bonding surfaces is beyond the aim of this thesis, but without deepening the details a further brief mention to some interesting works on the same topic is due. Galantucci *et al* [145] identified an increase by a factor higher than 70% of aluminium joints pre-treated with excimer laser with respect to the untreated specimens. Kim *et al* [22] concluded that the increase of contact area and the triggering of the interlocking effect due to the increase of surface roughness are the main responsible for the switch from adhesive to cohesive failure by laser pre-treating aluminium bonded joints. Gilbert *et al* [146] developed a model for evaluating the surface morphology in function of the energetic and kinematic parameters of the pulsed laser ablation process.

With refer to the influence over the aging resistance of aluminium joints, another work by Rechner *et al* [147] studied the shear strength of Nd:YAG laser treated single lap joints realized with AW 6016 aluminium substrates bonding together with a hot-curing epoxy adhesive Betamate 1496, before and after subjecting them to different aging procedures. In particular, the aging was carried out by means of the exposition to a salt spray atmosphere for 1000 and 2000 h, respectively. Moreover, before the accelerated ageing cycle, some specimens underwent an electrophoretic deposition process (EPD) to simulate the paintwork performed over bonded elements in the automotive industry, where the laser technology could be an interesting alternative to replace the hexavalent chromium compounds, banned

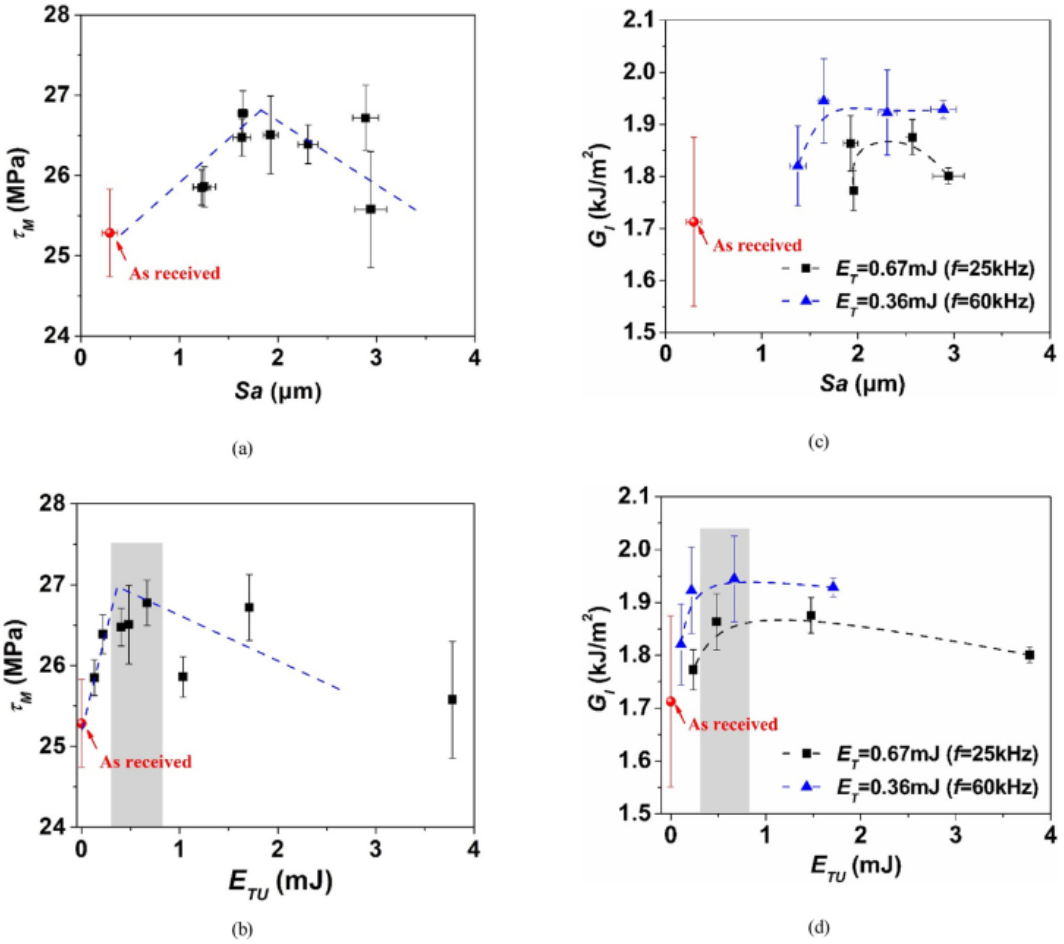

Fig. 2.26 Trends of the maximum shear strength τ_M and the critical Mode I strain energy release rate G_{Ic} in function of S_a and E_{TU}, respectively. In particular: in (a) and (b) τ_M from the SLJ tests, in (c) and (d) G_{Ic} from the DCB tests. The shaded area in (b) and (d) highlights the region in which the surface roughness decreases as E_{TU} grows up

since 2007 by the EU Directive 2000/53/EC. In Fig. 2.27 the mean values of shear strength, along with the standard deviations, of the laser treated and other two kinds of specimens produced for comparison purposes (the untreated and the samples subjected to atmospheric pressure plasma) are plotted.

While the atmospheric pressure plasma treatment does not reach in improving the tensile shear strength of EPD-passivated joints after the exposition to the salt spray atmosphere, the laser treatment enhances it by a different factor depending from the exposure time (26% and 15% for 1000 h and 2000 h of salt spray testing, respectively) with respect to the untreated joints. The increase of the shear strength in the AP-plasma and laser treated joints with respect to the reference samples when the EPD coating is not present is very marked. With

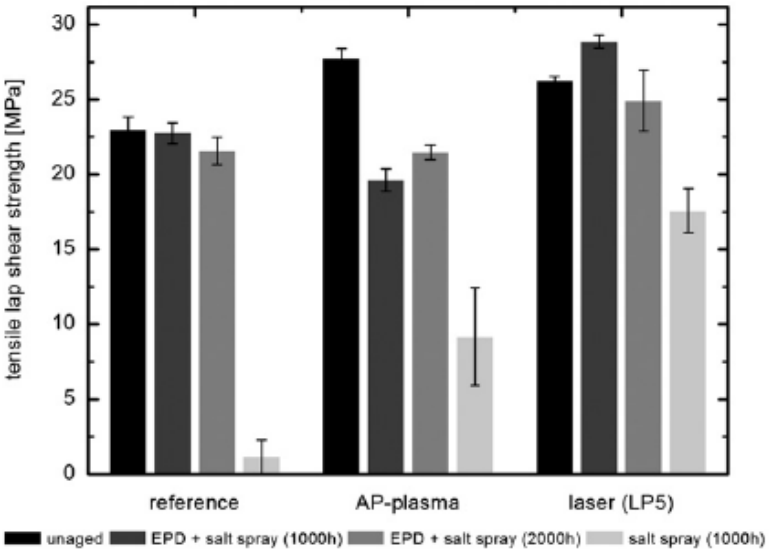

Fig. 2.27 Tensile shear strength of AW 6016 aluminium joints bonded with Betamate 1496 [147]

regard to the failure mode, in the unaged case the locus of failure was always in the adhesive, while after the ageing the amount of area subjected to interfacial failure became increasing in function of the exposure time to the ageing cycle. After 1000 h of ageing process, the untreated joints presented interfacial failure over the whole bonded area on one side, while in the plasma pre-treated samples the crack switched from one interface to the other and finally in the laser treated joints the adhesive failure occurred only along the edges of the bonding surface.

In a work by Wu *et al* [148] single lap adhesively bonded joints realized using AA6082-T4 aluminium sheets as substrates and Dow Betamate 1496 as adhesive were tested after being laser pre-treated with different parameters configurations and being immersed into water at 54°C for 7 days. Table 2.8 collects the different process parameters combinations used.

Table 2.8 Laser parameters configurations (numbered from L1 to L4) employed in [148]

Laser parameter	L1	L2	L3	L4
Pulse repetition frequency [kHz]	400	200	100	10
Scan speed [mm/s]	10000	5000	2500	250
Energy fluence [J/cm^2]	0.40	1.40	4.09	19.01

In Fig. 2.28 the results concerning the shear strength of untreated and laser treated joints after being exposed to the aforementioned aging process are compared with the corresponding data related to the unaged specimens. It is worth noting how a general reduction of the shear strength affects all the conditioned specimens, but, while the lower fluences treatments do not reach to significantly limit it, the laser ablation performed with higher fluences produces a slight decrease of the shear strength with respect to the unconditioned case. The extent of the amount of the fracture surface interested in cohesive failure went progressively increasing from the untreated specimens (where the crack propagated at the interface between adhesive and substrate) to the L4 treatment (where the failure occurred in a completely cohesive mode), both in the unaged and in aged conditions, even if in this last case the amount of adhesively failed area increased with respect to the former.

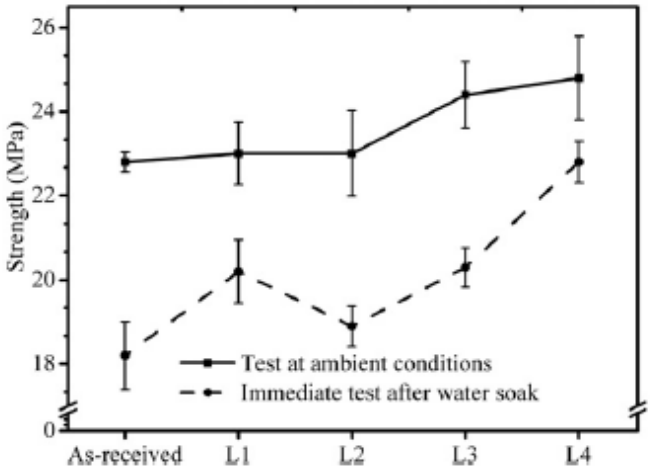

Fig. 2.28 Joint strength depending from the pre-treatment configuration and the occurrence of the water soak exposure measured in [148]; (b) variations of surface roughness and surface area induced by laser ablation; (c) comparison between shear strengths in untreated and high energy fluence L4 treatment joints depending from the aging

This result appears to be consistent with the surface roughness measurements and the findings of the XPS analysis over the treated surfaces. The first one was found to increase with the fluence until peaks when the laser configuration was set to L3, even if the value induced by the L4 combination is slightly lower than the maximum. Finally, the highest fluence configuration is able not only to clean the surface from the contaminants (as also the lower fluence treatments do) but also to generate a thick aluminium oxide layer, which is known to have a beneficial effect over the wettability of the surface.

Chapter 3

Materials and methods

3.1 Surface pre-treatment

In this work, laser is used to ablate the surfaces of some metal adherents, in order to make them suitable to be bonded.

The laser system used is composed by a Yb-fiber laser, featuring a z-axis positioning system for focus adjustment and a x-y galvo mirror scanner. The available process parameters are summarized in Table 3.1.

Table 3.1 Process parameters of laser equipment used in this work

Process parameter	Value
Laser nominal average power P_{ave}	1-20 W
Laser radiation wavelength λ	1055-1070 nm
Pulse repetition frequency f_r	20-80 kHz
Emission line width	<10 μm
Mode of operation	pulsed
Minimum pulse Full Width at Half Maximum (FWHM)	120 ns
Beam quality factor M^2	1.8
Laser beam mode	TEM00

Being the diameter of the collimated laser beam d_s kept fixed to 7 mm and the focus length f of the F-Theta laser focusing lens equal to 100 mm, the nominal diameter of the resulting spot, ϕ_s, can be calculated from the following equation:

$$\phi_s = \frac{4}{\pi} M^2 \frac{\lambda f}{d_s} = 35 \mu m \tag{3.1}$$

The laser scanning strategy varies according to the pattern which is desired to design over the surface, in particular several directions are taken into account with respect to the plane in which the rectangular process surface ideally lies, in particular the transverse (along the shortest side of the surface), the longitudinal (along the longest side) and the cross (both transverse and longitudinal) patterns are compared, as Fig. 3.1 shows.

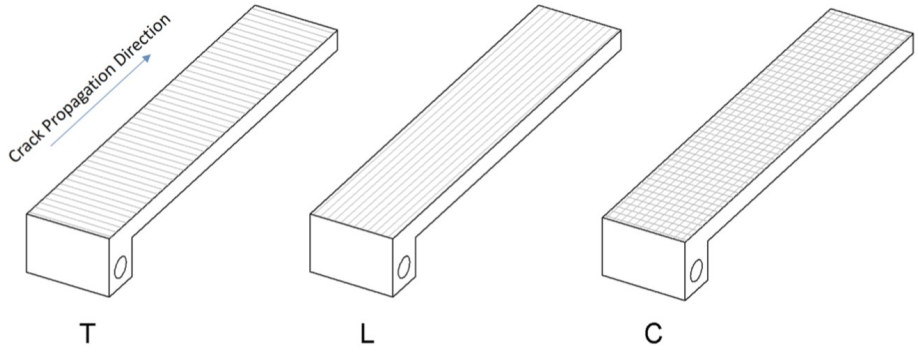

Fig. 3.1 Illustration of the lasing scanning directions employed [149]

The identifying names of the textures taken into account are:

- T - the laser beam follows perpendicular trajectories with respect to the crack propagation direction
- L - the laser beam follows parallel trajectories with respect to the crack propagation direction
- C - the laser beam moves following both the T and L direction, resulting in a sort of grid all over the surface

In general, the laser treatment is carried out by varying some peculiar parameters, in particular the average laser power (P) in a range 6-18 W, the tangential scan speed (v) in a range 90-1000 mm/s and the hatch distance (H), which measures the nominal space existing between adjacent grooves from center to center of the laser beam induced spots, ranging from 25 to 100 μm. The goal is to evaluate the quality of laser pre-treatment, in terms of surface morphology and mechanical performance of bonded joints, with respect to the energy

density, ED, which is the amount of energy per unit area transmitted by the laser to the surface [150][151] and is defined as:

$$ED = \frac{P}{v\phi_s} \tag{3.2}$$

In general, as one would expect, the depth of the grooves produced by the laser beam increases with ED, because a higher amount of emitted energy is able to melt a higher amount of material on the surface.

3.2 Surface assessment

3.2.1 Surface topology observation

To conduce an in-depth investigation over the changes induced by the laser treatment on the surface topography, using traditional optical microscope is not always sufficient, because of the poor depth of field which is typical of this tool. It is far preferable to employ the Scanning Electron Microscopy (SEM) technique, which exploits the interaction between the sampled surface and a focused beam of electrons impacting on it to record the different electrical signals emitted by every impacted point of the surface. In this way, it composes an high-resolution image which succeeds in focusing details which do not lie on the image plane and which would appear blurred if using the traditional optical microscope. The use of SEM allows to obtain high magnification images of the treated surfaces, allowing to visually compare them with two reference cases (as produced and grit-blasted).

SEM images provide an immediate snapshot of the enhancement in roughness which occurs passing from the as-produced to the grit-blasted and finally to the laser-treated samples. Sometimes it is useful to submit fracture surfaces to the SEM observation after the breaking of the joint. This can be an aid in identifying the mechanism (adhesive or cohesive) and the locus of failure, even if the amount of charge accumulated on non-conductive surfaces, like the one of the adhesive on which cohesive failure occurred, results in scanning faults, which is why it is always recommendable to coat non-conductive samples with an ultra-thin alloy of electrically conducting material.

In this work, SEM analysis are carried out using a Field-Emission SUPRA40 Zeiss SEM equipped with a GEMINI FESEM detection column and an Oxford Instrument EDX micro-analysis setup to analyse the laser treated surfaces before the production of the bonded joints to evaluate the differences brought by the ablation process with respect to the two aforementioned case and, within the laser ablated samples, by using different process conditions and parameters. The EDX microanalysis instrument embedded into the SEM equipment is also

used to get information about the chemical modifications induced by the treatment. Finally, a 50x optical microscopy is used to observe the surfaces of the joints after the breakage.

3.2.2 Surface morphology evaluation

The simple observation of the treated surfaces allows to get an idea of the surface topography, but, in order to assess the surface morphology not only from a qualitative point of view but in a way that allows to put the study cases in order with respect to it, it is always desirable to flank the SEM analysis with the determination of numerical indexes able to summarize the main characteristics of the surface morphology.

The first and primary parameter which aids in quantitatively characterizing a surface is the roughness. In this work, the roughness of the surface is measured according to ISO 25178-2 [130], in which areal methods to assess the surface texture are presented. In particular, in this work the average surface roughness, S_a, is preferred to the classic linear profile roughness, R_a, because of the strongly anisotropic nature of the surface texture which would make the classic parameter unrepresentative of the state of the surface. The surface roughness can be evaluated as:

$$S_a = \frac{1}{A} \int \int |z(x,y)| dxdy \tag{3.3}$$

In Eq. 3.3 A is the area whose roughness is to be calculated, z is the coordinate in the normal-to-the-surface direction while the x-y plane is the one on which the surface lies. Fig. 3.2 illustrates the definition of surface roughness.

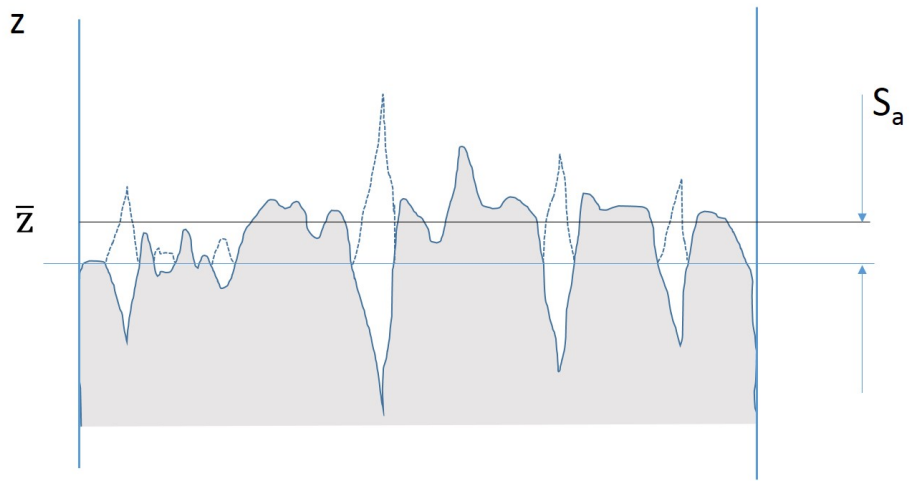

Fig. 3.2 A graphic illustration of the definition of S_a

The main disadvantage in using such a parameter to summarize the surface morphology is that it can provide information only about the deviation of the profile with respect to the medium plane, but it tells nothing about the distribution of peaks and valleys or the homogeneity of the texture. For this reason, another surface parameter is taken into account and supported the surface roughness in comprehensively describing the characteristics of the morphology, namely the Pearson's first coefficient of skewness S_{sk}. According to [130], the surface skewness is calculated as:

$$S_{sk} = \frac{1}{S_q^3 A} \int \int z^3(x,y) dxdy \tag{3.4}$$

In Eq. 3.4 S_q is the root mean square height of the surface, defined in Eq. 3.5.

$$S_q = \sqrt{\frac{1}{A} \int \int z^2(x,y) dxdy} \tag{3.5}$$

The surface skewness helps in understanding how the peaks and valleys are distributed over the surface with respect to the mean plane of the surface itself, resulting in height of the peaks higher than the depth of the valleys in case of positive values of S_{sk} and in the opposite situation in case of negative values of the index, as shown in Fig. 3.3.

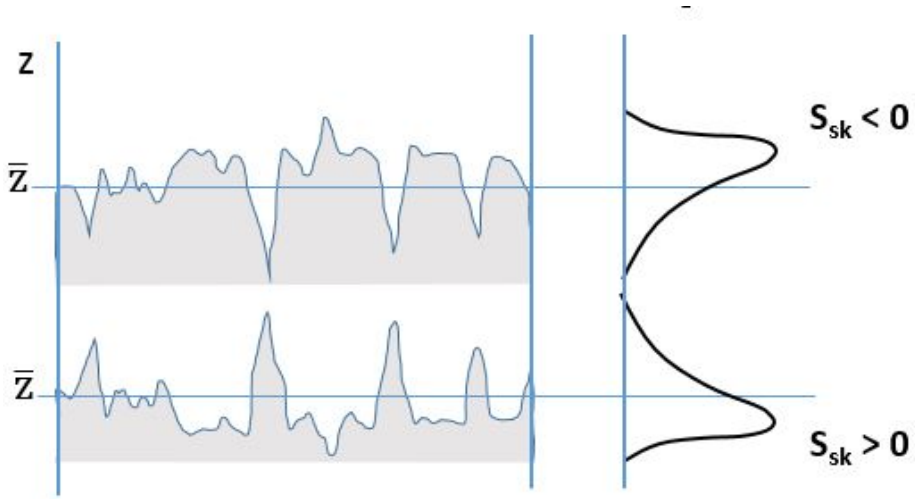

Fig. 3.3 A graphic illustration of the definition of S_{sk}

To assess the surface properties from a quantitative point of view, many techniques are available, including scanning probe or scanning tunnelling microscopy. In this work, the employed method to obtain information about the deviation of the profile and the distribution of peaks and valleys occurring naturally or induced by the laser treatment with respect to the mean plane of a processed surface is the laser profilometry. It consists in scanning the surface with a CCI Taylor-Hobson 3D optical profilometer with a resolution of 340 nm on

the longitudinal x-y plane and 1 nm on the vertical z-axis. This approach is by far more advantageous with respect to a classic contact profilometer because the tip of the diamond stylus does not succeed in penetrating in surface structures shaped by very narrow and deep grooves. On the other hand, if using a non-contact profilometer attention must be paid to the cleaning of the surfaces, because the presence of contaminants can alter and disturb the measure.

3.2.3 Wettability measurements

Some measurements of the modification of the static water contact angel are performed by means of a Dataphysics OCA20 (Optical Contact Angle) instrument. The sessile drop test is employed and the drop volume is set to 1 ml. The test is performed at room temperature. Fig. 3.4 provides an example of the method used for evaluating the contact angle from the tangent curve to the drop profile in the contact point between sessile drop and substrate surface.

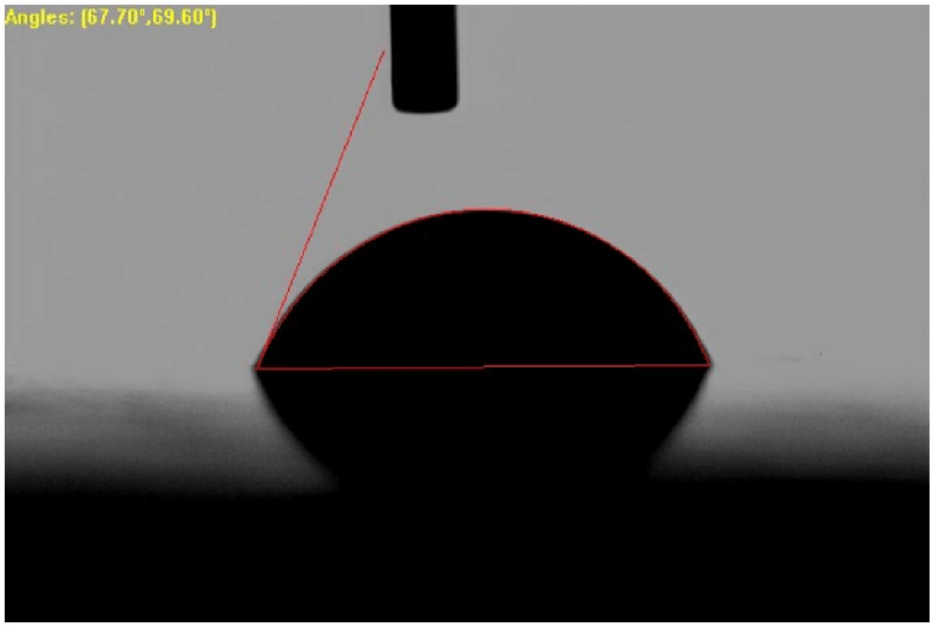

Fig. 3.4 Example of determination of tangent curve to the drop profile starting from which the contact angle is assessed [152]

3.3 Mechanical characterization

3.3.1 Joint geometry and preparation

The joint geometry employed in the tests is the Double Cantilever Beam (DCB) one represented in Fig. 3.5, while the dimensions are summarized in Tab. 3.2.

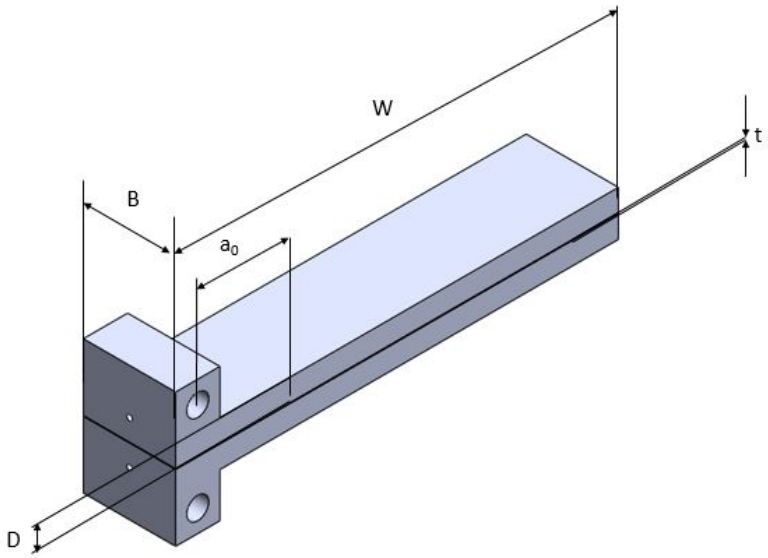

Fig. 3.5 DCB joint geometry [149]

Table 3.2 DCB joint dimensions

W [*mm*]	d [*mm*]	B [*mm*]	t [*mm*]	a_0 [*mm*]
120	6	25	0.15	25

The substrates are manufactured in AA6082-T6 aluminium alloy, whose mechanical properties are summarized in Tab. 3.3.

The transmission of load during the test is allowed thanks to the presence of two small steel drilled blocks which are glued on a side of each substrate. A toughened epoxy two component adhesive, Loctite Hysol 9466, is used to produce both the laser ablated bonded joints and the joints used as reference, namely the simply degreased and the grit blasted one. Its mechanical properties, taken from the data sheet provided by the producer, are summarized in Tab. 3.4.

Table 3.3 AA6082-T6 mechanical properties

Young Modulus E_s [GPa]	70
Poisson's ratio ν_s	0.33
Tensile Yield Strength Rp_s [MPa]	260
Tensile Ultimate Strength Ru_s [MPa]	310

Table 3.4 Loctite Hysol 9466 mechanical properties

Young Modulus E_a [MPa]	1718
Poisson's ratio ν_a	0.35
Tensile Ultimate Strength Ru_a [MPa]	32

After a wash with soap and water aimed at removing the contaminants remained on the surface due to the machining, the substrates are laser ablated with different combinations of process parameters in order to explore a wide range of values of energy density ED, using three different values of hatch distance H (25, 50 and 100 μm) to assess the influence of a superposition length lower, approximately equal and higher, respectively, to the groove width W.

After the laser ablation, within 1 hour the substrates are bonded together, placing a polyester sheet in the front extremity of the specimens to create an initial 25 mm long crack. The thickness of the bond line is controlled by positioning calibrated metal sheets at both the endpoints of the specimens. The bonded joints undergo a curing cycle in a temperature controlled oven at 80°C for 1 hour. Two kind of reference specimens are also produced: the simply degreased one is washed and then cleaned with a chemical degreaser (Henkel 7063 cleaner), while the grit blasted one is processed with alumina particles (grade 80), at a pressure of 0.5 MPa and keeping the nozzle at a distance approximately equal to 30 mm from the surface.

The cure of the bonded joints for all the experimental phases of the work, as well as the conditioning of the specimens aimed to undergo an accelerated ageing cycle as described in Par. 5.4, are performed using an ACS test chamber (model DY110).

3.3.2 Quasi-static test characteristics

The test for the assessment of the Mode I strain energy release rate of Double Cantilever Beam joints is performed according to ASTM D3433 [102] and consists in making a crack initiating and propagating along the bonded length of a specimen, within the adhesive (cohesive failure) or at the interface between adhesive and substrate (adhesive failure), because of a tensile force

acting in a normal direction with respect to the crack surface. The tests are performed using a servo-hydraulic testing machine MTS 810 equipped with a 3 kN load cell, in displacement control at a constant cross-head speed. A load-unload law in rate of displacement control (2 mm/min in the loading phase and 4 mm/min in the unloading phase) is imposed because the evolution of the crack length as the test proceeds is evaluated by using the compliance method, starting from the following equation due to the work of Krenk [106]:

$$C = \frac{\Delta}{P} = \frac{2\lambda_\sigma t}{E'_a B}\left[1 + 2(\lambda_\sigma a) + 2(\lambda_\sigma a)^2 + \frac{2}{3}(\lambda_\sigma a)^3\right] \tag{3.6}$$

where C is the compliance of the joint, Δ is the displacement of the loading point, P is the load, t is the thickness of the bondline, E'_a is the plane strain formulation of the Young Modulus of the adhesive given by $E'_a = E_a/1-\nu_a^2$, B is the width of the joint, a is the actual crack length and finally λ_σ is a parameter given by Eq. 3.7:

$$\lambda_\sigma = \sqrt[4]{\frac{6}{D^3 t}\frac{E'_a}{E_s}} \tag{3.7}$$

where D is the height of a substrate and E_s is the Young modulus of the substrates material.

The reason for using this formulation instead of the one proposed in [102] is due to the fact that the Krenk model assumes that, due to the symmetry of the DCB joint, every substrate could be treated as a beam on an elastic foundation and therefore takes directly into account the contributions to the mutual displacement of the substrates given by the elasticity of the adhesive layer (namely, the deformation and the rotation of the beams at the crack tip), without any need for experimental correction of the compliance value as stated in ASTM D3433.

Actually, for the implementation of the assessment of the Mode I strain energy release rate a Finite Element Model of the joint is realized and a series of linear static analysis are performed, by keeping the applied load constant and progressively increasing the crack length. For every analysis, the corresponding value of compliance C' evaluated as the ratio between the Crack Opening Displacement δ' (COD) measured at the front of the specimen and the applied load is extracted in order to obtain a polynomial law relating this compliance and the crack length which can be used to assess the actual crack length from the experimental data (in particular δ' is measured during the test with an omega clip gage).

The Mode I strain energy release rate G is finally evaluated through the following equation, extracted from [106]:

$$G = \frac{P^2}{2B}\frac{dC}{da} = \frac{(Pa)^2}{BE_sI}\left(1+\frac{1}{a\lambda_\sigma}\right)^2 \tag{3.8}$$

where I is the second moment of area of the beam section, given by $I = BD^3/12$.

An example of the force-opening plot typical as a result of a DCB test is given in Fig. 3.6, while in Fig. 3.7 the crack resistance curve (R curve) for the same specimen is offered.

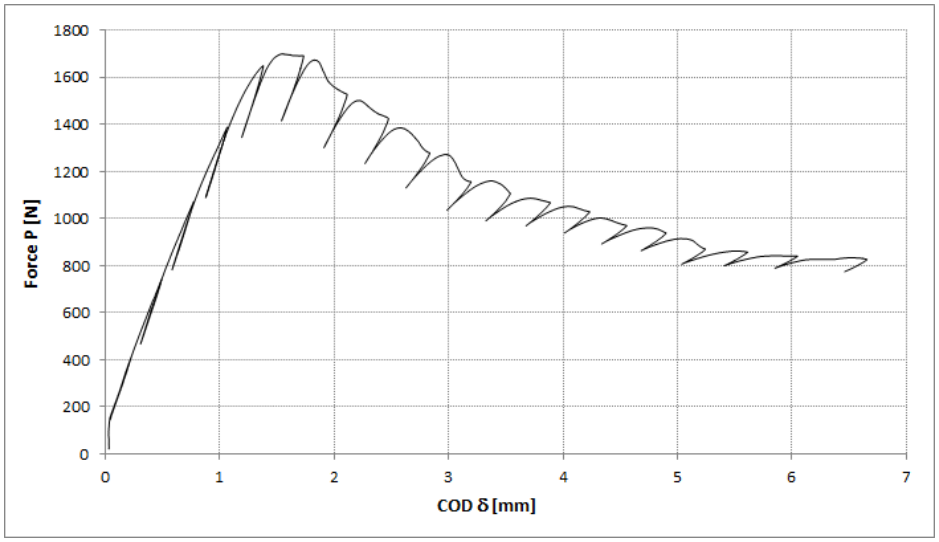

Fig. 3.6 Example of force vs. COD plot resulting from a DCB test

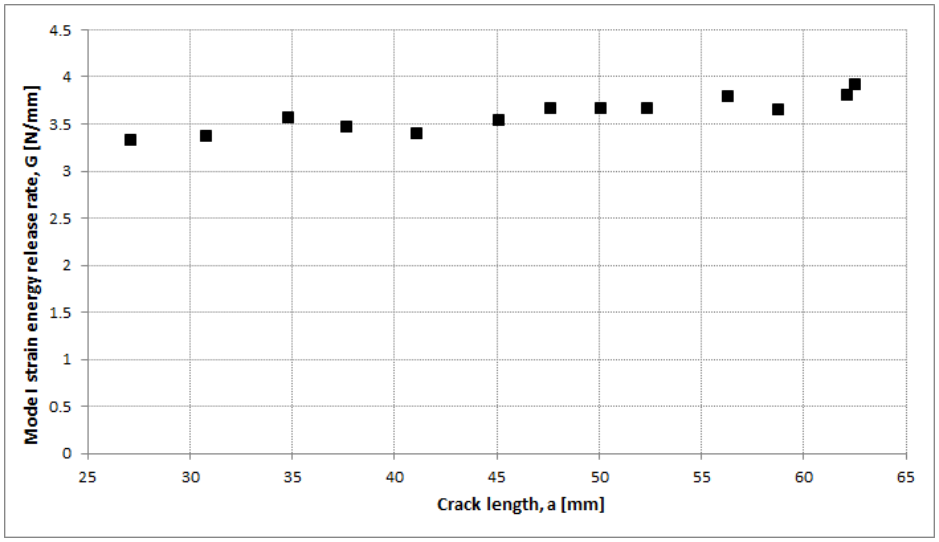

Fig. 3.7 Example of crack resistance curve resulting from a DCB test

From Fig. 3.7 it is notable how the crack resistance curve appears flat as the crack proceeds, that is why the critical value of the Mode I strain energy release rate, G_{Ic}, is evaluated as the average of the values that G assumes during the test in the plateau.

3.3.3 Fatigue test characteristics

The fatigue tests are running using the same experimental equipment using for the DCB quasi-static test. The test is performed in load control, according to ASTM E647 [153]. The compliance method is used in this case too for the evaluation of the actual crack length from which the range of Mode I strain energy release rate within a load cycle, ΔG, is periodically updated as the crack grows up according to Eq.3.9

$$\Delta G = G_{max} - G_{min} = G_{max}(1-R^2) = \frac{(P_{max}a)^2}{BE_sI}\left(1+\frac{1}{a\lambda_\sigma}\right)^2(1-R^2) \tag{3.9}$$

where G_{max} and G_{min} are the maximum and the minimum value, respectively, of the Mode I strain energy release rate in a load cycle, R is the load ratio and P_{max} is the maximum load achieved during a fatigue cycle. The other terms in Eq. 3.9 have been already presented in Par. 3.3.2. For the evaluation of G_{max} and G_{min}, the Krenk model [106] is used even in this case.

Chapter 4

Analysis of laser treated surfaces

The pre-treatment of surfaces intended to be bonded aims at modify both the morphology and the chemical status of the surface in order to improve the conditions of bonding (wettability, cleaning, interlocking effect, etc). Therefore, in order to begin understanding and evaluating the differences in surface morphology due to laser treatments carried out with different combinations of process parameters, the surface characterization plays a crucial role. It involves several means and techniques ranging from the visual inspection to the determination of topographic representative quantities able to summarize in an index the general framework of the surface morphology.

In this chapter, a description of the main results obtained in correlating the output of the surface analysis with the different process configurations is offered, with the aim of identifying a general trend between laser induced surface morphology and treatment conditions which acts as a predictive law. Part of the results here exposed has been published in [154] and [149].

4.1 Starting points

In this work, different laser process parameters are used for ablating surfaces belonging to adherents to be bonded. The material taken into account is aluminum AA6082-T6. The goal of the quantitative surface characterization through the laser profilometer is to assess the influence that different configurations of laser parameters employed for the ablation has over the surface texture representative indexes. The aforementioned energy density ED is the marker which is assumed as strictly representative of a single process sample, due to the fact that it is given by different combinations of power P and scan speed v, being the nominal spot diameter ϕ_s constant. In [155], the geometrical and dimensional characterization (depth and width) of a single groove realized with the laser ablation on an aluminum AA6082-T6

surface was conducted varying the energy density provided to the surface during the process. It was found that the trend of the width of the grooves, W, with the energy density ED strictly depends from the level of power P employed to perform the ablation: when the power is set to 20 W, a slight increase of W with ED is apparent; when the power is equal to 15 W, the slope of the curve is extremely low and W is considerable being constant to approximately 55 μm; finally, when the power is further lowered to 10 W a slow decrease of W with ED is observed, probably due to the fact that a lesser power implies also lower thermal losses and therefore a reduction of the energy conduction on a plane perpendicular to the optical axis. With refer to the groove depth, D, the identified relation between it and ED is much simpler, consisting in a approximately linear increase of D with ED. Fig. 4.1 and 4.2, taken from a work by the same authors [156], graphically illustrate these last remarks.

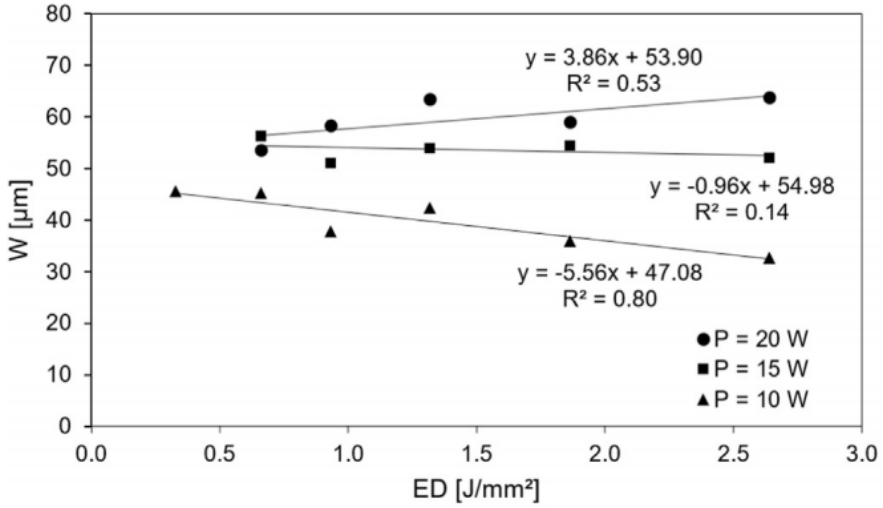

Fig. 4.1 Trend of groove width W in function of the energy density ED, varying the laser power P [156]

In order to segregate the effect of the energy density on the surface roughness from the contribution of the hatch distance H, different laser ablated surfaces obtained by varying the energy density and kept H fixed to 0.075 mm were evaluated through laser profilometry. In Fig. 4.3 it is possible to observe the trend of S_a in function of ED.

Observing the Fig. 4.3 the surface roughness S_a seems almost to linearly grow up with ED to a specific threshold value, approximately equal to 4 J/mm^2. When this level of energy density is exceeded, S_a steadily decreases. In [155] a possible explanation of this trend was offered and identified in the softening of the bulk material and the flattering of the crests the main responsible events of the phenomenon: the reduction in the peak-to-valley distance results in a general lowering of the surface roughness, the more marked, the higher the level of energy density reached after the threshold value. To better understand this, in Fig. 4.4 it is

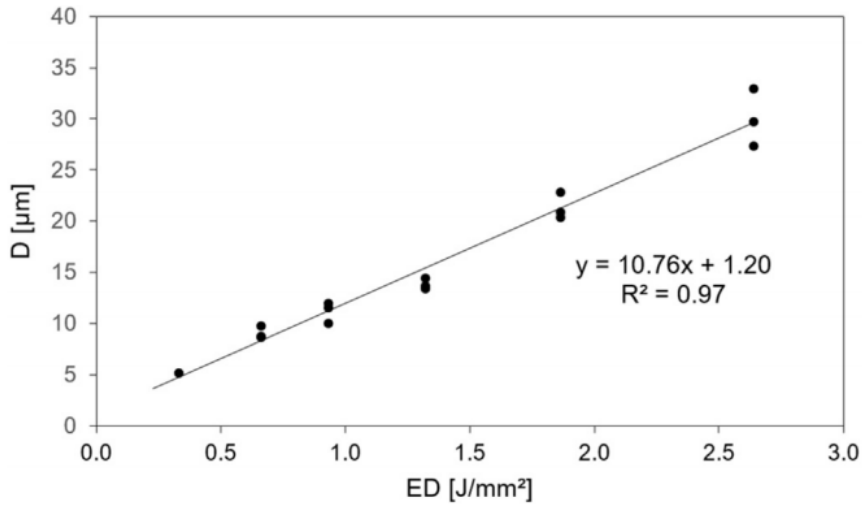

Fig. 4.2 Trend of groove width W in function of the energy density ED [156]

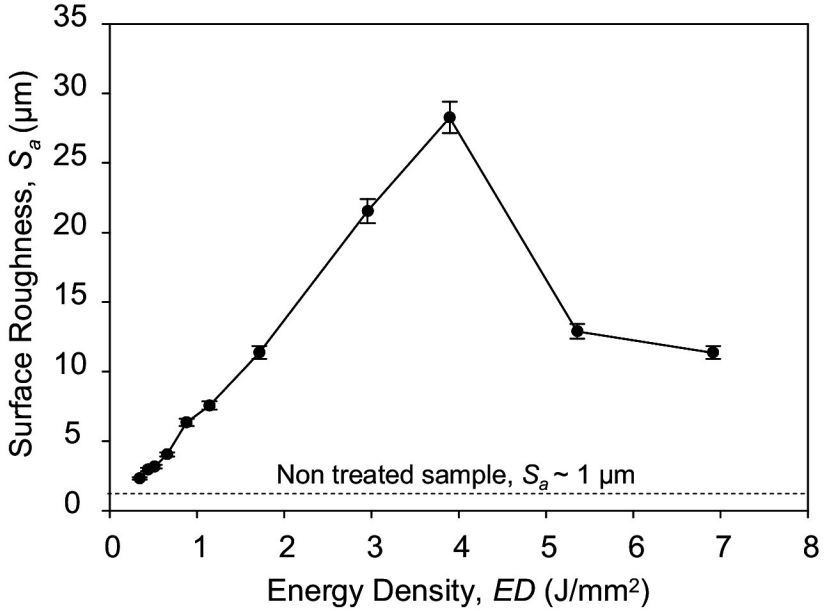

Fig. 4.3 Trend of S_a vs ED evaluated on aluminum AA6082-T6 surfaces, being the hatch distance H fixed to 0.075 mm [155]

possible to notice the evolution of surface roughness passing from a low value of ED (panel a, S_a very low) to the threshold value (panel b, increase of S_a) and finally to a high value of ED (panel c, slight but discernible decrease of S_a with respect to the panel b).

To take into account the effect of hatch distance H over the surface roughness, in [155] an approach based on an hypothesis presented in [157] was considered and an analytical model able to predict the surface roughness value of a laser ablated surface in function of H

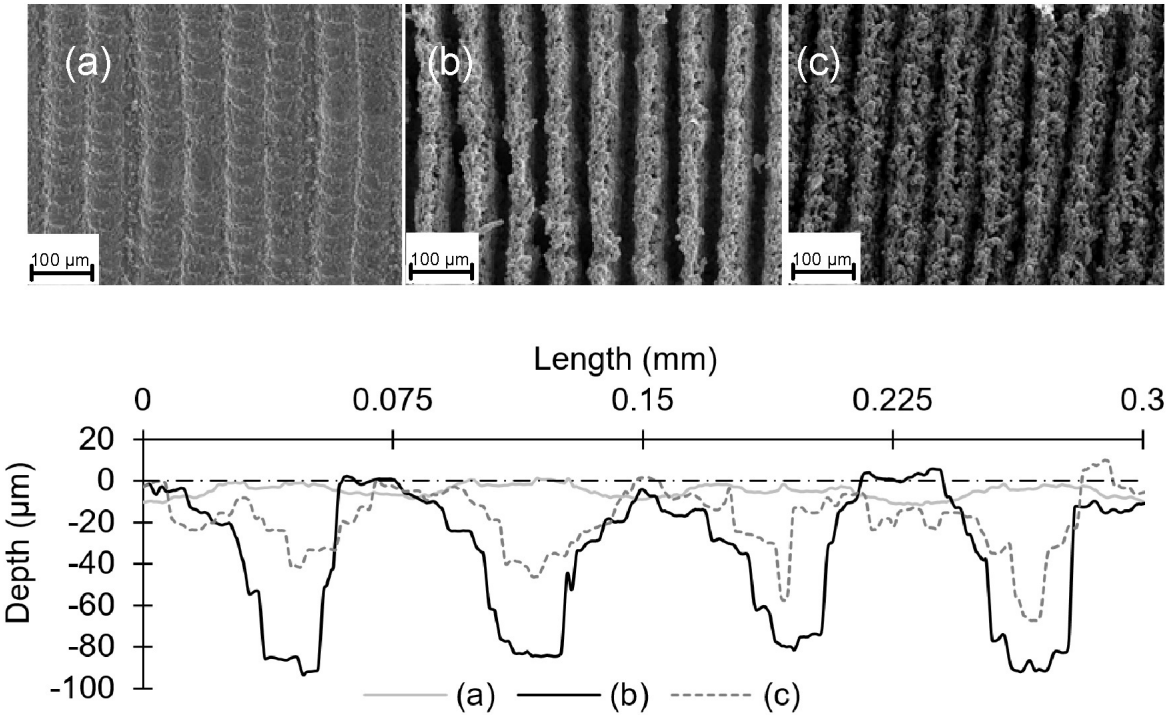

Fig. 4.4 SEM images at 600X (7 keV) and acquired profiles of aluminum AA6082-T6 surfaces ablated kept the hatch distance H constant to 0.075 mm and using different ED: (a) 0.438 J/mm^2, (b) 3.896 J/mm^2, (c) 6.912 J/mm^2 [155]

based on a predefined footprint of the profile was developed. In [151], the groove profile was assumed to be modeled as parabolic, considering the nearly Gaussian profile of the beam and the Beer-Lambert absorption law. After defining a mean plane of the profile by linearly fitting the profile of the surface far from the laser induced groove, the groove width W and the groove depth D were evaluated, respectively, as the distance between the intersections of the parabolic profile with the mean plane and the distance between the minimum of the parabolic curve and the mean plane, as Fig. 4.5 illustrates.

Because the surface pattern is composed by concentric grooves realized on the top surface of cylindrical samples, it was possible to assume that the linear roughness measured over a cross section of the laser induced grooves across a radial trajectory was representative of the surface roughness evaluated over the whole surface. To evaluate the influence of H on the surface roughness S_a two cases were considered: (1) superimposition of the grooves (H<W), case in which S_a can reasonably be expected to increase with H; (2) absence of overlap (H>W), case in which S_a was supposed to decrease with H. In Fig. 4.6 adjacent parabolic profiles used for the analytical evaluation of S_a are presented.

The mean plane identified by $\bar{z}$ was placed by balancing the areas segregated from peaks and valleys, modeling the laser induced grooves as parabolic profiles, so that the reference

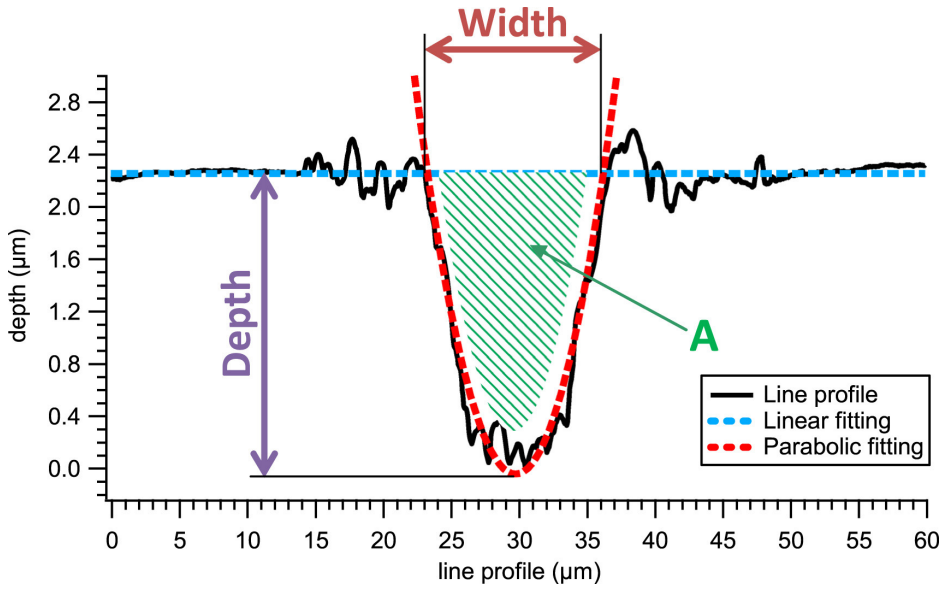

Fig. 4.5 Groove width and depth definitions [151]

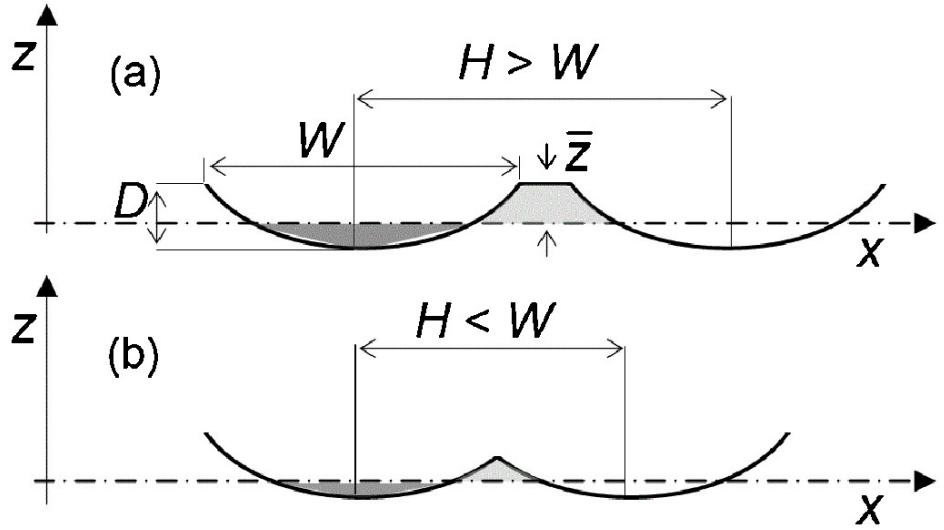

Fig. 4.6 Sketch used for the analytical evaluation of S_a in function of H: (a) H>W and (b) H<W, for a constant ED [155]

position on z-axis of the mean plane could be calculated by the following equations, valid for H<W or H≥W, respectively:

$$\bar{z} = \frac{2}{3}\left(\frac{DH^2}{W^2}\right) \tag{4.1}$$

$$\bar{z} = \frac{2DW}{3H} \tag{4.2}$$

Following the definition of S_a provided in [130], the surface roughness was evaluated for H<W and H≥W, respectively, in Eq. 4.3 and 4.4.

$$S_a = \frac{4}{9\sqrt{3}}\left(\frac{DH^2}{W^2}\right) \tag{4.3}$$

$$S_a = \left(\frac{4DW}{3H}\right)\left(1 - \frac{2W}{3H}\right)^{\frac{3}{2}} \tag{4.4}$$

The validation of the developed analytical model was carried out by measuring the surface roughness of laser ablated surfaces processed at the same value of ED (0.65 J/mm^2) varying the hatch distance H in a range between 0.035 mm (equal to the nominal spot diameter ϕ_s) and 0.200 mm. In Fig. 4.7 a comparison between the experimental and analytical trend obtained by Eq. 4.3 and 4.4 is proposed.

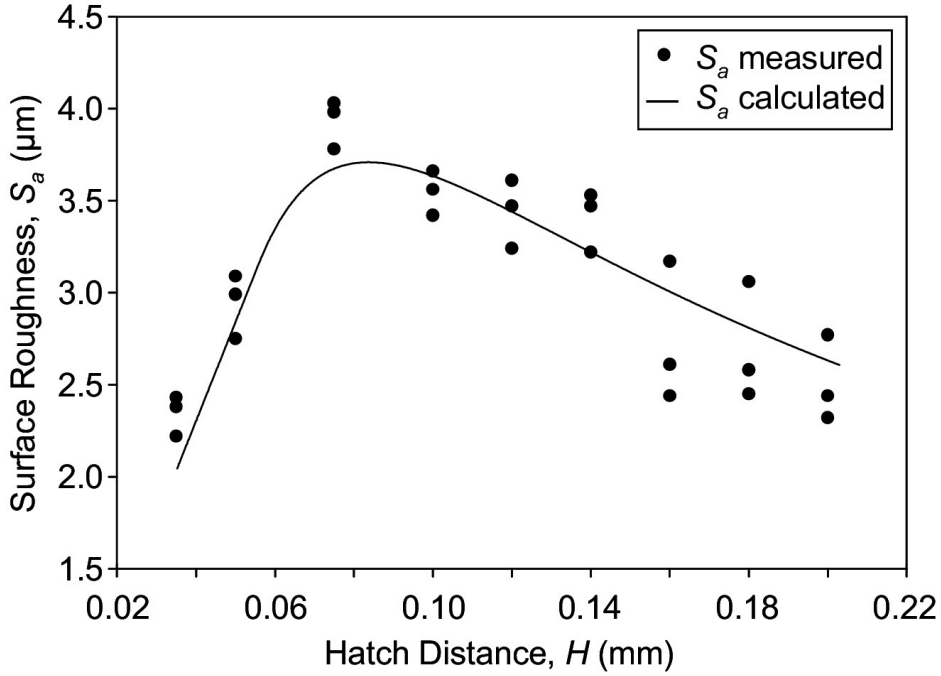

Fig. 4.7 Comparison between experimental and analytical trend of S_a in function of H, being ED constant at 0.65 J/mm^2 (W=55 μm and D=12 μm) [155]

The analytic curve followed the expected behavior, linearly increasing until a maximum of H=0.075 mm (slightly higher than the reference W, equal to 0.055 mm) and then steadily decreased as the amount of untreated area grew up. The percentage of error between the predicted values and the experimental data was in a quite low limit (5%). The model developed in [155] was therefore a good prediction tool for the surface roughness useful in

process optimization, provided that the ablation occurs without thermal effect that can induce surface unevenness.

4.2 Surface characterization results

In this work, surfaces treated varying the entity of ED and H are compared to each other and with two reference cases, represented by the as produced surface and the grit-blasted surface, respectively. On Fig. 4.8 some 400x400 μm 3D contour maps extracted with the laser profilometer and representing the height profile of the reference surfaces are provided, while Tab. 4.1 summarizes the evaluated values of S_a and S_{sk}.

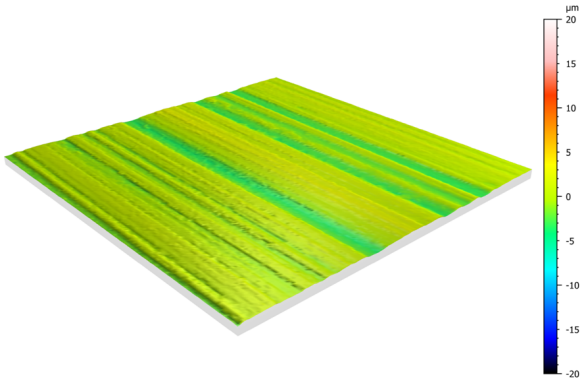

(a)

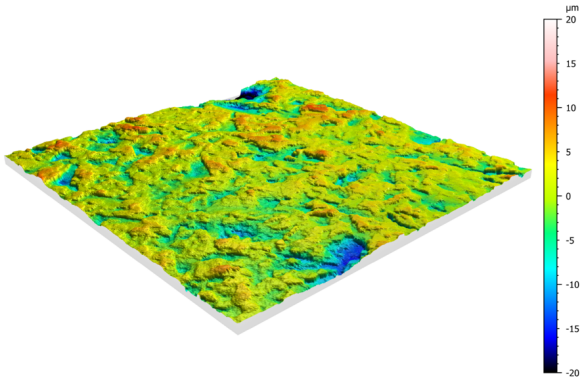

(b)

Fig. 4.8 AA6082-T6 aluminium surface morphology maps of the reference cases: (a) the untreated and (b) the grit blasted [154]

The morphology maps in Fig. 4.8 show how the untreated surface presents a smooth texture, in which very light grooves appear to have a preferential direction as a result of the extrusion process. The Pearson's first coefficient of skewness is approximately equal to zero, which denotes a substantial homogeneity and equal distribution of peaks and valleys. The

Table 4.1 Surface parameters for untreated and grit-blasted aluminum surfaces

Parameter	Untreated	Grit-blasted
S_a [μm]	1.20	3.16
S_{sk} [-]	-0.182	-1.07

grit-blasted surface has been treated with alumina particles (grade 80) and seems of course rougher than the untreated one, as it is confirmed by the surface roughness value. The surface skewness S_{sk} is lower than zero, indicating that the valleys are predominant with respect to the peaks.

In Fig. 4.9 the roughness values measured for aluminium AA6082-T6 surfaces are plotted against the energy density ED values for three different hatch distances (H=25, 50 and 100 μm). The trend exhibited by S_a in function of ED seems quite consistent with the one identified in [155]: the surface roughness steadily increases with ED until the energy density reaches a threshold value, confirmed approximately equal to 4 J/mm^2, beyond which the roughness begins to slightly lower as ED grows up. Investigating the behavior of S_a in function of the hatch distance H, the samples belonging to the series with H=100 μm have always a lower roughness with respect to the other two cases, except in correspondence of ED=1.71 J/mm^2, value at which the roughness of the surfaces with the highest H undergoes an unexpected increase.

The dependence of the surface skewness S_{sk} from the energy density ED is illustrated in Fig. 4.10.

When ED is very low (0.17 J/mm^2), S_{sk} is lower than zero because the low energy density beam is not able to significantly ablate the surface, only resulting in the generation of slightly deep valleys on the surface. Raising ED to 0.34 J/mm^2, it is possible to notice how the morphology is diversified depending on the hatch distance value: the treatments carried out with high values of H (H=100 μm) result in negative values of S_{sk}, while as H decreases the skewness becomes increasingly positive, until peaking in a range between 2.6 and 3 when H is equal to 25 μm. This appears to be reasonably explainable by noticing that a high level of superposition between adjacent grooves unavoidably results in a higher amount of melting material stacking on each other and inducing the formation of peaks. Then S_{sk} undergoes a lowering when ED is further increased until reaching a minimum in correspondence of ED=3.81 J/mm^2 and finally slightly raises up to values around zero, for high values of ED. An explanation of this trend is offered by considering that as ED increases the effectiveness of the laser process grows up and so the ablation is able to produce valleys characterized by a

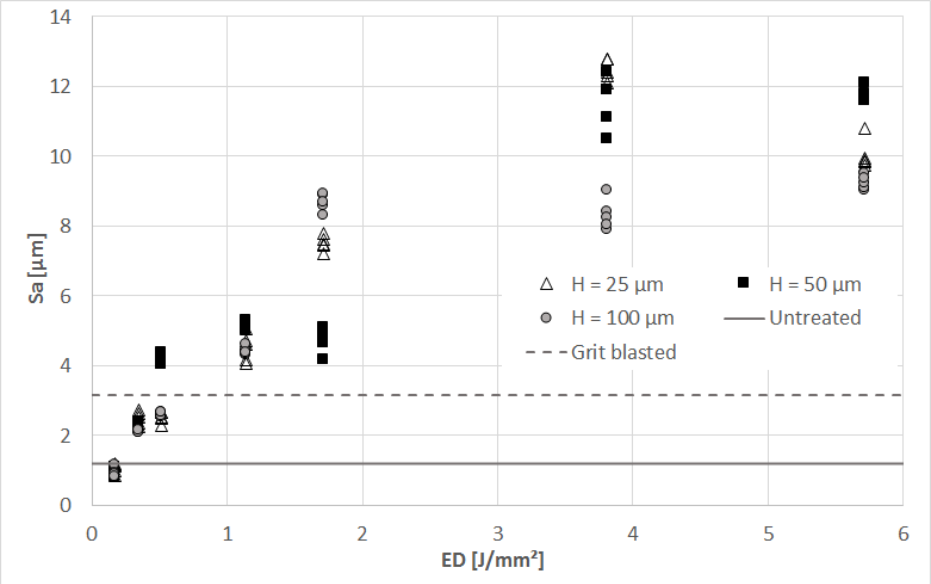

Fig. 4.9 Measured value of surface roughness S_a vs Energy density ED for different hatch distances H [154]

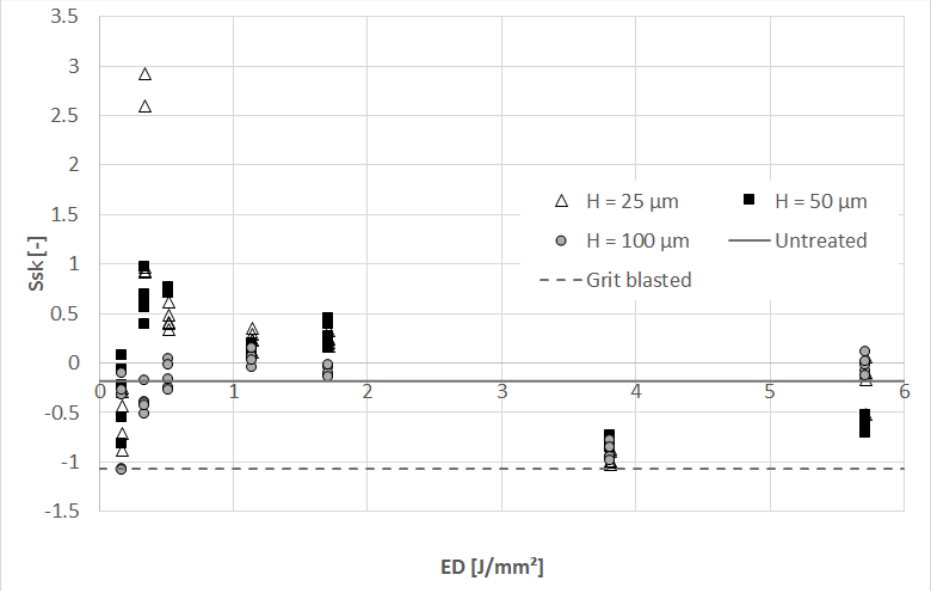

Fig. 4.10 Measured value of surface skewness S_{sk} vs Energy density ED for different hatch distances H [154]

more relevant depth that the one typical of low ED processes. It is worth noting that the set of values of S_{sk} with H=100 μm remains approximately always negative or slightly positive through the whole energy density range explored.

To better assess the behavior of the surface morphology with respect to the ablating process parameters, two different comparisons among surface morphology maps obtained through laser profilometry are proposed: in Fig. 4.11 the morphology of three different aluminium surfaces ablated varying the power and the speed but keeping constant the value of the hatch distance H is showed, while in Fig. 4.12 a comparison among surfaces morphology produced by the laser ablation varying the hatch distance H but keeping the energy density ED constant is offered. The first one is also accompanied by images taken from SEM analysis over the same surfaces.

With refer to Fig. 4.11, it is possible to notice, moving from the first image to the latter and thus from the lowest to the highest value of ED, how the surface changes from being approximately flat (panel a) to progressively increase the entity of its roughness with ED. In particular, in the surface showed in panel b the peaks are higher than the depth of the valleys resulting in positive values of S_{sk}. while the surface in panel c is characterized by valleys deeper than the height of the peaks and therefore by a negative value of S_{sk}.

Instead, the roughness of the three samples with constant ED represented in Fig. 4.12 is approximately the same, but the surface skewness assumes very different values according to the hatch distance value of the ablating process. In particular, in panel a) H is 25 μm and the surface is characterized by the presence of crests due to the interaction of adjacent grooves, in panel b) H is 50 μm and the medium plane appears to be slightly higher than in the previous case, while finally in panel c) H is 100 μm and the surface appearance alternates the untreated morphology and rows of spots induced by the laser treatment. Consequently, the surface skewness S_{sk} decreases from panel a) to panel c), as it is possible to verify in Fig. 4.10.

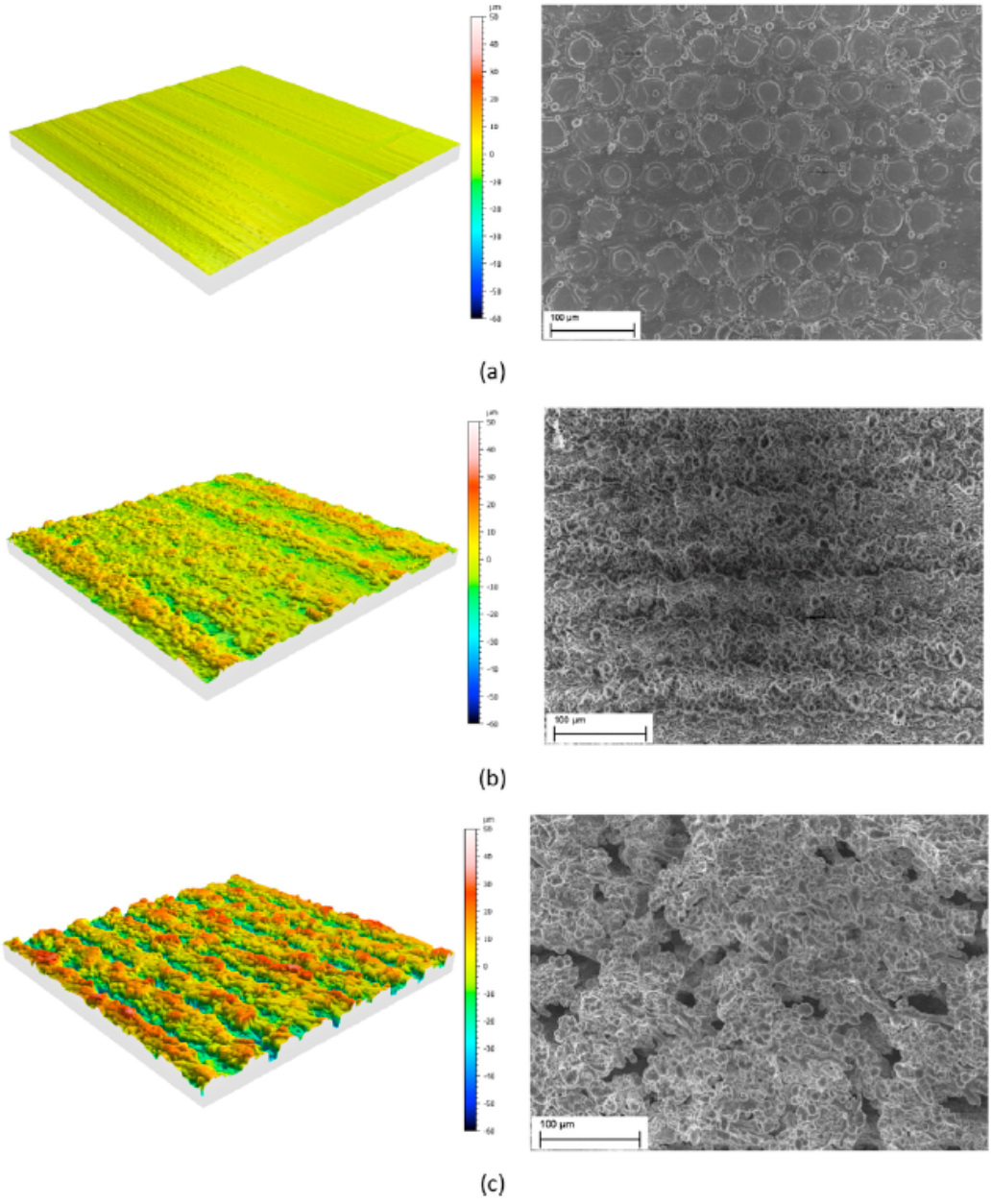

Fig. 4.11 Morphology maps and SEM images of aluminum surfaces ablated with H=50 μm and a) ED=0.17 J/mm^2, b) ED=1.71 J/mm^2, c) ED=5.71 J/mm^2 [154]

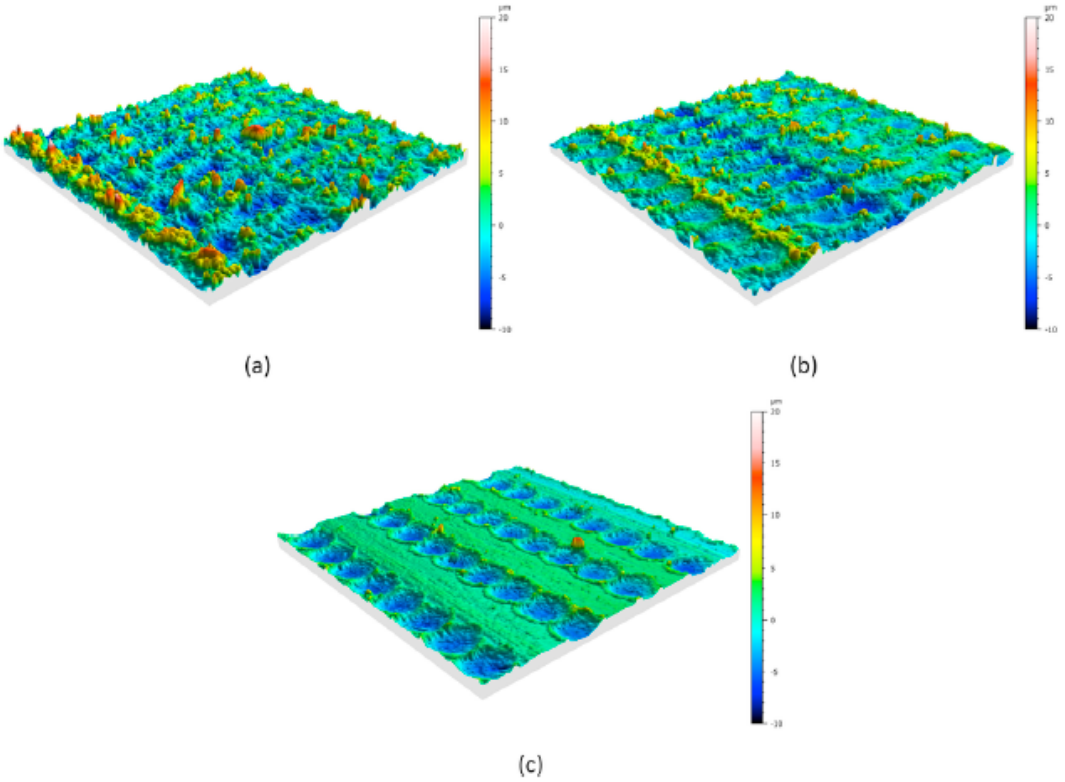

Fig. 4.12 Morphology maps of aluminum surfaces ablated with ED=0.34 J/mm^2 and a) H=25 μm, b) H=50 μm, c) H=100 μm [154]

4.2.1 Effect of the laser scanned pattern over the surface morphology

Another process parameter taken into account is the texture induced by the laser ablation on the treated surface. Besides the treatment carried out making the laser beam scan the surface along parallel lines from an extremity to the other, even a texture realized by means of perpendicular crossed trajectories is studied. Although a single transition along every trajectory is performed, there are of course several points, in correspondence of the crosses, which receive the pulse twice and therefore absorb a double amount of energy.

The influence of the employment of every ablated pattern over the surface morphology is evaluated by means of the same methods followed in the previously exposed characterization. In Fig. 4.13 the measured values of surface roughness induced by different energy density processes carried out with the intent of producing a sort of regular grid all over the treated surfaced are plotted. As in the unidirectional case, the hatch distance is varied between the same three values. The letter "C" in the graph legend stands for "crossed", it agrees with the nomenclature exposed in Chapter 3 and it is reported to promote the understanding of the figure when comparing it with Fig. 4.9.

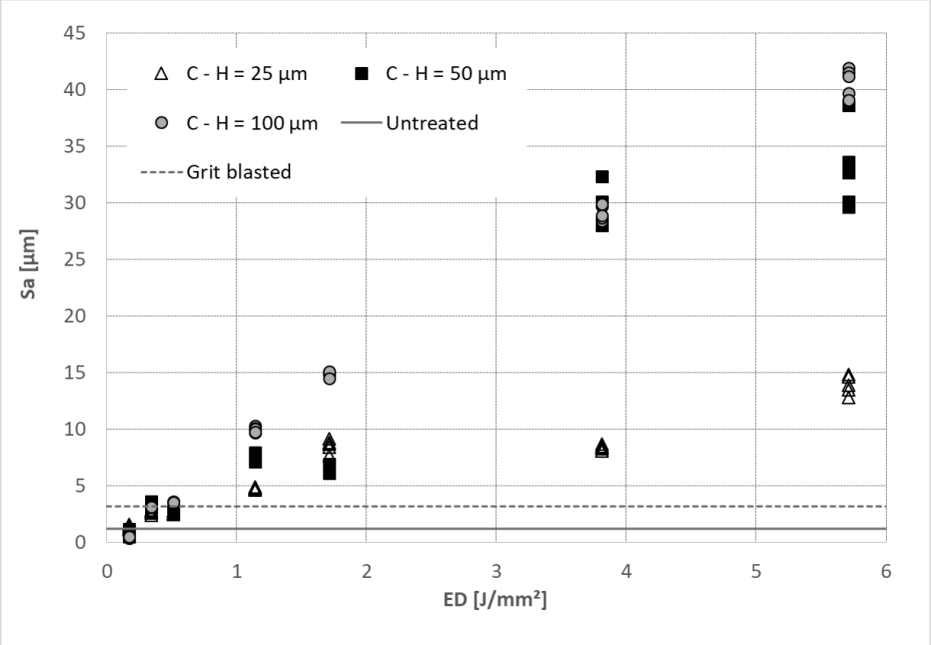

Fig. 4.13 Measured value of surface roughness obtained with crossed pattern treatment S_a vs Energy density ED for different hatch distances H [149]

Comparing Fig. 4.13 with the results of roughness for the laser scanning unidirectional direction (Fig. 4.9), it is possible to notice how the ablation with a grid pattern induces a surface morphology characterized by significantly higher values of S_a than in the previously

discussed case. The increase of roughness appears very strong especially for high values of hatch distance and energy density, while for the H=25 μm set the values are consistent with what was found for the unidirectional pattern. The dependence of the surface skewness from the energy density varying the hatch distance for the pattern realized with crossed trajectories is showed in Fig. 4.14.

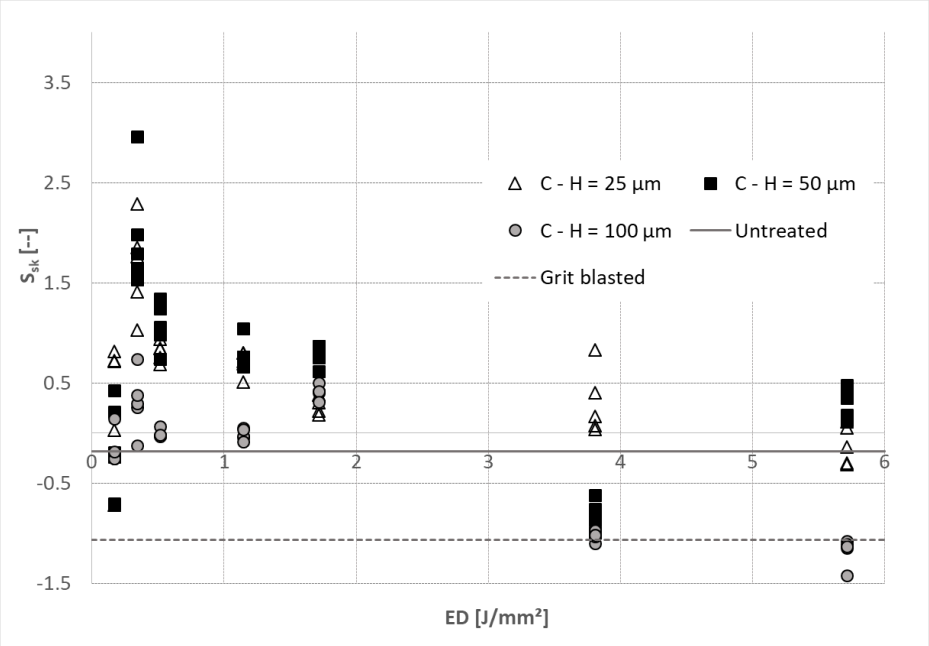

Fig. 4.14 Measured value of surface skewness S_{sk} vs Energy density ED for different hatch distances H,for the crossed pattern case [149]

In general, comparing Fig. 4.14 with Fig. 4.10, it is possible to state that the surfaces characterized by a grid pattern induced by the laser ablation present an increase of the S_{sk} value when the hatch distance is equal to 25 and 50 μm and the energy density is lower than 2 J/mm^2 with respect to the ones pre-treated unidirectionally. The set with H=100 μm of Fig. 4.14 present values of S_{sk} slightly higher than the corresponding ones of the unidirectional surfaces, with the exception of the highest ED values, in correspondence of which S_{sk} is very low.

In order to justify the differences achievable by means of a variation of the laser scanning direction, even for the crossed pattern case some images showing the morphology maps among the corresponding SEM images are provided in Figs. from 4.15 to 4.17.

Fig. 4.15 refers to a surface ablated with the lowest ED value considered in this work, with different values of H. It is possible to observe how when H is equal to 25 and 50 μm the interaction between grooves induced on adjacent lines is very high and the ablation coverage

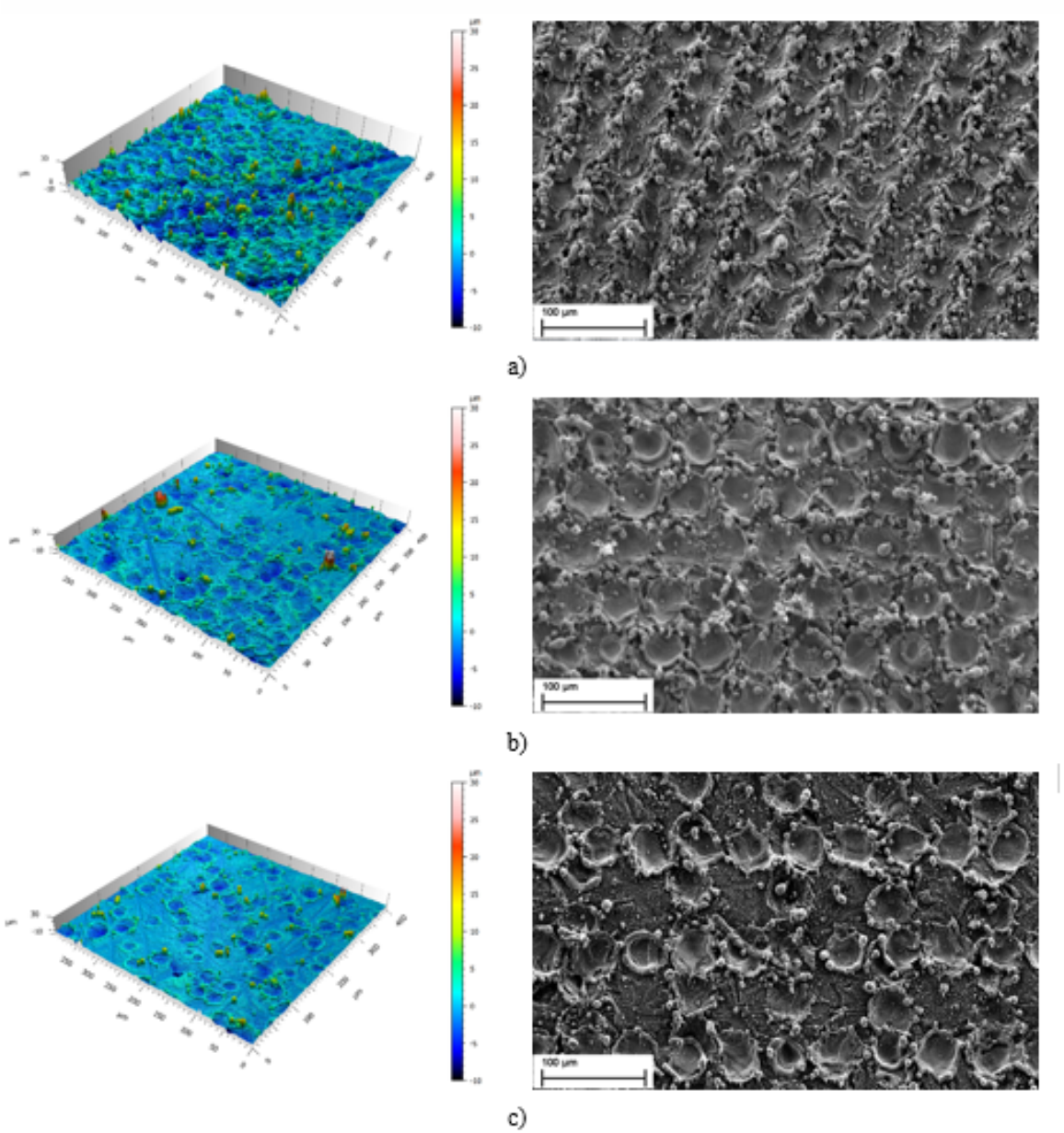

Fig. 4.15 Morphology maps and SEM images of surfaces ablated using a crossed pattern strategy with ED=0.17 J/mm^2 and a) H=25 μm, b) H=50 μm and c) H=100 μm [149]

of the surface is complete. Instead, in the H=100 μm case a wide portion of the surface remains untreated because of the poor interaction between adjacent craters.

Moving to consider the images corresponding to the ED=1.71 J/mm^2 case (Fig. 4.16), the first and the second one (H=25 μm and H=50 μm, respectively) do not exhibit any particular shape in terms of peaks and valleys, because of both the fact that the width of every groove is significantly higher than the hatch distance and the stacking of the debris ejected during the

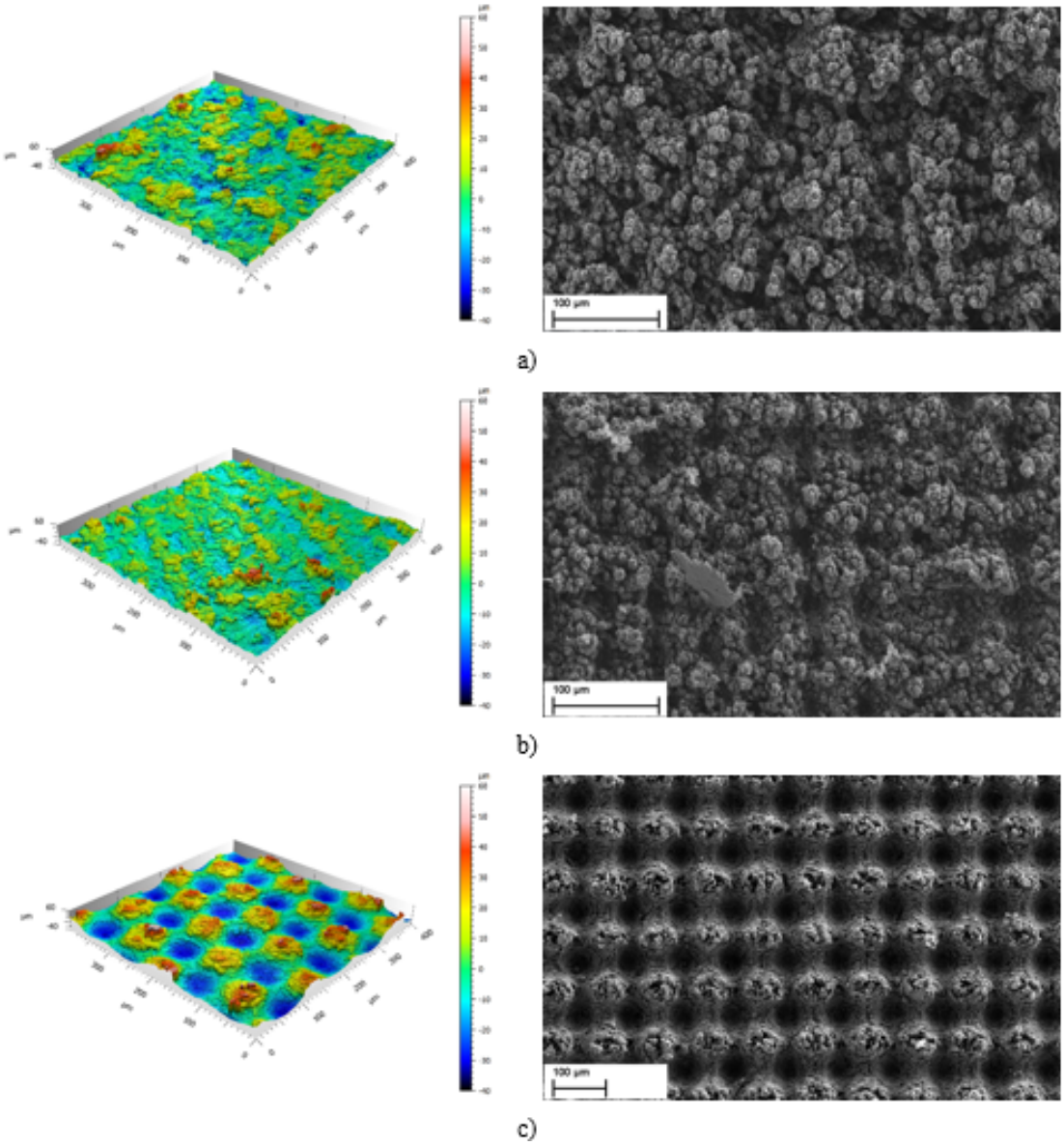

Fig. 4.16 Morphology maps and SEM images of surfaces ablated using a crossed pattern strategy with ED=1.71 J/mm^2 and a) H=25 μm, b) H=50 μm and c) H=100 μm [149]

treatment due to the material ablation. When H becomes significantly higher than the spot diameter (H=100 μm), there is not any trace of overlay and the surface appears organized in a sort of grid generated by the presence of high peaks, in the untreated zones where the ablated material is stacked, and deep valleys caused by the overlap of two perpendicular laser beam trajectories.

Finally considering the high ED treated samples presented in Fig. 4.17 , it is worth noting the high accumulation of the solidified melted material expelled during the treatment due to

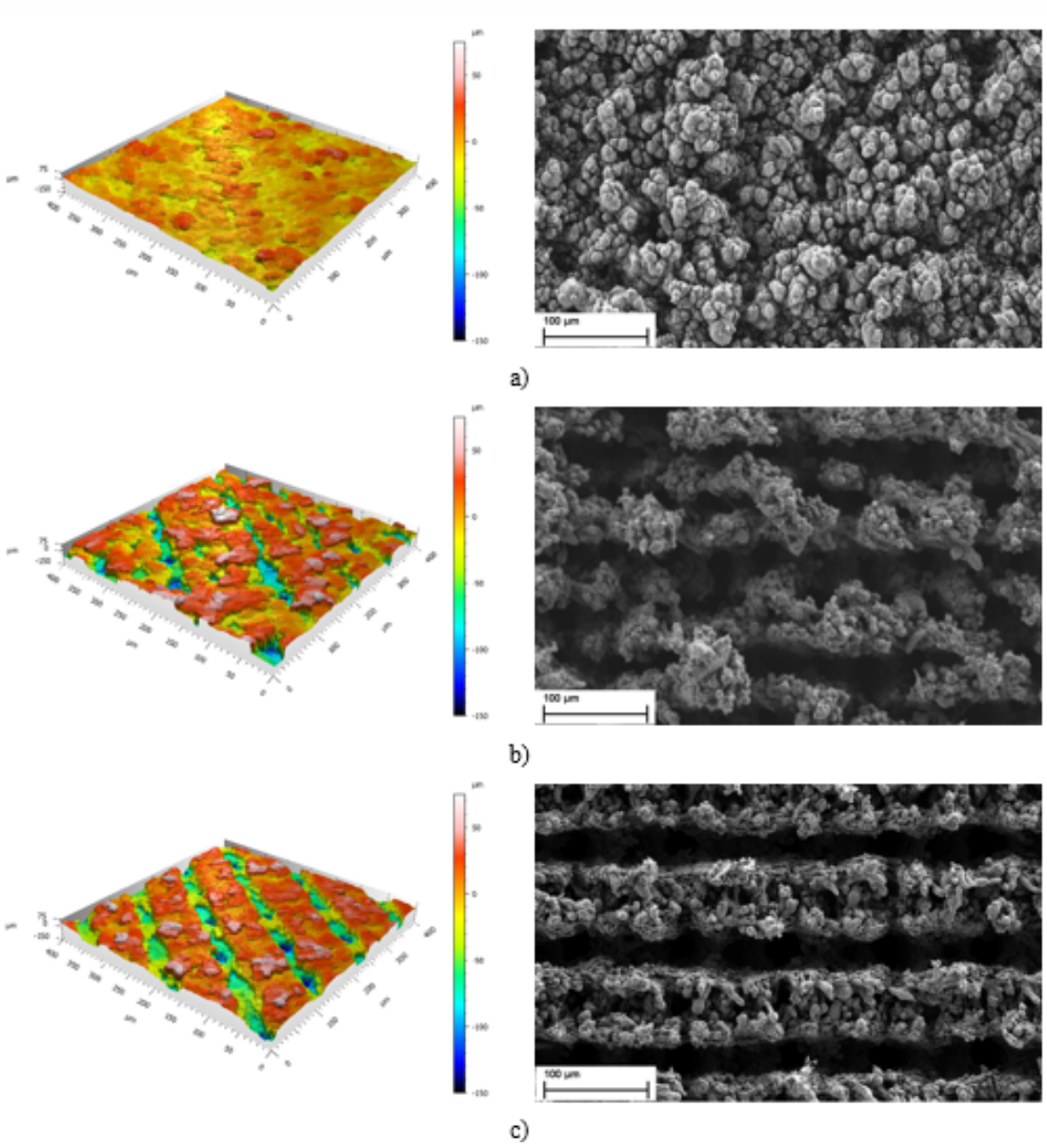

Fig. 4.17 Morphology maps and SEM images of surfaces ablated using a crossed pattern strategy with ED=3.81 J/mm^2 and a) H=25 μm, b) H=50 μm and c) H=100 μm [149]

the high amount of energy provided to the surface. As a direct consequence, although the laser scan is performed along two perpendicular directions, the final shape of the surface is essentially the result of the ablation carried out along the last followed direction. This is especially pronounced for the H=100 μm case, while when the hatch distance value is lower the grooves appear partially hidden by the debris. Additionally, the high ED value employed produces a surface characterized by remarkably deep valleys, which justifies both the high

surface roughness S_a and the very low surface skewness S_{sk} found for the H=100 μm set when ED is higher than 3 J/mm^2.

4.3 EDS measurements

In order to integrate the XPS analysis already performed in the aforementioned work by Alfano *et al* [138], some Energy Dispersion X-ray Spectrometry (EDS) measurements are carried out exploiting the capability of the SEM instrument. The results concerning the atomic content of oxygen and aluminium over AA6082-T6 aluminium surfaces ablated using different levels of ED are shown in Fig. 4.18.

The results demonstrate how the atomic content of oxygen seems increasing as ED grows up, while the aluminium content is characterized by the inverse trend. This seems to go towards the direction of the known phenomenon related to the formation of a thick oxide layer over the surface, which contributes to the enhancement of the wettability properties of the surface. In particular, these trends seem to be more marked as the hatch distance value decreases, which appears meaningful since the lower is H, the higher is the amount of area interested by the treatment. The maximum of the oxygen content occurs in correspondence of the same energy density value (3.81 J/mm^2) which induces the lowest content of alumininum, while a futher increase of the ED causes a slight inversion of the trend.

The presence of other contaminants (like Si, Mg and Mn) is detected, but their atomic content is so low (under 1%) to be considered negligible.

4.4 Contact angle measurements

In order to verify which is the influence of using the laser ablation as a pre-treatment for bonding purposes, an assessment of the changing induced over the wettability conditions is performed by means of a series of static water contact angle measurements upon surfaces laser-treated with different levels of energy density. To take into account the possible effect due to the direction of the grooves over the spread of the water drop (anisotropic wetting), the measurements are repeated in two different directions, according to Fig. 4.19, in presence of the unidirectional treatments.

The results are summarized in Fig. 4.20.

From the simply degreased and the grit blasted surfaces, where the average contact angle value is equal to 98° and 115°, respectively, showing an increase of the original hydrophobic status of the surface which appears consistent with the Wenzel's model, a decline of the contact angle towards values lower than 90° is observed in presence of the lowest tested

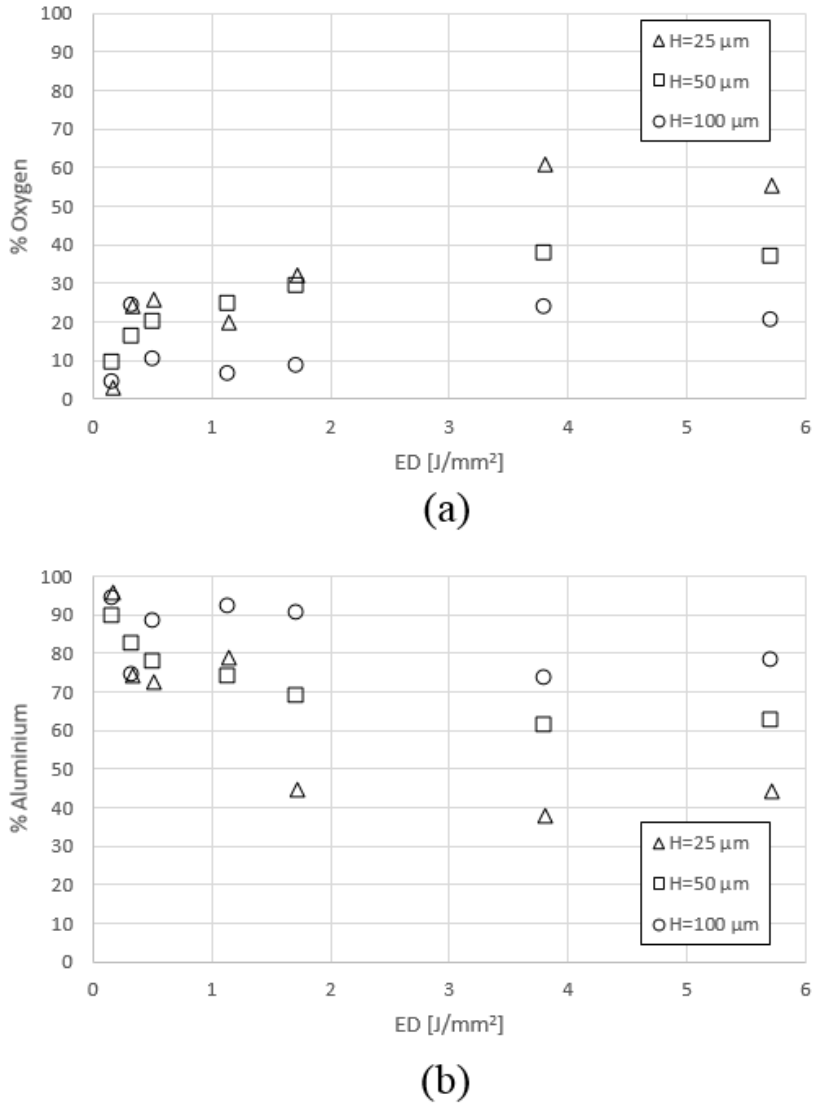

Fig. 4.18 EDS measurements concerning the atomic content of oxygen (a) and aluminium (b) of laser pre-treated AA6082-T6 aluminium surfaces in function of the energy density ED of the laser ablation

energy density laser ablation treatment (ED=0.17 J/mm^2). It is interesting to notice the influence of the hatch distance on the wettability, with the highest superimposition level between adjacent grooves producing the lowest value of contact angle because of the lower amount of untreated area with respect to the H=50 μm and H=100 μm surfaces and therefore the more marked difference from the original surface. Rising up the energy density value until 0.51 J/mm^2, the contact angle results impossible to be evaluated because the drop of water completely spreads over the surface, along the grooves direction, resulting in a fully

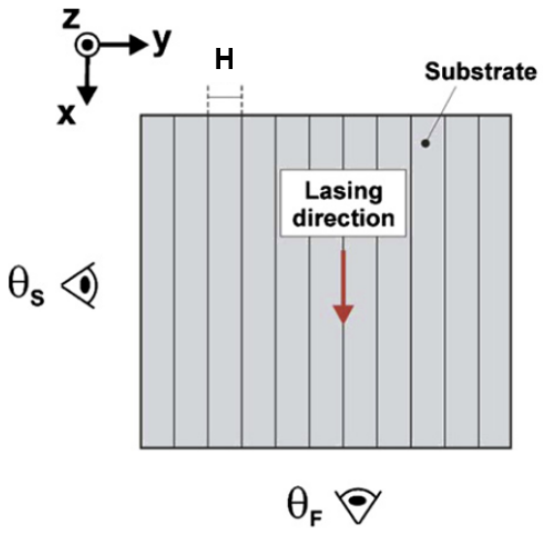

Fig. 4.19 Definition of the contact angles measured in the side (θ_S) and the front (θ_F directions, adapted from [137]

hydrophilic surface which does not behave according to the Wenzel's model. The described trend is regardless from the laser scanning direction.

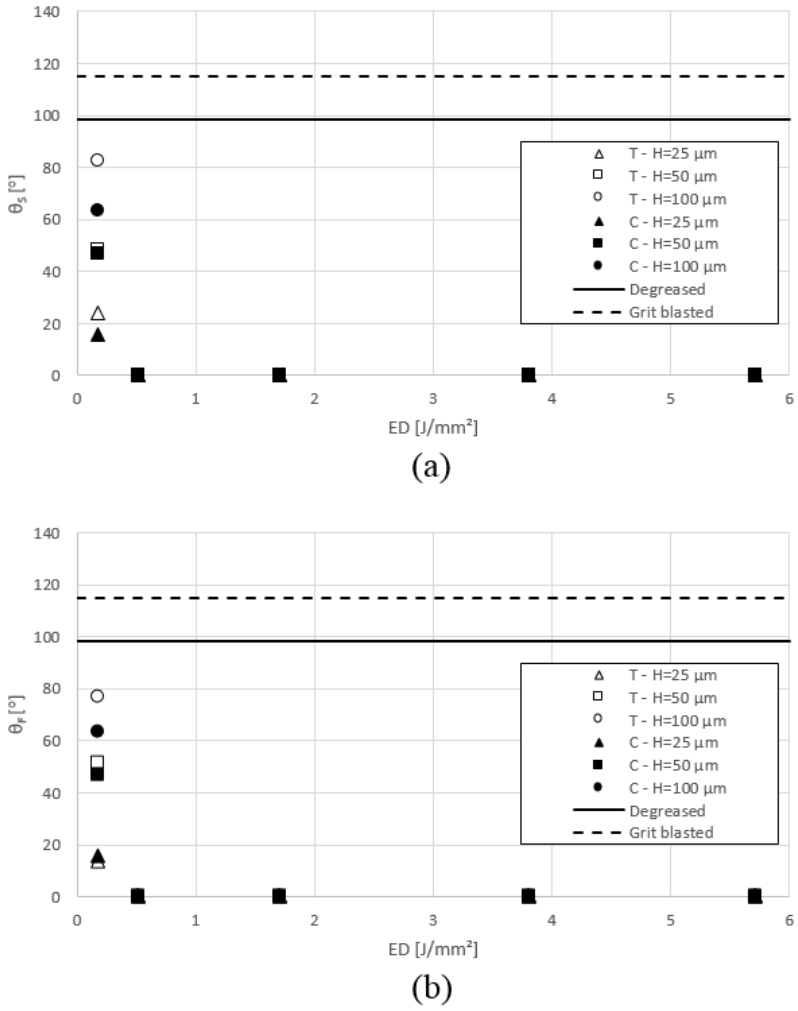

Fig. 4.20 Contact angle measurements in function of the energy density ED of the laser ablation process: (a) along the side direction; (b) along the front direction

Chapter 5

Mechanical characterization of laser ablated bonded joints

The optimization of the laser ablation process for surfaces aimed to be bonded together for food industrial applications is conduced with respect to the mechanical performances of the bonded joints. According to the aim of the thesis, the material chosen to be tested is AA6082-T6 aluminium. The mechanical characterization is carried out by means of the evaluation of the Mode I strain energy release rate of the joints, measured through Double Cantilever Beam (DCB) tests exploring a wide range of laser process parameters and diversifying both the direction of treatment and the test conditions (quasi static tests, fatigue tests, post-aging tests). Part of the results here exposed has been published in [154], [149] and [158].

5.1 Starting points

The work described in [155] and in [156], already used as a starting point for the surface assessment of the laser ablated substrates, is very useful as a starting point even for the mechanical characterization of the joints realized with them. In particular, the authors tensile tested some AA6082-T6 aluminium butt joints bonded with Loctite Hysol 9466, whose scheme is represented in Fig. 5.1.

The joint strength results in function of the energy density ED used to pre-treat the bonding surfaces are proposed in Fig. 5.2. From it, it is apparent that an initial threshold of energy density (approximately placed between 0.215 J/mm^2 and 0.438 J/mm^2) has to be overstepped in order to notice significant increases in the joint strength with respect to the untreated case. However, after reaching a maximum in correspondence of ED=0.438 J/mm^2 where the joint strength is higher by a factor of 30% than the untreated value, the curve

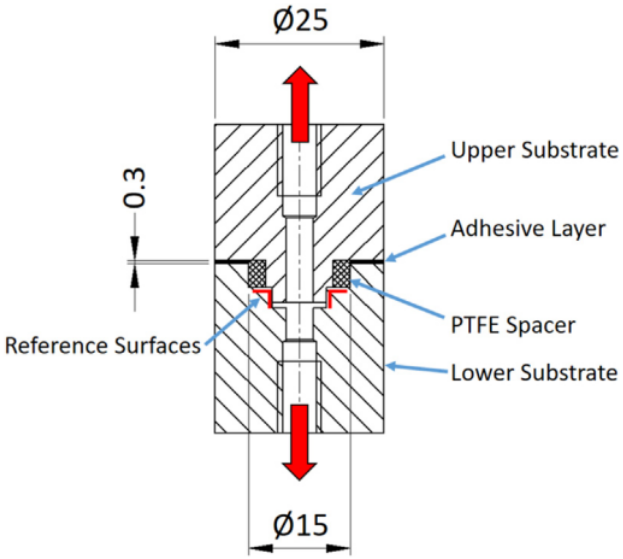

Fig. 5.1 Butt joint geometry tested in [156]

representing the joint strength suddenly plummets with a further increase of the ED level. A slight recovery occurs when the energy density is higher than about 4 J/mm^2.

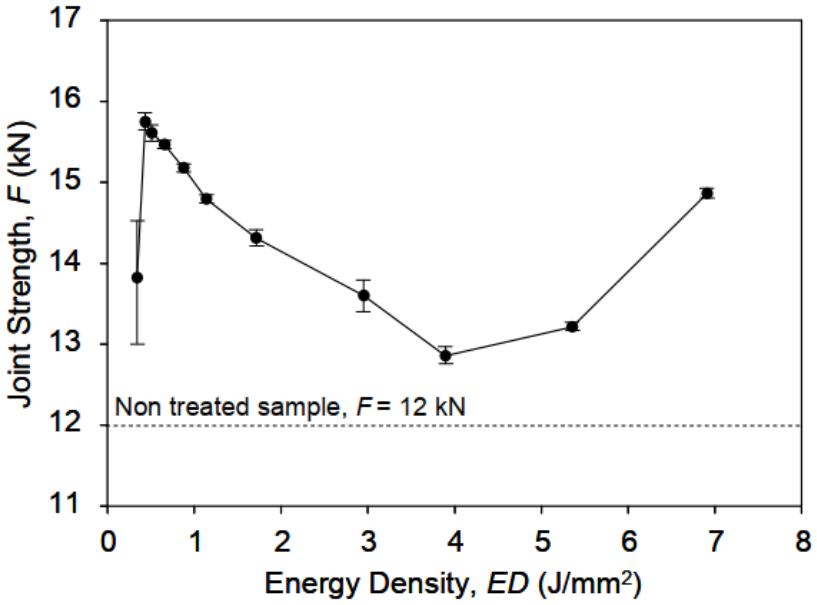

Fig. 5.2 Trend of the joint strength vs ED evaluated with tensile tests on aluminum AA6082-T6 butt joints, being the hatch distance H fixed to 0.075 mm [155]

To better understand the reasons for the peculiar trend of joint strength, a comparison between Fig. 5.2 and Fig. 4.3 where the trend of the measured surface roughness with ED

was plotted is meaningful. It clearly highlights that a progressive increase of the surface roughness does not offer any assurance concerning the obtainment of an analogue and concurrent progressive increase of the joint strength and instead is the main responsible for the suddenly decrease of the strength. In fact, by observing the fracture surfaces it can be noticed that higher the roughness, higher the detectable amount of air bubbles remained entrapped within the adhesive due to the surface morphology which does not allow the adhesive to completely flow into the grooves. Some images of the fracture surfaces, revealing also the change of the failure mode from adhesive (in the joint ablated with a very low ED value) to cohesive (in the higher energy laser ablated joints), are proposed in Fig. 5.3.

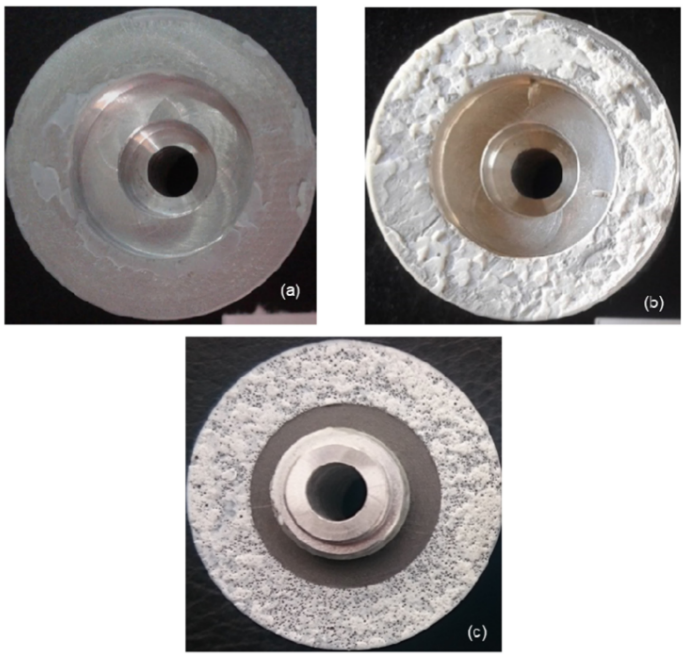

Fig. 5.3 Fracture surfaces of aluminium butt joints ablated with several levels of energy density: (a) ED=0.33 J/mm^2 (b) ED=0.66 J/mm^2 (c) ED=3.89 J/mm^2 [156]

As a concluding result, it was possible to describe the trend of the joint strength in function of the surface roughness (visible in Fig. 5.4), removing the dependence from the laser parameters employed to realize the pattern.

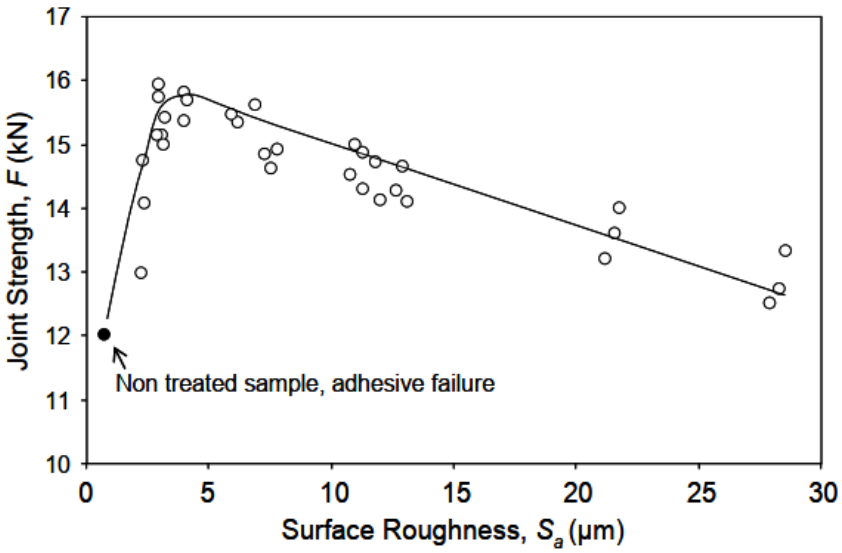

Fig. 5.4 Trend of AA6082-T6 aluminium butt joint strength in function of the surface roughness [155]

5.2 Quasi static characterization of the joints as produced

Firstly, the experimental campaign aimed at evaluating the influence of the laser ablation process parameter configurations over the mechanical response exhibited during quasi-static tests by the bonded joints is described. The materials and methods employed for the production and the testing of the specimens was described in Chapter 3.

5.2.1 Test results

In this section the results of the DCB tests are discussed with the intent of relating the value of fracture toughness evaluated with the mechanical test with the results of the morphological analysis of the surface and with the energy density and hatch distance parameters used during the ablation process. Moreover, the influence of the laser scanning direction over the mechanical response of the bonded joints is addressed.

Firstly, the focus is placed over the unidirectional results (T and L patterns). Because it is reasonable to assume that the behaviors of the T and L joints are similar to each other, only one value of hatch distance (H=50 μm) is selected for the assessment of the L joints, with the intent of not excessively burdening the experimental campaign. In Fig. 5.5 the critical Mode I strain energy release rate G_{Ic} values from DCB tests on T joints are plotted against the surface roughness S_a values, discussed in section 4.2. The values of S_a plotted are obtained

evaluating the average of the surface roughness values measured with the laser profilometer on surfaces treated with the same laser parameters (see Fig. 4.9).

First of all, the basic assumption related to the fact that the fracture toughness of the L samples is in line with the corresponding T samples is confirmed. This suggests that, being fixed the surface morphology induced by the laser ablation, since the adhesive is tensile strained, the interlocking effect provided by rotating the textures by 90° is reasonably the same of the texture perpendicular to the crack propagation direction. Then, it is possible to notice how the laser ablated joints reaches, in some cases, values of G_{Ic} higher up to 65% than the one of the grit blasted joint. Moreover, G_{Ic} apparently seems to be influenced by the hatch distance, even if the trend exhibited by the Mode I strain energy release rate as S_a increases is the same regardless from the value of H: G_{Ic} rises up until a maximum value, different depending on the value of H, and then decreases as S_a further increases.

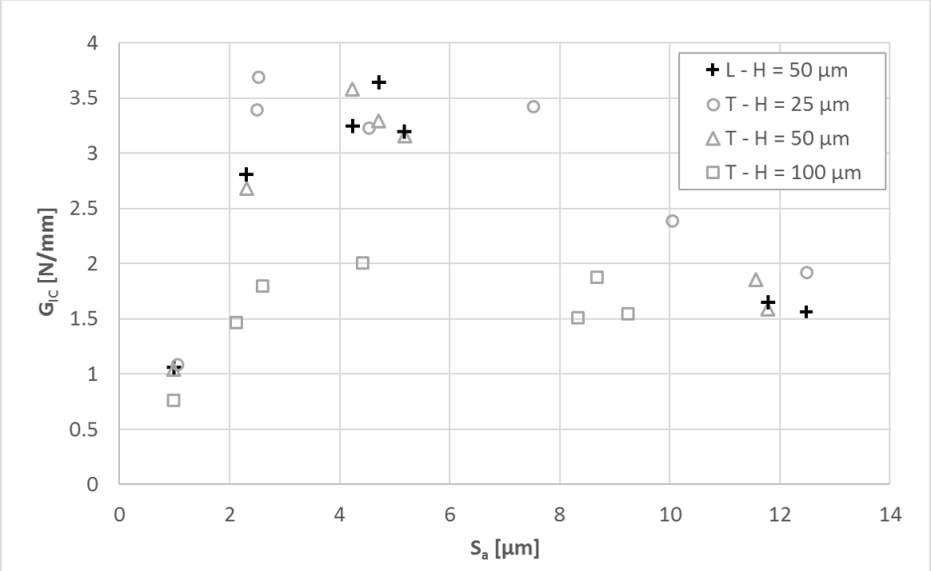

Fig. 5.5 Critical Mode I strain energy release rate (G_{Ic}) vs. surface roughness (S_a) plot for laser ablated joints obtained with a T/L pattern and reference bonded joints [149]

Approximately the same trend is encountered by analyzing the plot of G_{Ic} against the energy density ED values, Fig. 5.6.

In agreement with the S_a vs. ED trend (Fig. 4.9) and with the G_{Ic} vs. S_a trend (Fig. 5.5), the Mode I strain energy release rate increases as ED grows up until it peaks in a narrow range of values of ED, after which it becomes decreasing as ED further rises up. With respect to the influence of the hatch distance, it is possible to notice that, when H is much higher than the spot diameter ϕ_s, the resulting values of G_{Ic} are significantly lower than the ones belonging to joints characterized by hatch distance values lower or slightly higher than ϕ_s.

In this latter case, the hatch distance does not seem to have a particular influence on the mechanical toughness, resulting in values of the strain energy release rate similar to each other regardless of the specific value of H.

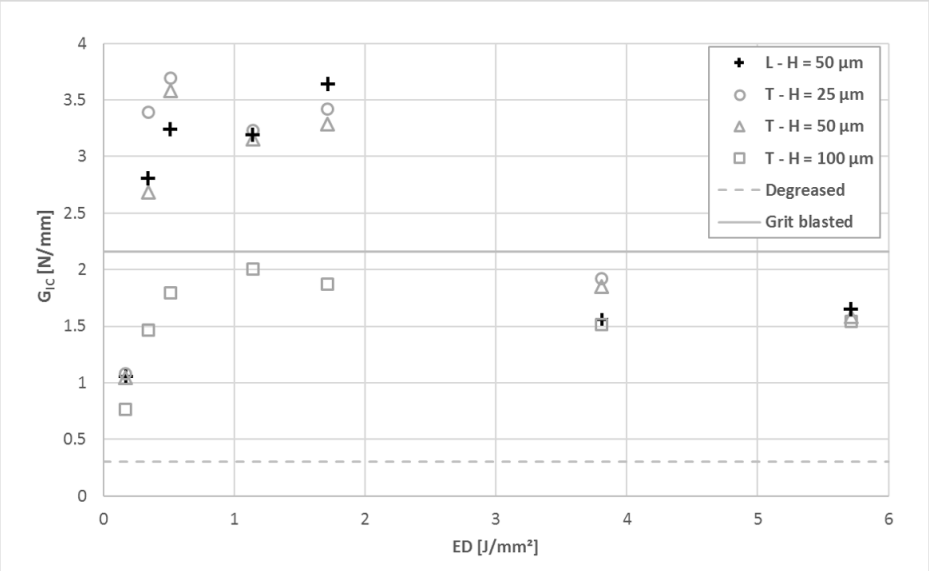

Fig. 5.6 Critical Mode I strain energy release rate (G_{Ic}) vs. energy density (ED) plot for laser ablated joints obtained with T/L pattern. The values of G_{Ic} belonging to the reference joints are also presented for comparison[149]

Analyzing the fracture surfaces of T joints with the optical microscopy, it is possible to notice a peculiar behavior according to the level of energy density at which the laser ablation of the bonded surface is performed. To better illustrate the phenomenon, Figs. from 5.7 to 5.11 provide a photograph of the fracture surface accompanied by the relative shot taken with the microscopy, for surfaces ablated with different process parameters.

As it was possible to notice in previous considerations (see 4.2), when the energy density is very low the treatment is not able to significantly alter the morphological properties of the surface, resulting in a completely adhesive debonding (Fig. 5.7). As ED grows up and H is kept constant at 25 or 50 μm (Figs.from 5.8 to 5.10), the failure mode progressively switches from completely adhesive to completely cohesive, which denotes that the laser ablation succeeds in enhancing the surface morphology for the purpose of bonding. With respect to the influence of H over the adhesion phenomenon, a treatment carried out with a value of hatch distance significantly higher than the spot diameter ϕ_s carries to an increase of the surface area of the joint not involved in the laser ablation. This goes towards an increase of the amount of surface which undergoes adhesive failure, resulting thereby in a reduction of the toughness with respect to a joint with the whole surface ablated, being equal the energy

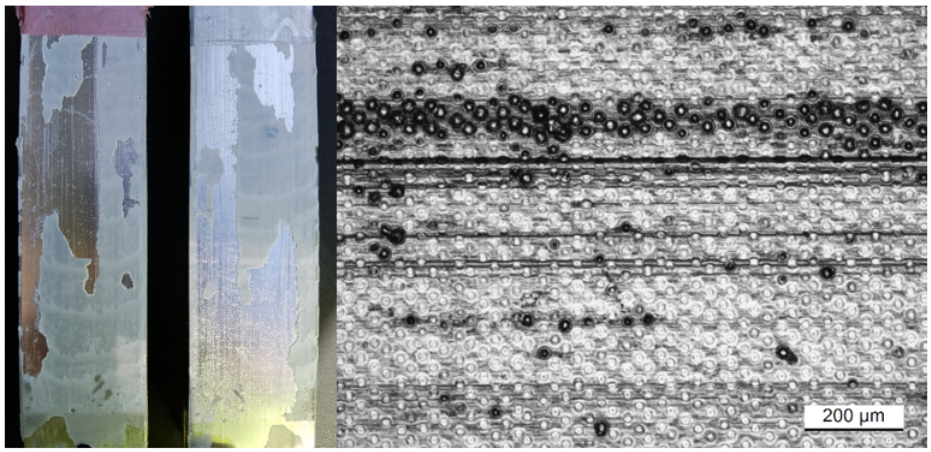

Fig. 5.7 Fracture surface of a T-joint ablated with ED=0.17 J/mm^2 and H=25 μm [154]

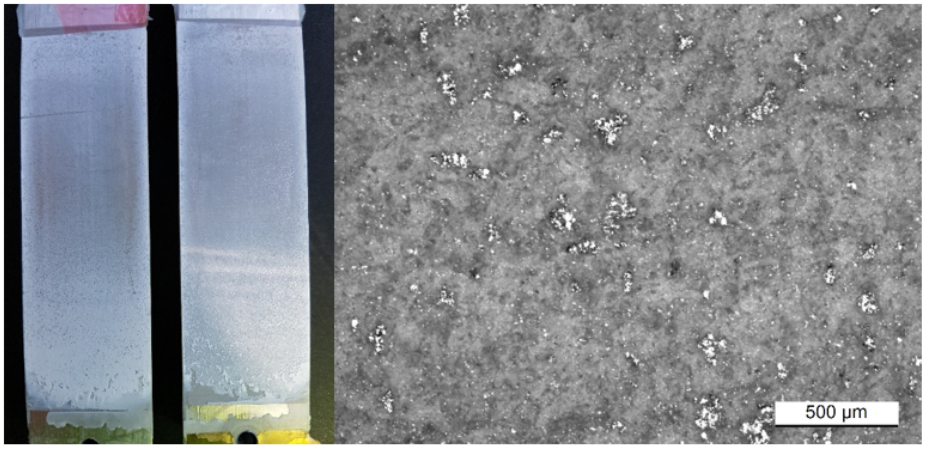

Fig. 5.8 Fracture surface of a T-joint ablated with ED=0.51 J/mm^2 and H=50 μm [154]

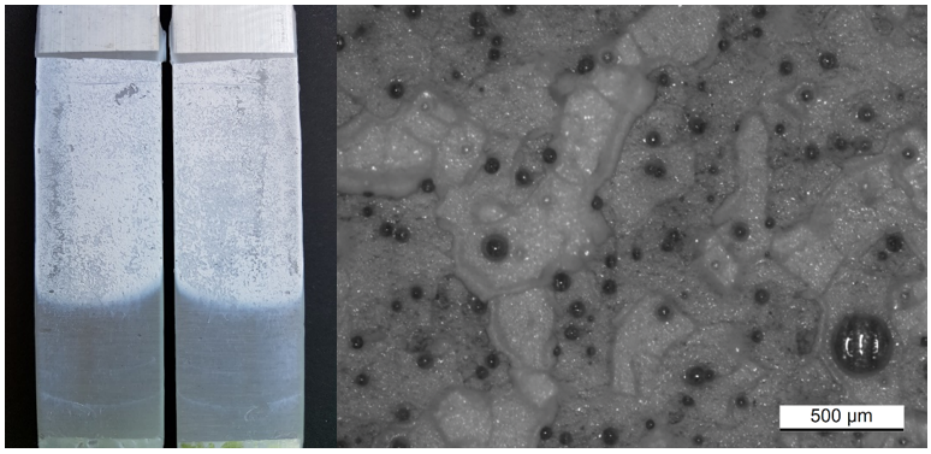

Fig. 5.9 Fracture surface of a T-joint ablated with ED=1.14 J/mm^2 and H=50 μm [154]

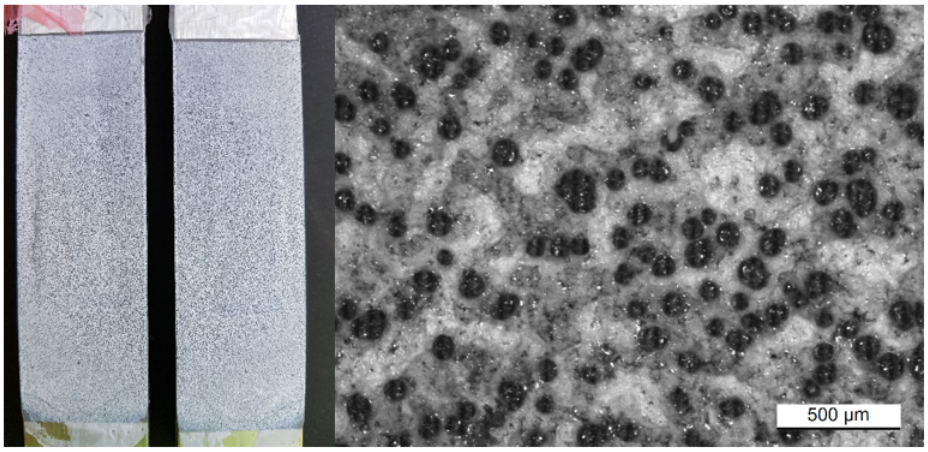

Fig. 5.10 Fracture surface of a T-joint ablated with ED=3.81 J/mm^2 and H=50 μm [154]

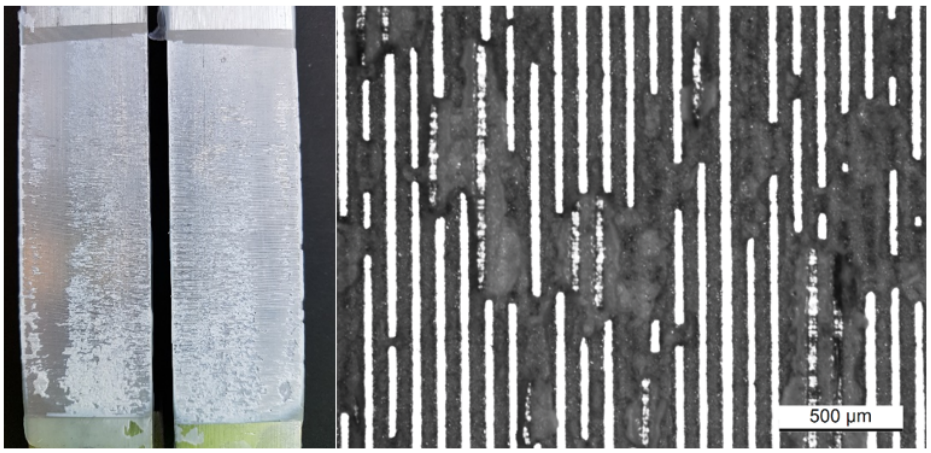

Fig. 5.11 Fracture surface of a T-joint ablated with ED=1.71 J/mm^2 and H=100 μm [154]

density. This appears evident looking at the specimen depicted in Fig. 5.11, where a mixed adhesive/cohesive failure occurred.

Considering the images taken by means of the microscopy, it is possible to state that a certain amount of air remains entrapped within the laser induced grooves during the adhesive deposition, resulting in a presence of air bubbles which, being fixed the hatch distance, is much more relevant as the energy density and thus the depth of the grooves increases (Figs. from 5.8 to 5.10). The increase of the air trapped within the grooves as ED grows up well explains the trend exhibited by the G_{Ic} vs. ED curve after a certain value of energy density, which depends from the hatch distance value. When ED is lower than that threshold value, the strain energy release rate rises as ED grows up because the enhancement in the interlocking effect provided by the grooves prevails over the progressive increase of the trapped air, which

instead becomes the leading phenomenon when ED overtakes the threshold value at which G_{Ic} reaches its maximum value.

To better understand the relationship between the energy density and the entrapment of air within the grooves, it is useful to refer to Fig. 4.10, in which the Pearson's first coefficient of skewness S_{sk} representing the distribution of peaks and valleys with respect to the mean plane of a surface is plotted against the energy density ED, and to relate S_{sk} with G_{Ic}, Fig. 5.12.

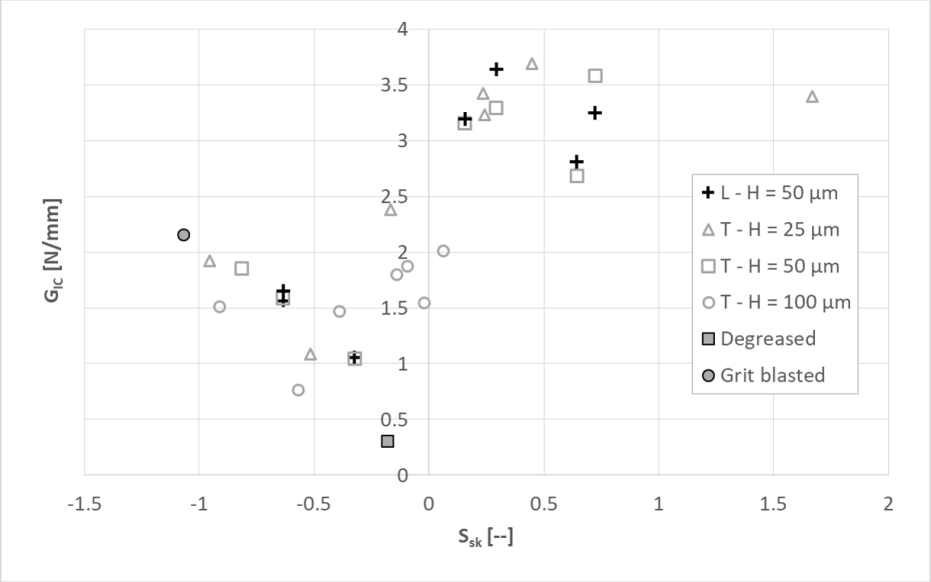

Fig. 5.12 Critical Mode I strain energy release rate (G_{Ic}) vs. surface skewness (S_{sk}) plot for laser ablated joints obtained with a T/L pattern and reference bonded joints [149]

Although the data dispersion is considerable, it is possible to notice that G_{Ic} tends to increase with S_{sk}, which seems reasonable since the prevalence of peaks with respect to the mean plane of the surface promotes the occurrence of an interlocking mechanism between adhesive and surface, which directly affects the mechanical toughness of the joint. It is here more appreciable what already stated about the joints characterized by an high value of hatch distance (H=100 μm): because of the lower amount of surface area involved in the laser ablation treatment, the valleys prevail over the peaks with respect to the mean plane and an adhesive failure occurs in the not treated areas, resulting in a general lowering of the toughness values of the joint. Moreover, by means of a crossed comparison it is possible to investigate how the samples with the lower values of S_{sk} are also the ones in which the presence of air bubbles within the grooves is much relevant, since the depth of the valleys is more pronounced than the height of the peaks and therefore the adhesive does not succeed in deeply penetrating into the groove bottom. This phenomenon is the main responsible for the

decrease of G_{Ic} when the energy density ED becomes greater than a threshold, over which the values of S_{sk} are lower than zero (Fig. 4.10).

Moving to consider the effect provided to the mechanical toughness by the crossed pattern, a comparison with the T-samples results (chosen as representative of the unidirectional texture) is offered in Fig. 5.13 with refer to the trend of G_{Ic} in function of S_a.

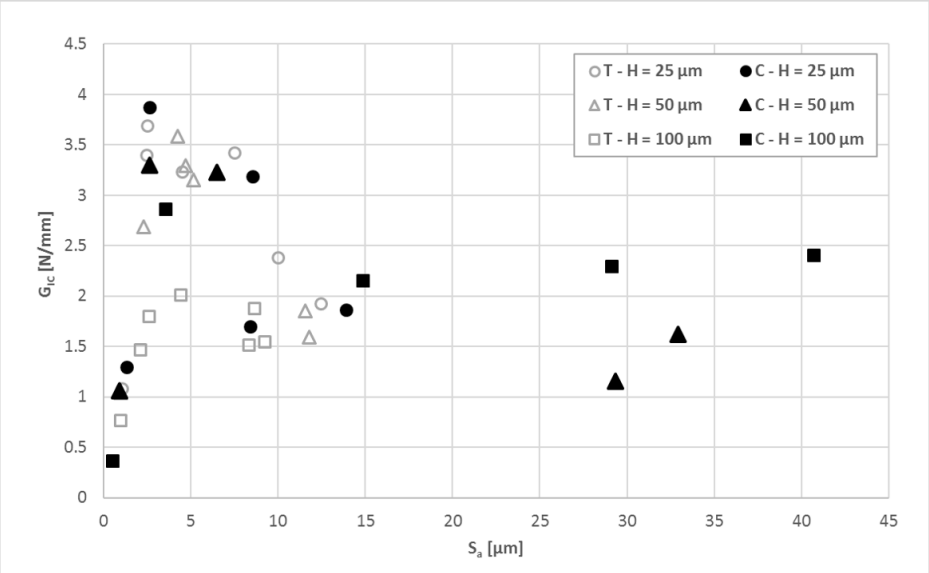

Fig. 5.13 Critical Mode I strain energy release rate (G_{Ic}) vs. surface roughness (S_a) plot for laser ablated (T and C pattern) and reference bonded joints [149]

From the graph, it is apparent that the crossed pattern treatment generates extremely high values of surface roughness compared with the T-samples results, but at the same time this improvement in roughness does not correspond in an analogue increment of toughness. In fact, it is immediately perceptible looking at Fig. 5.13 how the values of the critical Mode I strain energy release rate of the C-samples presenting values of roughness equal or higher than 30 μm is approximately the same belonging to T-samples whose roughness is 80% lower than S_a of C-samples. A comparison between the trends of G_{Ic} in function of the energy density ED for the T and the C-joints, respectively, is showed in Fig. 5.14.

The trend exhibited by the C-samples is approximately the same previously analyzed for the unidirectional case: regardless of the hatch distance value, the critical Mode I strain energy release rate of the C-joints seems to progressively increase as ED grows up, until reaching a maximum in correspondence of ED=0.51 J/mm^2. Similarly to the T-samples case previously studied, after this threshold value G_{Ic} descends as ED further grows up. The differences between the values of G_{Ic} achieved by means of the C pattern and the ones obtained by using the T pattern are not remarkable, the only exception being the fact that the

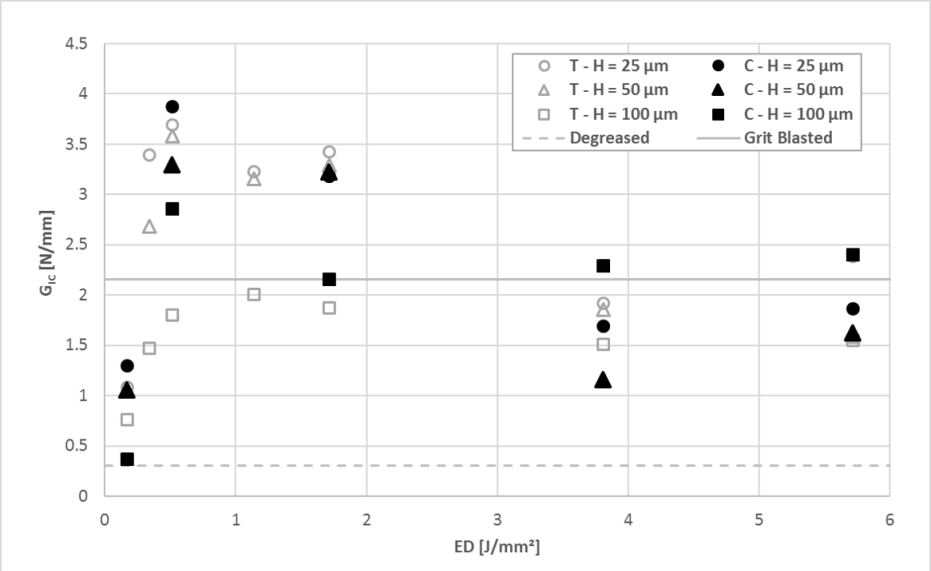

Fig. 5.14 Critical Mode I strain energy release rate (G_{Ic}) vs. energy density (ED) plot for laser ablated joints (T and C pattern). The values of G_{Ic} belonging to the reference joints are also presented for comparison [149]

sensitivity of the toughness to the hatch distance value seems less marked in the C-samples case than in the T-joints. In particular, the H=100 μm set is not so segregated with respect to the other two sets as it is in the T-samples case, so much so an overtune with respect to the usual hierarchy between the sets with low and high values of H occurs in correspondence of ED=3.81 J/mm^2. The main reasons for the lowering of the sensitivity of the fracture toughness to the hatch distance are to be found in the fact that even when the hatch distance is higher than the spot diameter value the C-samples present a lower amount of untreated area with respect to the corresponding T-joints, resulting in an increase of the load bearing area and in a higher benefit given to the adhesion.

In Fig. 5.15 the relation between the fracture toughness and the Pearson's first coefficient of skewness, representative of the distribution of the peaks and valleys with respect to the mean plane, is plotted.

Even in this case the data dispersion is very significant, but similarly to the T-samples case it is possible to identify an approximately increasing trend of G_{Ic} with the skewness coefficient S_{sk}, which means that higher is the height of the peaks of the surface with respect to the depth of the valleys, higher is the fracture toughness of the joint. In order to validate this experimental observation from a statistical point of view, the Pearson's correlation factor, defined as the covariance between two variables and the product of their standard deviations, is evaluated applying it to G_{Ic} and S_{sk}. Given that the coefficient can range between -1 and +1 and the probability related to the existence of an actual relation between the two

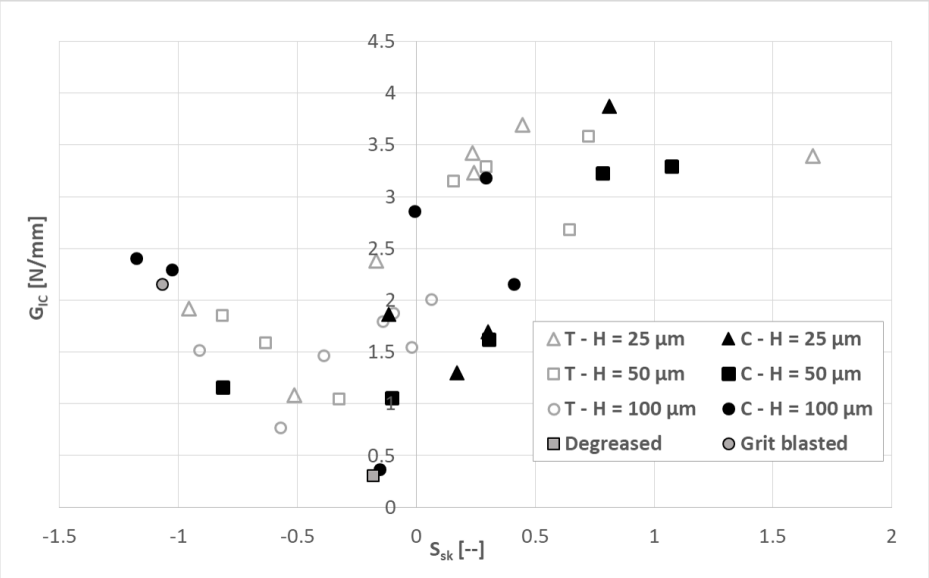

Fig. 5.15 Critical Mode I strain energy release rate (G_{Ic}) vs. surface skewness (S_{sk}) plot for laser ablated (T and C pattern) and reference bonded joints [149]

variables increases if the absolute value of the coefficient does the same, the correlation factor of 0.65 for the data presented in Fig. 5.15 means that a link between G_{Ic} and S_{sk} is statistically quite likely. Moreover, an investigation is conduced about the correlation between the mechanical toughness and the amount of air bubbles remained entrapped within the grooves, which is typical of the surfaces with a low value of the skewness coefficient due to the very deep grooves associated. From Fig. 5.16 to Fig. 5.19 some photographs of the fracture surfaces of the C-joints ablated with a constant H (H=50 μm) and different ED values and the corresponding images taken by means of the 50x optical microscope are juxtaposed.

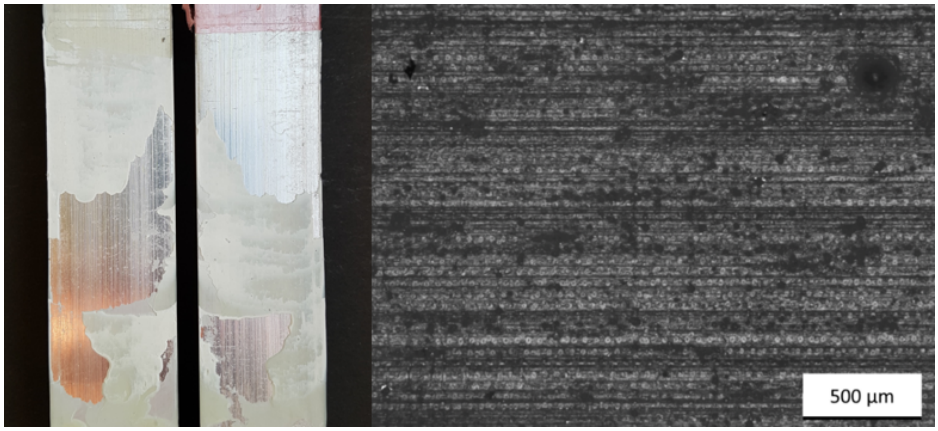

Fig. 5.16 Fracture surface of a C-joint ablated with ED=0.17 J/mm^2 and H=50 μm [149]

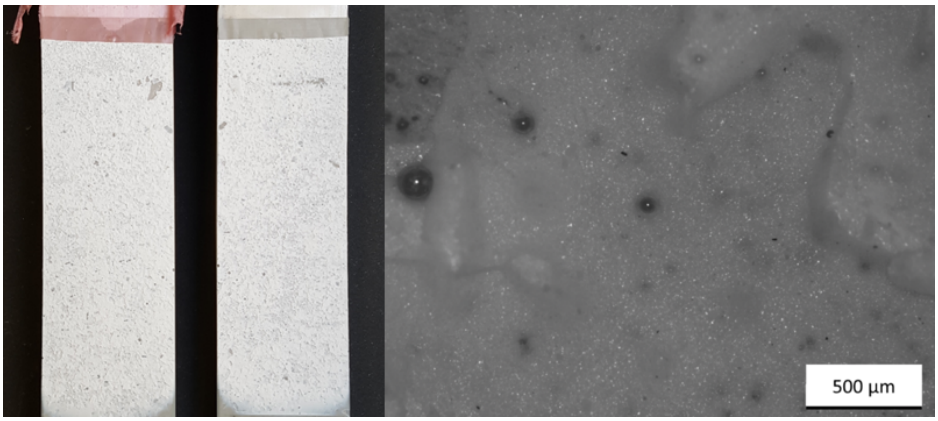

Fig. 5.17 Fracture surface of a C-joint ablated with ED=0.51 J/mm^2 and H=50 μm [149]

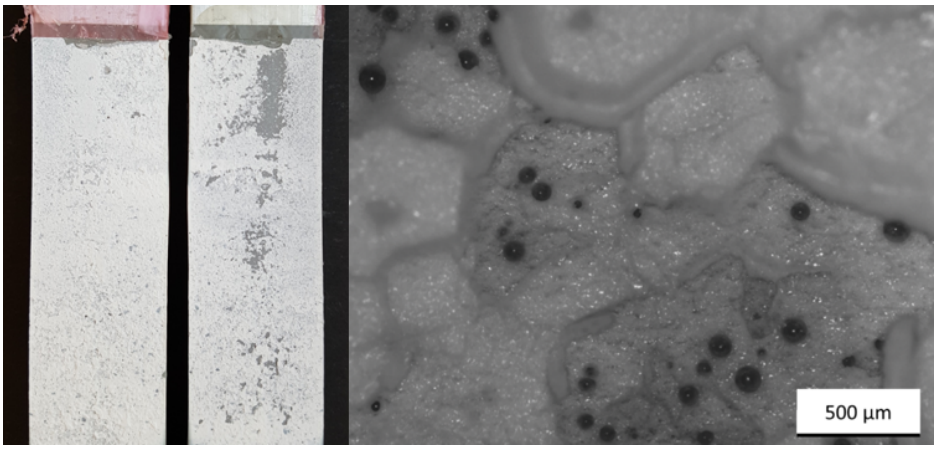

Fig. 5.18 Fracture surface of a C-joint ablated with ED=1.71 J/mm^2 and H=50 μm [149]

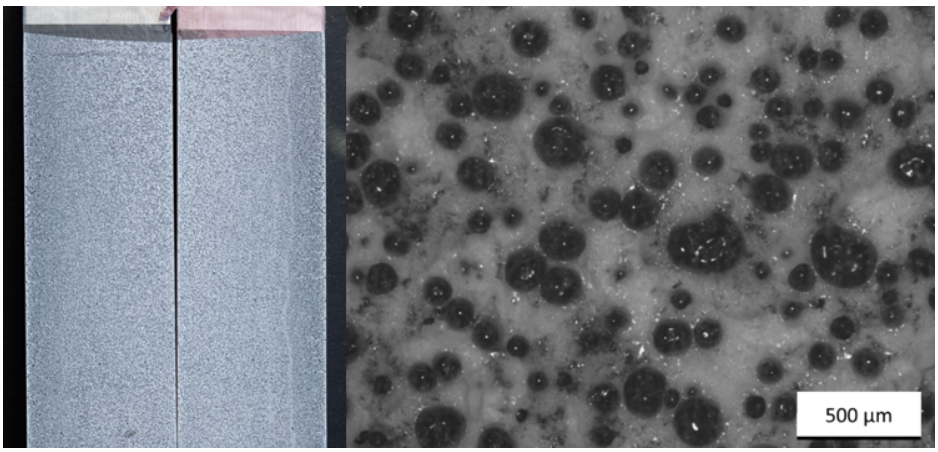

Fig. 5.19 Fracture surface of a C-joint ablated with ED=3.81 J/mm^2 and H=50 μm [149]

An ablation treatment carried out with a very low value of ED (ED=0.17 J/mm^2, Fig. 5.16) even in the C-sample case does not succeed in enhancing the surface morphology, resulting in a failure of the bonded joints in a completely interfacial mode. No air bubble is detected by means of the microscope, probably because the failure must be imputed to the incapability by the surface morphology to significantly enhance the strength of the interface between adhesive and substrate. When the energy density reaches its threshold value (ED=0.51 J/mm^2, Fig. 5.17), a switch of the failure mode from adhesive to cohesive occurs and only a few air bubbles are detectable. Therefore, the mechanical toughness grows up, as it is appreciable in Fig. 5.14. The slight decrease of the fracture toughness value occurring when ED=1.71 J/mm^2 is justified by the observation of Fig. 5.18, in which the fact that the dimension and the number of the air bubbles become more prominent with respect to the previous case is apparent. Moving towards higher energy density values (ED=3.81 J/mm^2, Fig. 5.19), the occurrence of the air bubbles is high, resulting in a significant decrease of the critical Mode I strain energy release rate.

With the aim of assessing the influence of the hatch distance over the air entrapment phenomenon, two additional images are provided, showing the fracture surfaces of C-joints ablated at ED=1.71 J/mm^2, the first one with H=25 μm (Fig. 5.20) and the second one with H=100 μm (Fig. 5.21), to be compared with the appearance of the fracture surface of the bonded joint ablated with H=50 μm, at the same level of ED, depicted in Fig. 5.18.

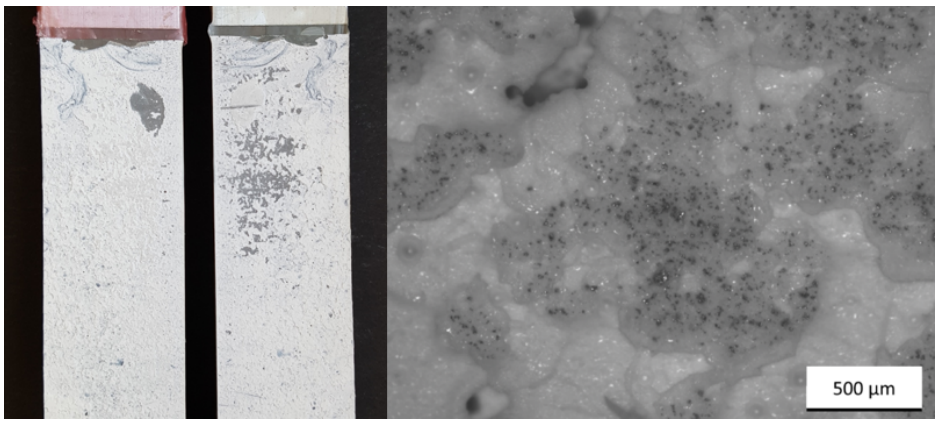

Fig. 5.20 Fracture surface of a C-joint ablated with ED=1.71 J/mm^2 and H=25 μm [149]

From the Fig. 5.20, it is possible to notice how the failure locus is within the adhesive and how a wide amount of small bubbles is detectable all over the surface. With refer to the specimen with H=100 μm in Fig. 5.21, firstly it is worth noting that unlike the corresponding T-joint (Fig. 5.11) the failure mode is cohesive, probably as a result of the lowering of the untreated amount of area provided by the C treatment and of the subsequent enhancement of the adhesion. Nevertheless, the surface morphology already discussed in Chapter 4 and

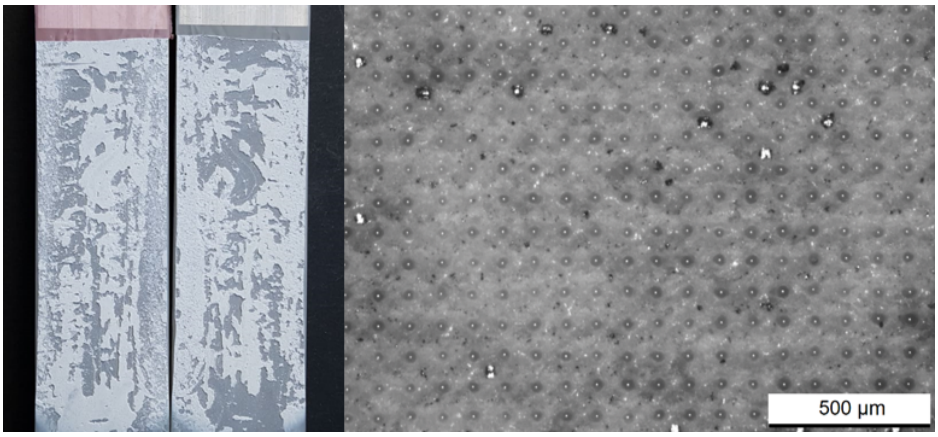

Fig. 5.21 Fracture surface of a C-joint ablated with ED=1.71 J/mm^2 and H=100 μm [149]

showed in Fig. 4.16 induces the entrapment of air in correspondence of the narrow and deep grooves generated by the double scan, resulting in an alignment of the air bubbles with the grooves and in the formation of a sort of regular grid of air inclusions.

5.3 Fatigue characterization

After the quasi-static characterization, the subsequent step is dealing with taking into account the passing of time. To do this, firstly a series of fatigue experiments is set-up with the aim of extending the knowledge acquired about the relation between laser parameters, surface morphology and mechanical behavior of bonded joints by means of loading some tested configurations as similarly as possible to the real application. The methods employed and the results obtained related to the fatigue characterization are exposed in this section.

5.3.1 Variations of the set-up

The fatigue test campaign is based upon the results of the quasi-static experiments exposed in Par. 5.2. Therefore, only a restricted range of laser parameters configurations resulting from the experimental optimization carried out in the previous phase of the work is selected for the fatigue characterization of the bonded joints. The choice is driven by the attempt to explore as better as possible the design space identified with the quasi-static tests and is based on the representativeness of the different grades of toughening provided by the treatment to the bonded joints, resulting in the selection of the ranges listed in Tab. 5.1.

The test methodology adopted for the fatigue test, as well as the dimensions and the procedure for the preparation of the joints, is the same employed for the quasi-static case. The effect of different laser scanning direction is evaluated exclusively for the T and the C-pattern

Table 5.1 Laser parameters employed for the treatment of the joints aimed to be fatigue tested

Process parameter	Value
Laser nominal average power P_{ave}	6-12-18 W
Scan speed v	90-300-1000 mm/s
Hatch distance H	50-100 μm
Pulse repetition frequency f_r	20 kHz
Diameter of the spot ϕ_s	35 μm

configurations. Even in this case, the simply degreased and the grit blasted specimens, produced as described in Par. 3.3.1, are realized.

5.3.2 Fatigue test results

The results of the fatigue tests are presented in terms of crack growth rate, da/dN, in function of the range of Mode I strain energy release rate within a cycle. The data obtained from the different sets of specimens are showed separately for a better comprehension. Firstly, the results related from the T-samples with a value of hatch distance H=50 μm are proposed. Fig. 5.22 shows the trend of the crack growth rate associated to both the reference specimens and the lowest energy density laser treated sample (ED=0.17 J/mm^2).

It is noticeable how the slopes of the curves referred to the degreased and the grit blasted specimens seem very similar to each other, although the value of ΔG required for the crack propagation in the grit blasted specimen, keeping fixed the crack growth rate, is considerably higher than the corresponding value of the degreased sample. Moreover, considering the laser ablated joint curve, when the crack growth rate oversteps 1.9e-4 mm/cycle the values of ΔG become slightly bigger than the ones of the degreased sample, which however achieves crack growth rates much higher. In Fig. 5.23, the results related to the other tested T-specimens belonging to the H=50 μm set are shown.

Although all the data in Fig. 5.23 appear gathered around the grit blasted sample curve and it is not easy to make significant distinctions between the fatigue behaviors of the different specimens, it is however possible to rank the laser configurations employed according to their capability to slightly enhance the value of ΔG with respect to the one exhibited by the grit blasted specimen, being equal the crack growth rate. Analyzing the graph following this approach, it is possible to notice how the highest energy density laser ablated joint presents values of ΔG slightly lower than the ones of the grit blasted specimen and the same trend

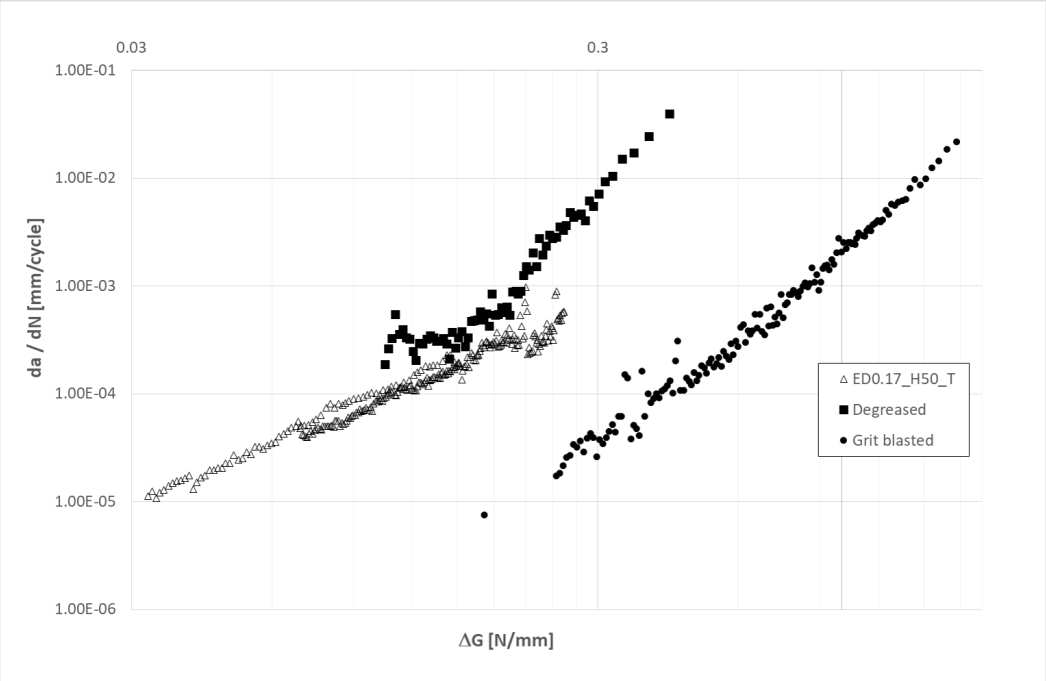

Fig. 5.22 Crack growth rate vs ΔG resulting from a fatigue test over the simply degreased, the grit blasted and the laser ablated T-sample with ED=0.17 J/mm^2 and H=50 μm [158]

is found for the curve related to the ED=3.81 J/mm^2 set. Considering the ED=0.34 J/mm^2 data, they appear to be overlapped to the grit blasted joint curve when the crack growth rate is not too high before increasing with da/dN. The improvement brought by the three lowest energy density treated samples to the ΔG value is quite low but discernible. With the intent of quantitatively validating these remarks, the coefficients of the Paris' law [159], presented in Eq. 5.1, are evaluated by means of a power law regression carried out for every experimental curve.

$$\frac{da}{dN} = C(\Delta G)^m \tag{5.1}$$

These coefficients, namely the intercept C and the slope m of the aforementioned regression curves, are collected in Tab. 5.2.

The values of the slopes summarized in Tab. 5.2 are not very different to each other, with the exception of the ED=0.17 J/mm^2 sample which presents a lower value of m. There are more remarkable differences in the value of the intercept C, in particular the intercept C of the curve associated to the simply degreased sample is two order of magnitude higher than the others. The laser ablated joints present values of C which appear consistent with what noticed before about the ranking of the laser parameters configurations according to the comparison with the grit blasted specimen: the two families of joints ablated with ED$\leq$1.71

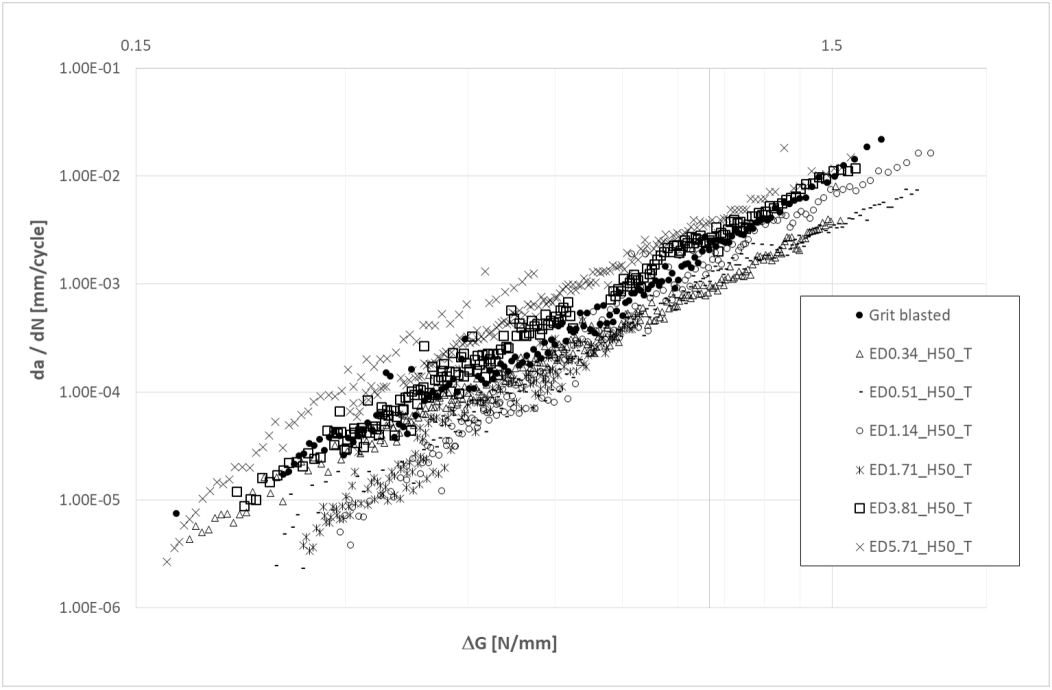

Fig. 5.23 Crack growth rate vs ΔG resulting from a fatigue test over the simply degreased, the grit blasted and the laser ablated T-sample with ED ranging from 0.34 to 5.71 J/mm^2 and H=50 μm [158]

Table 5.2 Coefficients of Paris' law for the sets showed in Fig. 5.22 and 5.23

DCB joint (when laser ablated: T pattern and H=50 μm)	C [mm^{m+1}N^{-m}cycle]	m
Degreased	5.7 10^{-1}	3.76
Grit blasted	2.0 10^{-3}	3.37
ED=0.17 J/mm^2	5.6 10^{-3}	1.79
ED=0.34 J/mm^2	1.0 10^{-3}	2.99
ED=0.51 J/mm^2	1.0 10^{-3}	3.41
ED=1.14 J/mm^2	1.4 10^{-3}	4.24
ED=1.71 J/mm^2	1.4 10^{-3}	4.13
ED=3.81 J/mm^2	2.7 10^{-3}	3.50
ED=5.71 J/mm^2	4.1 10^{-3}	3.29

J/mm^2 and ED>1.71 J/mm^2 have values of C lower and higher, respectively, than the grit blasted sample one.

A visual inspection of the fracture surfaces is useful to understand the failure mode occurring depending on the laser parameter configurations. An overview of photographs of the degreased and grit blasted samples, besides of the laser ablated T-specimens with H=50 μm, is offered in Figs. from 5.24 to 5.32.

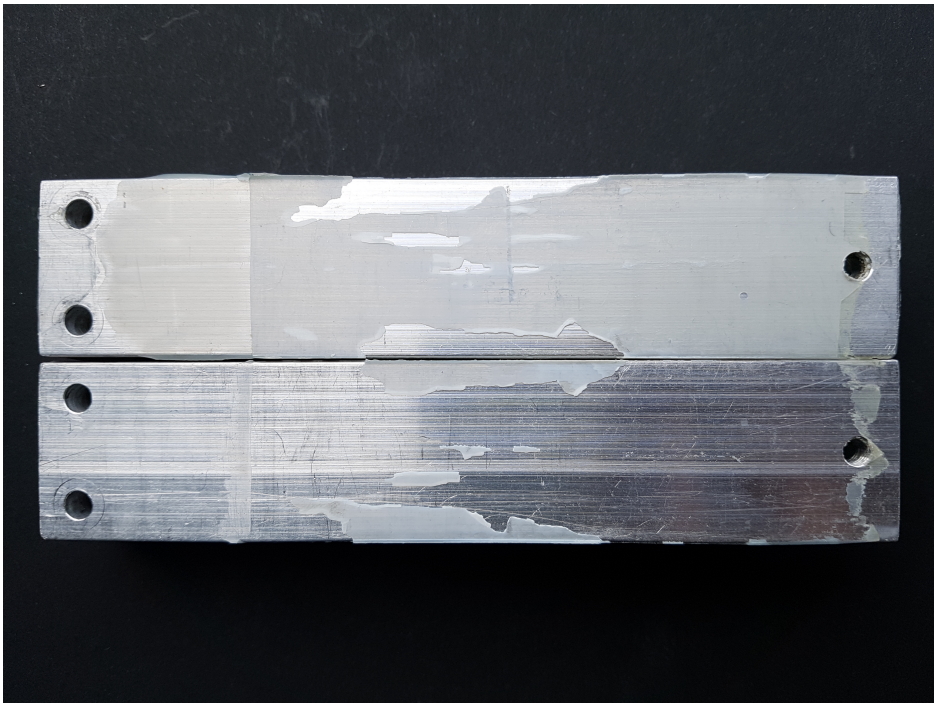

Fig. 5.24 Fracture surface of a fatigue tested degreased joint [158]

Fig. 5.25 Fracture surface of a fatigue tested grit blasted joint [158]

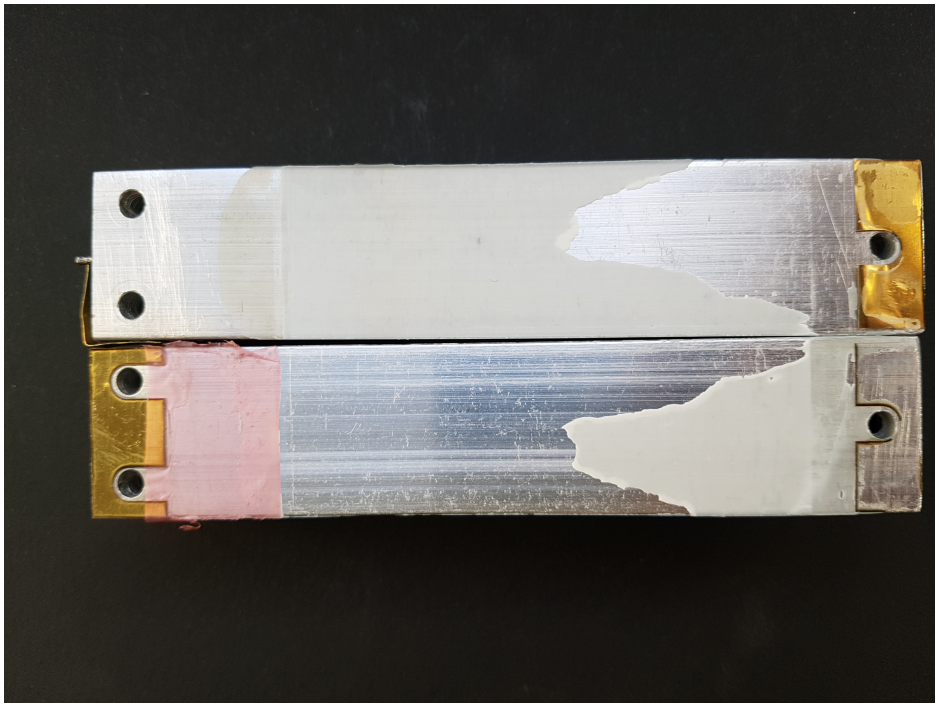

Fig. 5.26 Fracture surface of a fatigue tested T-joint (ED=0.17 J/mm^2 and H=50 μm) [158]

Fig. 5.27 Fracture surface of a fatigue tested T-joint (ED=0.34 J/mm^2 and H=50 μm) [158]

Fig. 5.28 Fracture surface of a fatigue tested T-joint (ED=0.51 J/mm^2 and H=50 μm) [158]

Fig. 5.29 Fracture surface of a fatigue tested T-joint (ED=1.14 J/mm^2 and H=50 μm) [158]

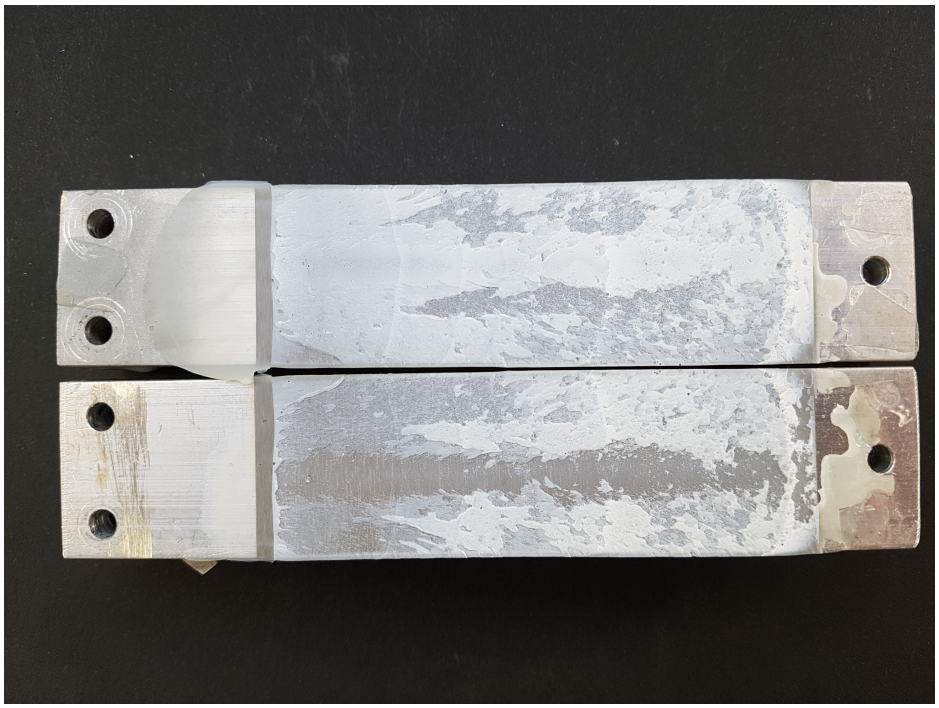

Fig. 5.30 Fracture surface of a fatigue tested T-joint (ED=1.71 J/mm^2 and H=50 μm) [158]

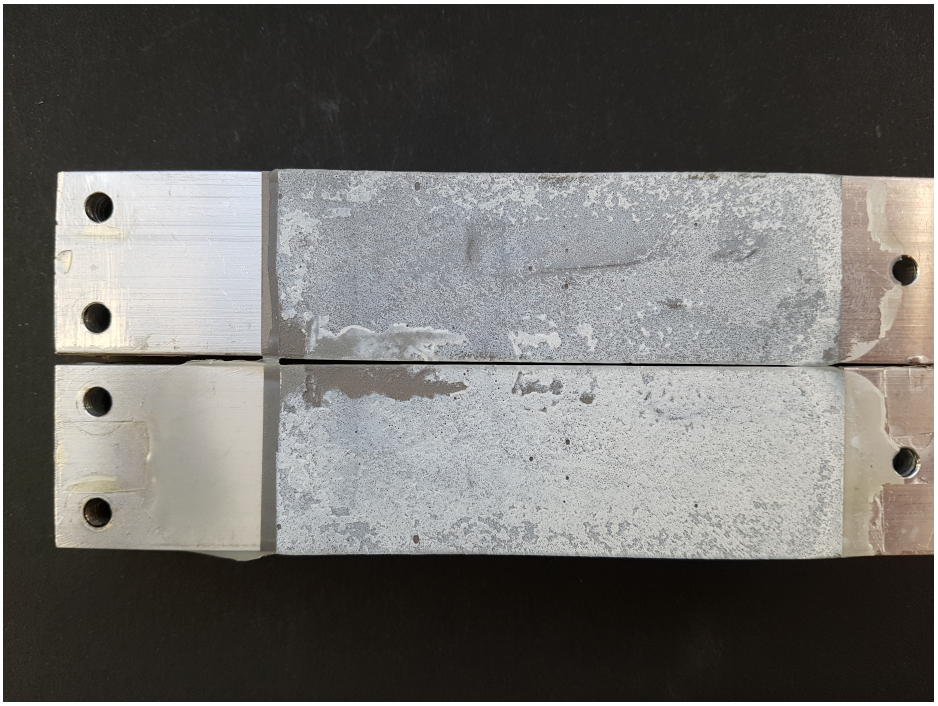

Fig. 5.31 Fracture surface of a fatigue tested T-joint (ED=3.81 J/mm^2 and H=50 μm) [158]

Fig. 5.32 Fracture surface of a fatigue tested T-joint (ED=5.71 J/mm^2 and H=50 μm) [158]

In the lowest energy density ablated sample (Fig. 5.26) the fracture surface presents the same appearance of the simply degreased specimen (Fig. 5.24) and analogously the failure occurs in a completely adhesive mode. As ED grows up to 0.34 J/mm^2 (Fig. 5.27) and 0.51 J/mm^2 (Fig. 5.28), the failure mode progressively moves from interfacial to cohesive and the fracture surface appears similar to the grit blasted one (Fig. 5.25). Further rising the energy density, it is possible to detect a switch from the occurring of the crack propagation within the adhesive (ED=1.14 J/mm^2, Fig. 5.29) to an increase of the amount of the zones undergoing adhesive failure (ED=1.71 J/mm^2, Fig. 5.30) and finally to a crack occurring within the adhesive but very close to the interface (ED=3.81 J/mm^2 and ED=5.71 J/mm^2, Fig. 5.31 and 5.32, respectively). All the remarks carried out with regard to the ranking of the laser parameters configurations and the dependence between the configuration employed and the failure mode recorded are consistent with what found for the quasi-static case. Therefore, it is meaningful to assume that even in this case the cause of the differentiation of the mechanical behavior according to the laser parameter configuration employed is to be ascribed to the presence of air bubbles in the laser ablation induced grooves. Even the fracture surfaces observed after the occurrence of a fatigue test are subjected to the entrapment of air between the adhesive and the substrate, generating inclusions which, in this case, seem to behave as tension points from which the crack initiates and propagates, often for small distances, along an interface. This behavior is appreciable in Fig. 5.33, panel a, while on panel b the corresponding fracture surface for the quasi-static case is juxtaposed.

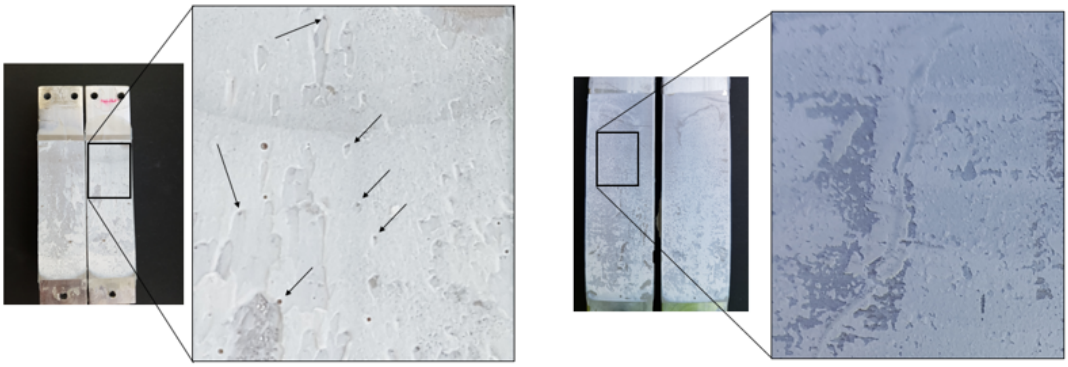

Fig. 5.33 Fracture surface of joints ablated with ED=0.34 J/mm^2, H=50 μm and T pattern, after fatigue test (panel a) and quasi-static test (panel b). In panel a the arrows are placed to point the air inclusions out [158]

In order to assess the influence of the hatch distance over the fatigue behavior, H is varied between 50 and 100 μm keeping constant the other process parameters for specific ED treated samples. The results for the T-joints are presented in Fig. 5.34.

The differences between results belonging to samples realized with different H values are not so marked as in the quasi-static case, but some similarities are however recognizable. Due to the higher amount of untreated area, the samples with H significantly higher than the spot diameter are characterized by slightly lower values of ΔG with respect to the joints realized with H=50 μm. The values of the coefficients of Paris' law provided in Tab. 5.3 for the H=100 μm set confirm these comments, in particular noticing the higher values of the intercept C with respect to the H=50 μm set case (Tab. 5.2).

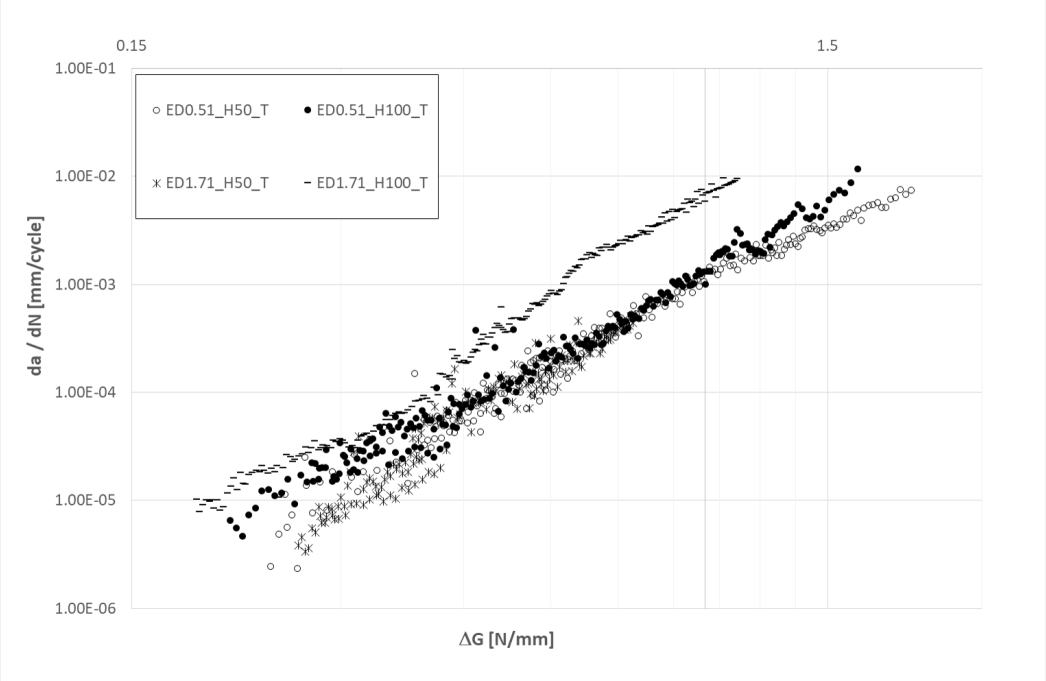

Fig. 5.34 Crack growth rate vs ΔG resulting from a fatigue test over two couples of laser ablated samples, treated with the same ED (ED=0.51 J/mm^2 and ED=1.71 J/mm^2) and the same pattern (T), but testing both the hatch distance values H=50 μm and H=100 μm [158]

Table 5.3 Coefficients of Paris' law for the sets showed in Fig. 5.34

DCB joint (T pattern and H=100 μm)	C [mm^{m+1}N^{-m}cycle]	m
ED=0.51 J/mm^2	1.3 10^{-3}	3.46
ED=1.71 J/mm^2	6.8 10^{-3}	4.21

A similar trend is detectable even for the C-samples, as shown in Fig. 5.35, especially for the case ED=0.51 J/mm^2 for which the gap between the curve referred to the H=50 μm sample and the curve referred to the H=100 μm joint is significant. When ED=1.71 J/mm^2 the behavior seems less sensitive to the hatch distance value, especially when the crack growth rate is quite high.

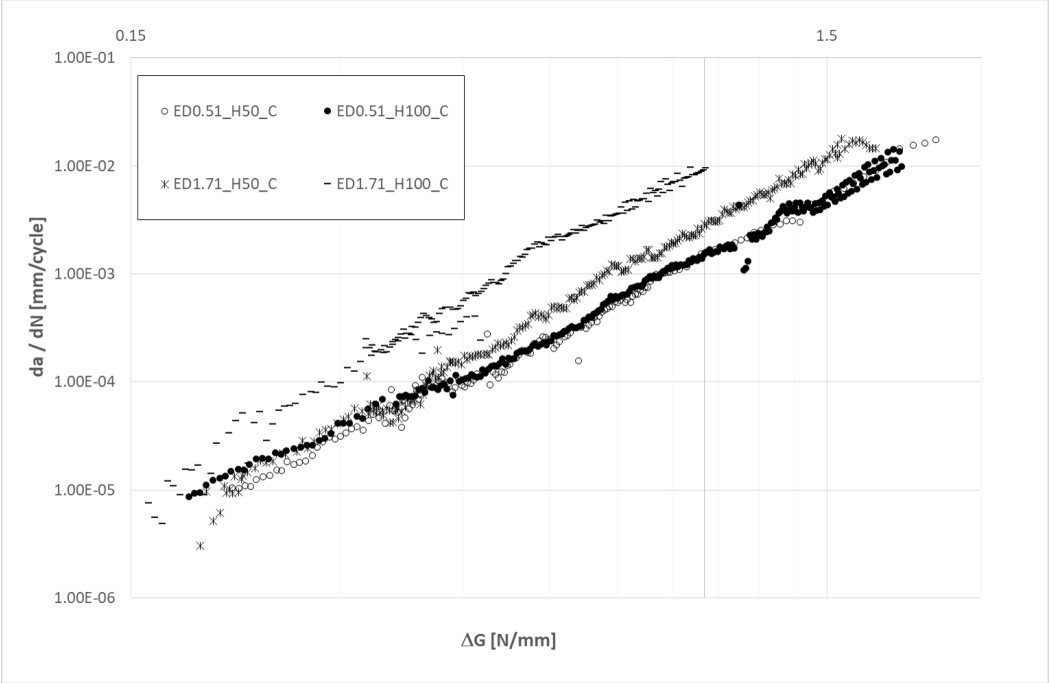

Fig. 5.35 Crack growth rate vs ΔG resulting from a fatigue test over two couples of laser ablated samples, treated with the same ED (ED=0.51 J/mm^2 and ED=1.71 J/mm^2) and the same pattern (C), but testing both the hatch distance values H=50 μm and H=100 μm [158]

Finally, the effect of a variation of the laser scanning strategy (unidirectional or grid pattern) is evaluated by means of the comparisons provided in Figs. 5.36 and 5.37, performed by keeping the hatch distance fixed to 50 μm and 100 μm, respectively.

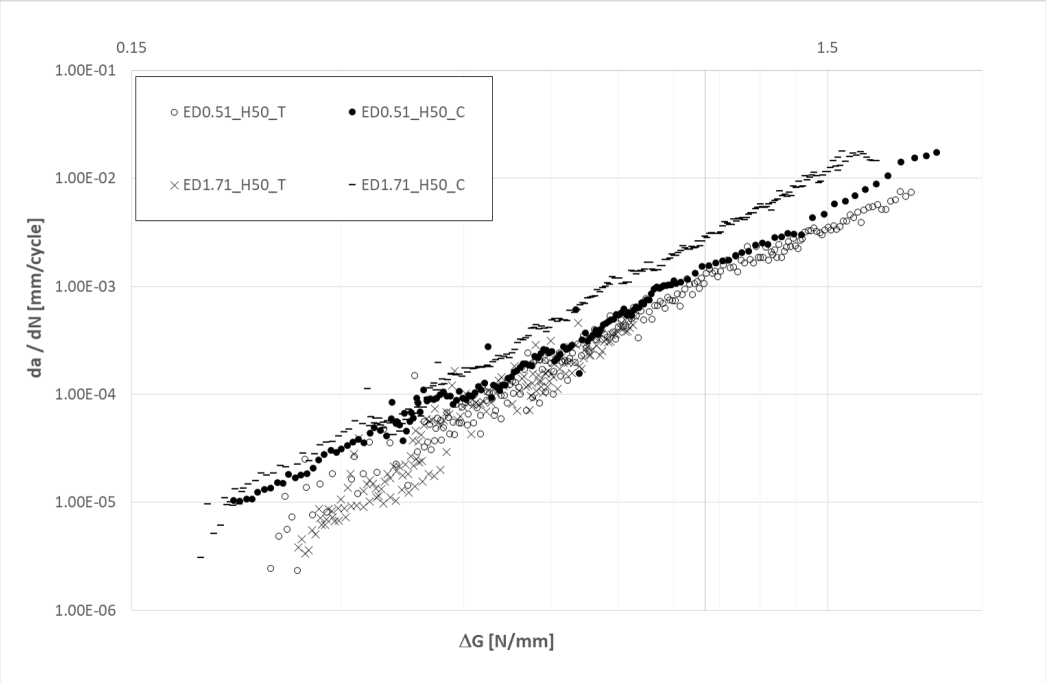

Fig. 5.36 Crack growth rate vs ΔG resulting from a fatigue test over two couples of laser ablated samples, treated with the same ED (ED=0.51 J/mm^2 and ED=1.71 J/mm^2) and the same hatch distance (H=50 μm), but testing both the T and the C textures [158]

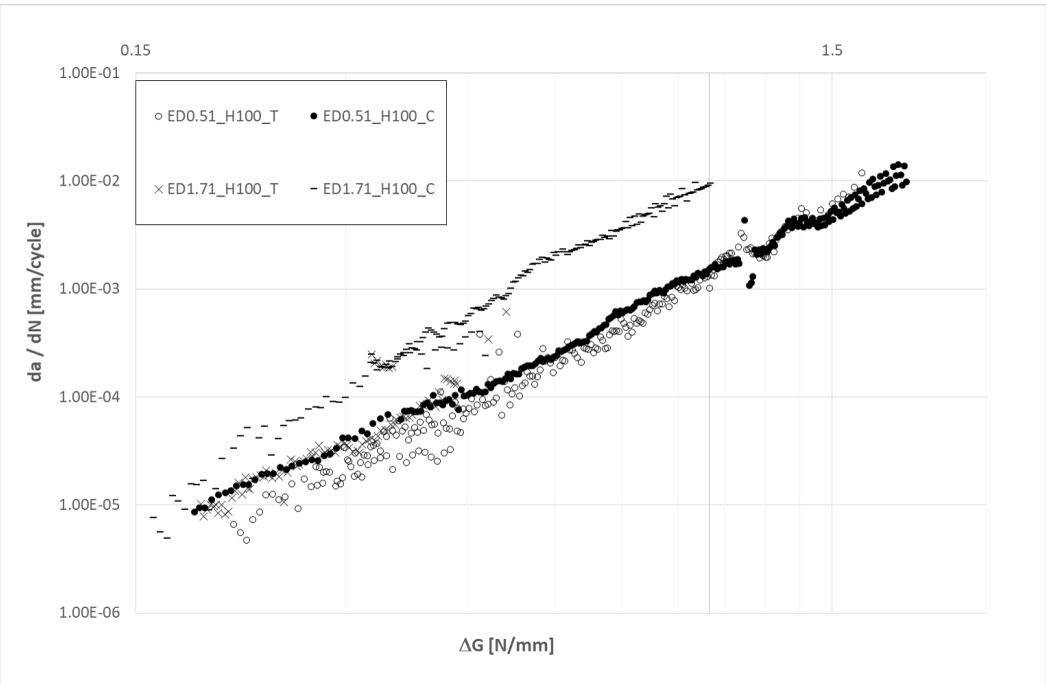

Fig. 5.37 Crack growth rate vs ΔG resulting from a fatigue test over two couples of laser ablated samples, treated with the same ED (ED=0.51 J/mm^2 and ED=1.71 J/mm^2) and the same hatch distance (H=100 μm), but testing both the T and the C textures [158]

Regardless of the hatch distance, a decrease of ΔG is recorded in the C-specimens with respect to the unidirectional case, more evident for the ED=1.71 J/mm^2 case and when the crack growth rate is low (for high da/dN an overtune with respect to the usual hierarchy happens in the ED=0.51 J/mm^2 and H=100 μm curves), while in the quasi-static test the results belonging to the T and the C-joints appear very close to each other and, even when a difference is apparent, it is very slight. Tab. 5.4 collects the coefficients of the Paris' law for every C-joint analyzed.

Table 5.4 Coefficients of Paris' law for the C-joints

DCB joint (C pattern)	H [μm]	C [mm^{m+1}N^{-m}cycle]	m
ED=0.51 J/mm^2	50	1.4 10^{-3}	3.20
ED=0.51 J/mm^2	100	1.4 10^{-3}	3.08
ED=1.71 J/mm^2	50	2.8 10^{-3}	3.59
ED=1.71 J/mm^2	100	1.2 10^{-2}	3.89

The value of C relative to the curve associated with the joint treated with ED=1.71 J/mm^2 and H=100 μm, which is one order of magnitude higher than the others, provides a quantitative validation of the previous remarks. The images of the fracture surfaces of two C-joints treated with ED=0.51 J/mm^2 for both the cases H=50 μm and H=100 μm are offered in Figs. 5.38 and 5.39, respectively. A switch of the failure locus from the inner adhesive to the interface occurs when using H=100 μm instead of H=50 μm for ablating the surface, at the same energy density level.

Fig. 5.38 Fracture surface of a fatigue tested C-joint ablated with ED=0.51 J/mm^2 and H=50 μm [158]

Fig. 5.39 Fracture surface of a fatigue tested C-joint ablated with ED=0.51 J/mm^2 and H=100 μm [158]

5.4 Quasi static characterization of the joints after an accelerated ageing

The second series of experiments used for taking into account the effect of the passing of time over the mechanical response of the laser ablated bonded joints is a repetition of some quasi static tests over various joints realized with already tested configurations, but after exposing them for some time to hot-humid critical environmental conditions. The aim is to complete the quasi static characterization and to extend the assessment of the mechanical behavior of the laser ablated joints to their durability characteristics.

5.4.1 Variations of the set-up

The set-up of the experimental campaign after the conditioning is directly related to the results of the previous quasi-static tests described in Par. 5.2, because the aim of this phase is the direct comparison of the fracture toughness achieved by bonded joints unaged and aged, respectively, keeping fixed all the other boundary conditions. Therefore, the choice of the DCB geometry with the same dimensions than the ones used in the unaged quasi-static campaign appears clear. For the aforementioned reason, even the selection of the laser parameter configurations used to ablate the samples directly descends from the results of the quasi-static campaign. Only a few values of ED are used for this phase of the work, limiting to the ones which have provided the best (ED=0.51 J/mm^2) and the worst (ED=0.17 J/mm^2) results, respectively, in the quasi-static campaign and to a couple of configurations whose associated quasi-static toughness has placed in the descending part of the G vs ED curve, near (ED=1.71 J/mm^2) and far (ED=5.71 J/mm^2) from the maximum. The hatch distance is kept fixed to 50 μm due to the fact that the best results have been detected for this value in the previous tests. Finally, only a unidirectional pattern (the so called T-texture) is employed since the conditioning is supposed to affect the mechanical toughness in the same way regardless of the laser scanning direction, suggesting that it is possible to scale the results for different patterns according to the differences recorded in the quasi-static unaged campaign.

After the cure of the adhesive inside the bonded joint, the specimens are placed in the climatic chamber where they are subjected to the standard accelerated ageing cycle D3 referred in the international standard DIN ISO 9142 [160]. This choice appears in line with what stated by Adams referring to poor representativeness of the degradation mechanisms triggered by excessive temperature and humidity [2]. According to this cycle, both the temperature (T) and the relative humidity (RH) are periodically varied after applying to the

specimens a preliminary conditioning for 24 h at T=23°C and RH 50 %. The cycle is divided into 4 phases, hereinafter summarized and illustrated in Fig. 5.40:

1. exposure for 15 h at T=40°C and RH 90%
2. change in 60 min to T=-20°C and exposure for 2 h
3. change in 60 min to T=70°C and RH 50% and exposure for 4 h
4. change in 60 min to T=40°C and RH 90%

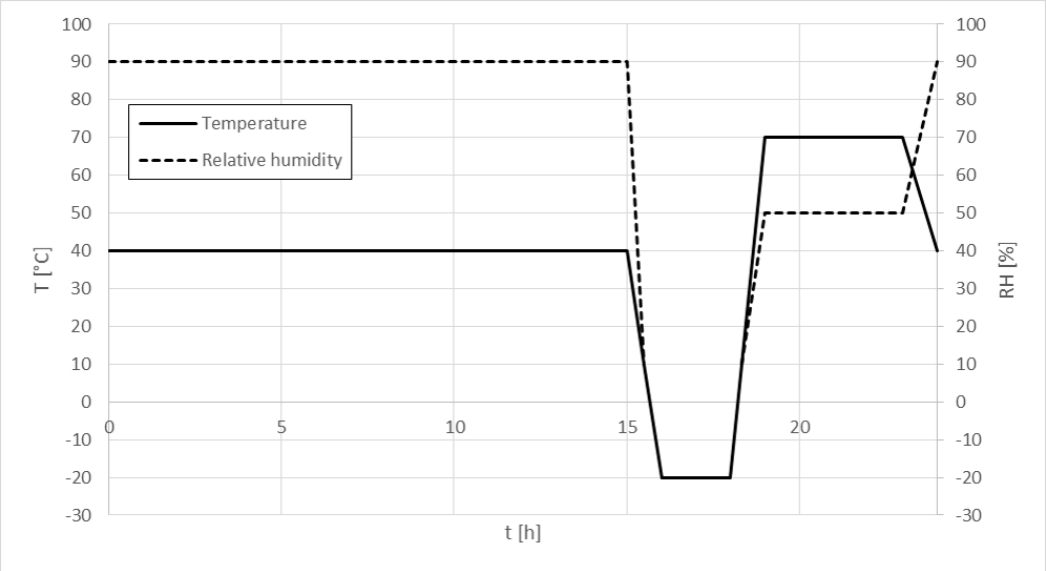

Fig. 5.40 Accelerated ageing cycle D3 according to DIN ISO 9142 [158]

Just before the reaching of the freezing point, the control of the relative humidity is deactivated and so remains until the temperature does not increase to 10°C during the third step. The total number of cycle repetition is set to 30 days consistently with what performed in other works in which the same cycle has been employed [161] [162].

5.4.2 Test results

Fig. 5.41 shows the average values and the standard deviation of G_{Ic} for the conditioned specimens, plotted together with the previous quasi-static test data.

Firstly, the trend of the toughness in function of ED is nearly untouched by the conditioning, with the only exception represented by a sliding of the maximum toughness towards higher values of the energy density. The reasons for the shape of the trend have already been

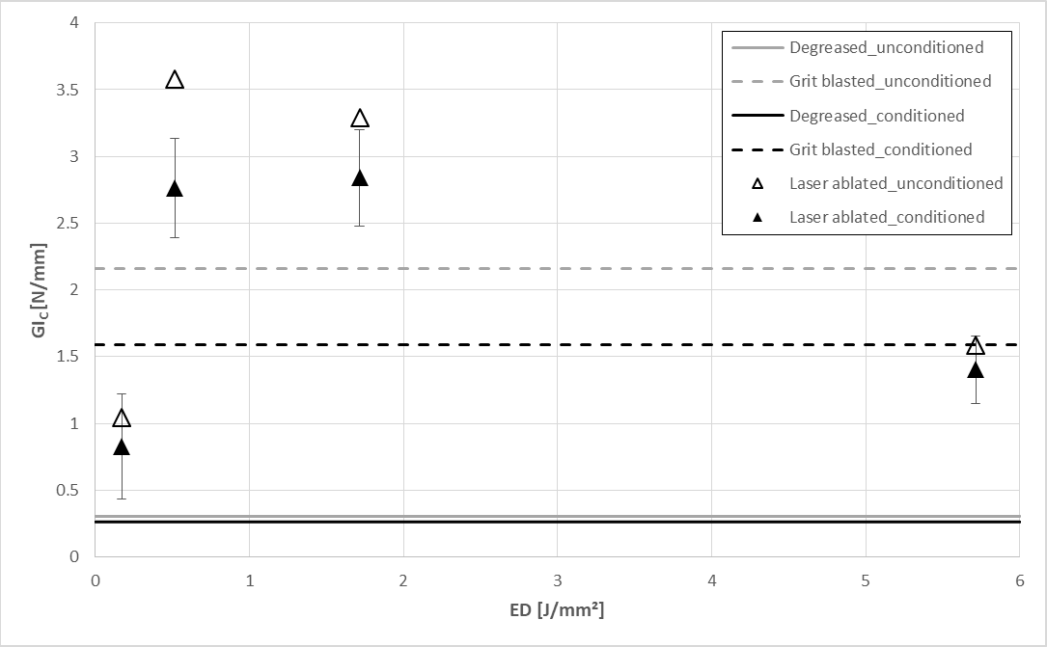

Fig. 5.41 Critical Mode I strain energy release rate G_{Ic} vs energy density ED for unconditioned and conditioned laser ablated joints. The simply degreased and grit blasted joints data are reported with continuous and stippled line, respectively [158]

discussed in Par. 5.2.1. Then, it is worth noting how, as one could expect, the average level of the critical Mode I strain energy release rate decreases for every conditioned set with respect to the corresponding unconditioned one. This lowering is not the same regardless to the process parameter configurations but depends from it. In particular, the rate of decrease of G_{Ic} goes from about 12% when ED is equal to 5.71 J/mm^2 to 14% for the degreased and the ED=1.71 J/mm^2 joints, to approximately 21% exhibited by the ED=0.17 J/mm^2, to 22.8% for the ED=0.51 J/mm^2 samples and finally to 26% in the grit blasted case. Just this last decrease involving the fracture toughness of grit blasted joints appears remarkable because it results in a relative improvement of toughness for some laser ablated sets with respect to the grit blasted one. In particular, the increment of toughness achievable by the ED=1.71 J/mm^2 laser ablated joint with respect to the grit blasted one, being equal the amount of time passed from the production and the type of conditioning applied to the sample, moves from 52% in the as produced test conditions to 78% after the conditioning. Instead, the difference in the value of G_{Ic} from the ED=0.51 J/mm^2 laser ablated joint and the grit blasted one jumps from 66% in the unconditioned case to 74% after the accelerated ageing cycle. In general, this behavior goes towards the existence of a benefit in adopting the laser ablation as a pre-treatment, appropriately selecting the process parameters configuration, instead of the grit blasting when the exposure to some environmental hot-humid critical conditions is expected during

the service life of the bonded joint. With regard to the deep reasons for the decrease of the toughness in every conditioned specimens with respect to the original unaged values, it is possible only to do some assumptions based on literature review. For instance, Zheng [71] ascribed the worsening of the lap shear maximum load of aluminum adhesive-bonded lap shear joints exposed for 240 h to T=40°C and RH 98% to an acceleration of the corrosion of the aluminum substrates by the high temperature and to a degradation of the Van der Waals forces responsible for the polar component of the work of adhesion by the moisture. In this work, however, no change in the failure locus occurs due to the ageing effect, so the provided explanation does not optimally fit with the presented results. As an illustration of the inability of recognizing any macroscopic sign of degradation or modification of the failure mode with respect to the unconditioned case, in Fig. 5.42 an image of a fracture surface for the ED=5.71 J/mm^2 conditioned joint (panel b) is juxtaposed to the picture of the fracture surface belonging to the corresponding unaged specimen (panel a).

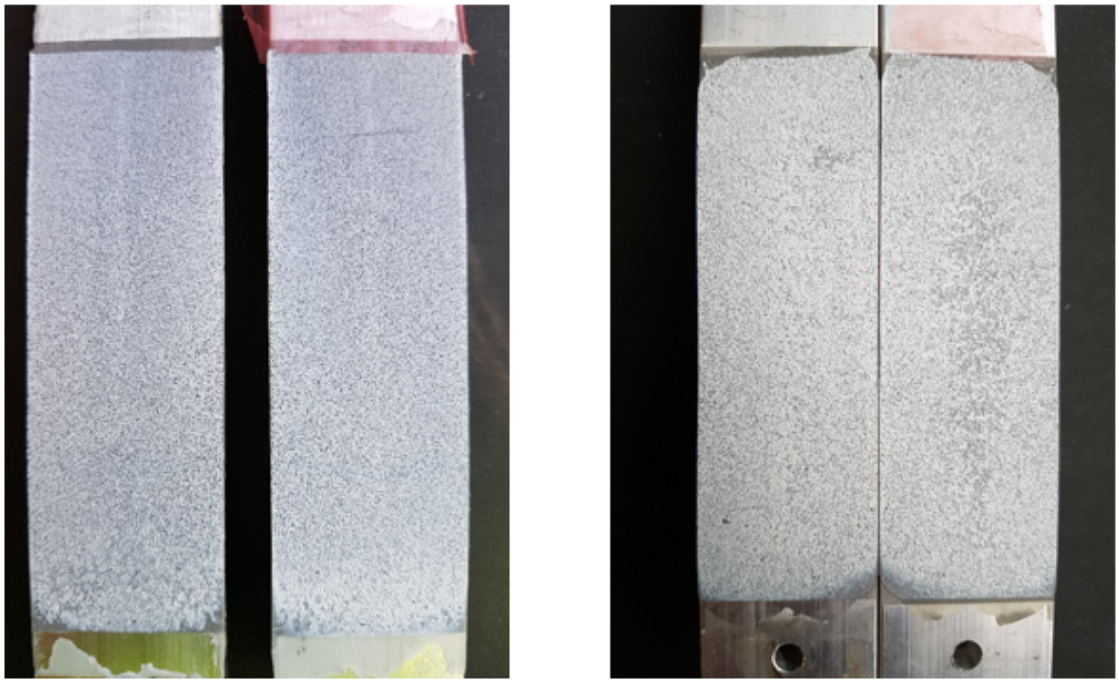

Fig. 5.42 Fracture surface of joints ablated with ED=0.51 J/mm^2, H=50μm and T-pattern tested as produced (panel a) and after the exposure to the accelerated ageing cycle (panel b) [158]

Conclusions

The aim of this work of thesis was to go deepen in exploring the influence that laser ablation has when it is chosen as surface pre-treatment to apply for the production of adhesively bonded joints. In particular, the focus went over the effect provided by the variation of some laser process parameters upon the quality of the pre-treated bonded joints, in order to discern in which operating range the laser behaves as an effective replacement to the traditional mechanical and chemical pre-treatments for bonding. To do this, a strategy consisting in the definition of the combinations of parameters to be tested was developed, in particular the laser power and the scan speed were varied to assume a discreet set of values. Therefore the energy density ED, defined as the energy provided to the ablated surface per unit area, was chosen as the driven indicator, able to summarize the configurations of parameters employed. Moreover, the nominal distance between adjacent ablated grooves, namely the hatch distance, was varied in order to test different levels of superimposition between grooves, in particular an overlap lower, equal and higher than zero, respectively, were induced. Finally, the laser scanning direction was taken into account by realizing three different surface textures, two of which (T and L-patterns, respectively) obtained by scanning straight parallel lines and by rotating them by 90°, while the last one (the C-pattern) consisted in creating a sort of grid over the ablated surface. The material selected for the analysis was AA6082-T6 alumininium alloy and a Yb-fiber laser equipment was used to ablate the surfaces. The surface morphology was evaluated through SEM observations recording high magnification images of the laser induced changing in the external appearance, while a quantitative assessment was performed by means of a measurement of the average surface roughness and of the Pearson's first coefficient of skewness using a 3D laser profilometer. The peculiar trend of the surface roughness with the energy density contemplates a linear increase with ED until the achievement of a threshold after which a further rise of the energy density value makes the roughness decrease, probably because of the softening of the bulk material and the flattering of the crests. The surface skewness, which represents the distribution of peaks and valleys with respect to the mean plane over the surface, underwent an increase when ED was raised from the lowest values, which was marked for low values of hatch distance able to produce high peaks due to the

stacked ablated and re-solidified material. As the energy density was risen up, the coefficient of skewness presented a significant decrease due to the effectiveness of the laser ablation process in generating a surface characterized by deep valleys. Concerning the differences induced over the surface morphology by using the unidirectional (T or L) rather than the crossed (C) pattern, this last one was noticed to generate a strong increase of the surface roughness with respect to the values obtained with the unidirectional textures, especially comparing data recorded after the application of low superimposition treatments. Even the coefficient of skewness of the crossed surfaces, although behaving as previously described in function of the energy density, presented in general higher values than the unidirectional ones. Also some EDS measurements and contact angle evaluation for the assessment of the wettability were executed on the ablated surfaces, revealing on one hand that by rising up the energy density used for the ablation it is possible to encourage the formation of a thick oxide layer, which on the other hand was proven to promote the wettability since the contact angles for energy densities equal or higher than 0.51 J/mm^2 were equal to zero, resulting in complete hydrophilic surfaces. For the evaluation of the mechanical response of the bonded joints, the Double Cantilever Beam (DCB) geometry was selected and several joints were produced by bonding laser pre-treated aluminium substrates with Loctite Hysol 9466 epoxy adhesive. Even the simply degreased and the grit blasted specimens were produced to be compared with the laser ablated ones. The mechanical characterization of the bonded joints was performed along a threefold front, based in all cases on the determination of the critical value of the Mode I strain energy release rate of the bonded joints: the quasi-static tests of the just produced joints and a durability evaluation consisting on one hand in a series of fatigue tests and on the other in the repetition of a quasi-static characterization over joints previously undergoing an accelerated aging cycle. Concerning the results of the quasi-static DCB tests, the energy density was found to be an effective parameter in order to promote the cohesive failure of the joint instead of the adhesive one occurring in the simply degreased joints, as well as to drive a strong enhancement of the fracture toughness with respect to the degreased and the grit blasted treated joints when it was kept in a range between 0.5 J/mm^2 (which produced the optimal conditions) and 2 J/mm^2. The coefficient of skewness was proven to be a good parameter to catch the asymmetric distribution of peaks and valleys and thus allows to identify the surface morphology conditions in which a higher amount of air remained entrapped within the grooves, as it was detected with an optical microscope for high ED treated samples. With refer to the influence of the hatch distance value, the lesser amount of treated area characterizing the joints whose surfaces were ablated with higher hatch distances resulted in a lower toughness with respect to the joints treated with a superimposition between adjacent grooves higher or equal to zero. With respect to the

laser scanning direction, no meaningful difference between T and L-textured joints were recorded as it was expected, but even for the C-pattern joints the values of strain energy release rate remained quite similar, with the exception of the set related to the highest hatch distance in which the amount of untreated area was lower than in the unidirectional case. This is essentially due to the fact that the improvement of the mechanical interlocking effect provided by the higher surface roughness was accompanied by an increase of the amount of air entrapped withint the asperities. Thereby, the critical Mode I strain energy release rate of the bonded joints seemed to be related, more than to the laser scanning direction or the surface roughness, to the value of the coefficient of skewness, correlation which was statistically validated. The fatigue characterization of the joints was performed using a selection of the laser parameters tested during the quasi-static tests. The data obtained by evaluating the crack growth rate in function of the range of the Mode I strain energy release rate required for the crack propagation within a load cycle, whose trend was assessed by computing the coefficients of the Paris' law for every experimental curve, were quite consistent with the ranking of the laser parameter configurations resulting from the quasi-static campaign. Even the influence of the hatch distance was similar to the trend previously identified, while with regard to the laser scanning direction the C-textured treatment was found to lead a slight reduction of the toughness with respect to the unidirectional one, especially for low crack growth rates. Finally, after being exposed to a conditioning realized by cyclically varying the temperature and the relative humidity of a controlled chamber according to a proper standard, some joints underwent a quasi-static DCB test, from which a general lowering of the Mode I strain energy release rate for every specimen (regardless from the type of pre-treatment applied) was evaluated, even if any apparent sign of degradation was distinguished from a visual inspection of the fracture surfaces. Nevertheless, in correspondence of specific energy density values (ED=0.51 J/mm^2 and 1.71 J/mm^2, respectively) comprised in a mid-zone of the explored range, a relative improvement of the fracture toughness of the corresponding laser treated joints with respect to the grit blasted sample was recorded being even higher than the one found for the unaged tests.

References

[1] A. Kinloch, *Adhesion and adhesives: science and technology*. Chapman and Hall, 1987.

[2] R. D. Adams, *Adhesive bonding: science, technology and applications*. Elsevier, 2005.

[3] G. W. Critchlow, "Pretreatments for metal-to-metal bonding," PhD thesis, © Gary Critchlow, 1997.

[4] K. L. Johnson, K. Kendall, and A. Roberts, "Surface energy and the contact of elastic solids," *Proc. R. Soc. Lond. A*, vol. 324, no. 1558, pp. 301–313, 1971.

[5] J. Huntsberger, "The nature of adhesion," *Adhesives Age*, vol. 13, no. 11, p. 43, 1970.

[6] F. Fowkes, D. McCarthy, and M. Mostafa, "Contact angles and the equilibrium spreading pressures of liquids on hydrophobic solids," *Journal of colloid and interface science*, vol. 78, no. 1, pp. 200–206, 1980.

[7] W. Dukes and A. Kinloch, *Developments in adhesives—1*, edited by WC Wake, 1977.

[8] F. Fowkes, "Acid-base interactions in polymer adhesion," in *Tribology Series*, vol. 7, Elsevier, 1981, pp. 119–137.

[9] J. Koenig and P. T. Shih, "Raman studies of the glass fiber-silane-resin interface," *Journal of Colloid and Interface Science*, vol. 36, no. 2, pp. 247–253, 1971.

[10] C. Chiang, H. Ishida, and J. Koenig, "The structure of γ-aminopropyltiethoxysilane on glass surfaces," *Journal of Colloid and Interface Science*, vol. 74, pp. 396–404, 1980.

[11] I. Klein, J. Sharon, A. Yaniv, H. Dodiuk, and D. Katz, "Chemical interactions in the system anodized aluminum—primer—adhesive," *International journal of adhesion and adhesives*, vol. 3, no. 3, pp. 159–162, 1983.

[12] H. Chu, N. Eib, A. Gent, and P. Henriksen, *Advances in chemistry series 174*, edited by JL Loenig, 1979.

[13] X. Zhou and C. E. Frazier, "Double labeled isocyanate resins for the solid-state nmr detection of urethane linkages to wood," *International journal of adhesion and adhesives*, vol. 21, no. 3, pp. 259–264, 2001.

[14] D. Tabor and R. Winterton, "The direct measurement of normal and retarded van der waals forces," *Proc. R. Soc. Lond. A*, vol. 312, no. 1511, pp. 435–450, 1969.

[15] C. Jennings, "Surface roughness and bond strength of adhesives," *The Journal of Adhesion*, vol. 4, no. 1, pp. 25–38, 1972.

[16] J. Evans and D. Packham, "Adhesion of polyethylene to metals: The role of surface topography," *Journal of Adhesion*, vol. 10, no. 3, pp. 177–191, 1979.

[17] E. M. Petrie, "Handbook of adhesives and sealants," 2000.

[18] J. Sargent, "Adherend surface morphology and its influence on the peel strength of adhesive joints bonded with modified phenolic and epoxy structural adhesives," *International journal of adhesion and adhesives*, vol. 14, no. 1, pp. 21–30, 1994.

[19] M. Shahid and S. Hashim, "Effect of surface roughness on the strength of cleavage joints," *International Journal of Adhesion and Adhesives*, vol. 22, no. 3, pp. 235–244, 2002.

[20] G. Critchlow and D. Brewis, "Influence of surface macroroughness on the durability of epoxide-aluminium joints," *International journal of adhesion and adhesives*, vol. 15, no. 3, pp. 173–176, 1995.

[21] S. Thery, P. Balladon, and A. Legros, "Study of parameters influencing the mechanical behaviour of and damage to steel/polymer interfaces," *Mechanical Engineering Publications Limited(UK),*, pp. 339–350, 1991.

[22] W.-S. Kim, I.-H. Yun, J.-J. Lee, and H.-T. Jung, "Evaluation of mechanical interlock effect on adhesion strength of polymer–metal interfaces using micro-patterned surface topography," *International Journal of Adhesion and Adhesives*, vol. 30, no. 6, pp. 408–417, 2010.

[23] Y. Zuo, H. Wang, J. Zhao, and J. Xiong, "The effects of some anions on metastable pitting of 316l stainless steel," *Corrosion Science*, vol. 44, no. 1, pp. 13–24, 2002.

[24] G. Critchlow and D. Brewis, "Review of surface pretreatments for aluminium alloys," *International Journal of Adhesion and Adhesives*, vol. 16, no. 4, pp. 255–275, 1996.

[25] J. Zhang, X. Zhao, Y. Zuo, J. Xiong, and X. Zhang, "Effect of surface pretreatment on adhesive properties of aluminum alloys," *Journal of Materials Science & Technology*, vol. 24, no. 2, pp. 236–240, 2008.

[26] M. Gude, S. Prolongo, and A. Ureña, "Adhesive bonding of carbon fibre/epoxy laminates: Correlation between surface and mechanical properties," *Surface and Coatings Technology*, vol. 207, pp. 602–607, 2012.

[27] K. Uehara and M. Sakurai, "Bonding strength of adhesives and surface roughness of joined parts," *Journal of Materials Processing Technology*, vol. 127, no. 2, pp. 178–181, 2002.

[28] R. N. Wenzel, "Resistance of solid surfaces to wetting by water," *Industrial & Engineering Chemistry*, vol. 28, no. 8, pp. 988–994, 1936.

[29] A. Cassie and S. Baxter, "Wettability of porous surfaces," *Transactions of the Faraday society*, vol. 40, pp. 546–551, 1944.

[30] R. Hebbar, A. Isloor, and A. Ismail, "Contact angle measurements," in *Membrane Characterization*, Elsevier, 2017, pp. 219–255.

[31] A. Harris and A. Beevers, "The effects of grit-blasting on surface properties for adhesion," *International Journal of Adhesion and Adhesives*, vol. 19, no. 6, pp. 445–452, 1999.

[32] Y. Boutar, S. Naımi, S. Mezlini, and M. B. S. Ali, "Effect of surface treatment on the shear strength of aluminium adhesive single-lap joints for automotive applications," *International Journal of Adhesion and Adhesives*, vol. 67, pp. 38–43, 2016.

[33] S. Voyutskii, "Adhesion and autohesion of high polymers," *Interscience, New York*, 1963.

[34] H. Krupp and W. Schnabel, "Light-modulated electrostatic double layer adhesion," *The Journal of Adhesion*, vol. 5, no. 4, pp. 269–277, 1973.

[35] B. Derjaguin, "Research 8, 70 (1955)," *Proc. 3rd Int. Congr. Surf. Activity*, vol. 28, p. 399, 1957.

[36] J. J. Bikerman, "The science of adhesive joints," Academic Press, Tech. Rep., 1961.

[37] P. Poole and J. Watts, "Effect of alloy composition and surface pretreatment on the durability of adhesive-bonded aluminium alloy joints," *International journal of adhesion and adhesives*, vol. 5, no. 1, pp. 33–39, 1985.

[38] J. Minford, "Durability of structural adhesive bonded aluminum joints," *Adhesives Age*, vol. 21, no. 3, pp. 17–23, 1978.

[39] P. Bijlmer and R. Schliekelmann, *The relation of surface condition after pretreatment to bondability of aluminium alloys*, SAMPE Quarterly, 1973.

[40] T. Sun, D. McNamara, J. Ahearn, J. Chen, B. Ditchek, and J. Venables, "Interpretation of aes depth profiles of porous al anodic oxides," *Applications of Surface Science*, vol. 5, no. 4, pp. 406–425, 1980.

[41] R. Digby and D. Packham, "Pretreatment of aluminium: Topography, surface chemistry and adhesive bond durability," *International Journal of Adhesion and Adhesives*, vol. 15, no. 2, pp. 61–71, 1995.

[42] W. Russell and E. Garnis, "A chromate-free low toxicity method of preparing aluminum surfaces for adhesive bonding," *SAMPE Journal*, vol. 17, pp. 19–23, 1981.

[43] W. Marwick and P. Sheasby, "Evaluation of adhesives for aluminum structured vehicles," *SAE transactions*, pp. 577–585, 1987.

[44] G. Brown, K. Shimizu, K. Kobayashi, G. Thompson, and G. Wood, "The morphology, structure and mechanism of growth of chemical conversion coatings on aluminium," *Corrosion science*, vol. 33, no. 9, pp. 1371–1385, 1992.

[45] M. Takai and M. Takaya, "Influence of conversion coating on magnesium and aluminum alloys by adhesion method," *Materials transactions*, vol. 49, no. 5, pp. 1065–1070, 2008.

[46] J. Venables, D. McNamara, T. Sun, B. Ditchek, and J. Chen, "Characterization of aluminum surfaces prepared for adhesive bonding.," MARTIN MARIETTA LABS BALTIMORE MD, Tech. Rep., 1979.

[47] J. Minford, "Etching and anodizing pretreatments and aluminum joint durability," *SAMPE Quarterly*, vol. 9, pp. 18–27, 1978.

[48] O.-D. Hennemann and W. Brockmann, "Surface morphology and its influence on adhesion," *The Journal of Adhesion*, vol. 12, no. 4, pp. 297–315, 1981.

[49] A. Spaggiari and E. Dragoni, "Effect of mechanical surface treatment on the static strength of adhesive lap joints," *The Journal of Adhesion*, vol. 89, no. 9, pp. 677–696, 2013.

[50] G. Davis, J. Ahearn, L. Matienzo, and J. Venables, "Use of hydration inhibitors to improve bond durability of aluminium adhesive joints," *Journal of materials science*, vol. 20, no. 3, pp. 975–988, 1985.

[51] J. Bishopp, E. Sim, G. Thompson, and G. Wood, "Effects of the environment on bonded aluminium joints: An examination by electron microscopy," in *Adhesion 13*, Springer, 1989, pp. 201–220.

[52] J. Bell and W. McCarvill, "Surface interaction between aluminum and epoxy resin," *Journal of Applied Polymer Science*, vol. 18, no. 8, pp. 2243–2247, 1974.

[53] D. Brewis, J. Comyn, and J. Tegg, "The durability of some epoxide adhesive-bonded joints on exposure to moist warm air," *International Journal of Adhesion and Adhesives*, vol. 1, no. 1, pp. 35–39, 1980.

[54] R. Pike, V. Patarini, R. Zatorski, and F. Lamm, "Plasma-sprayed coatings as adherend surface pretreatments," *International journal of adhesion and adhesives*, vol. 12, no. 4, pp. 227–231, 1992.

[55] J. F. Watts and J. Wolstenholme, *An introduction to surface analysis by XPS and AES*. Wiley, 2003.

[56] H. Zhuang and J. A. Gardella, "Spectroscopic characterization of polymer surfaces," *MRS Bulletin*, vol. 21, no. 1, pp. 43–48, 1996.

[57] W. Werner, D. Briggs, and J. Grant, "Surface analysis by auger and x-ray photoelectron spectroscopy," *IMPublications: Chichester*, 2003.

[58] A. Benninghoven, "Beobachtung von oberflächenreaktionen mit der statischen methode der sekundärionen-massenspektroskopie. i die methode," *Surface Science*, vol. 28, no. 2, pp. 541–562, 1971.

[59] R. Schubert and J. Tracy, "A simple, inexpensive sims apparatus," *Review of Scientific Instruments*, vol. 44, no. 4, pp. 487–491, 1973.

[60] T. Jones and N. Williams, "The fatigue properties of spot welded, adhesive bonded and weldbonded joints in high strength steels," SAE Technical Paper, Tech. Rep., 1986.

[61] L. Hart-Smith, "Stress analysis- a continuum mechanics approach in adhesive bonded joints," *Developments in adhesives- 2.(A 82-28576 13-39) London, Applied Science Publishers, 1981,*, pp. 1–44, 1981.

[62] J. Romanko and W. Knauss, "Developments in adhesives-2," *Applied Science Pub., London*, p. 173, 1981.

[63] S. Mostovoy and E. Ripling, *Adhesion science and technology 9b*, 1975.

[64] E. Papirer, "Characterization of fibers and fillers for composite materials using inverse gas chromatography," *Composite Interfaces*, pp. 203–213, 1986.

[65] P. Goodhew, J. Humphreys, and R. Beanland, *Electron microscopy and analysis*. (3rd Ed.) Taylor & Francis, 2000.

[66] J. Venables, "Adhesion and durability of metal-polymer bonds," *Journal of Materials Science*, vol. 19, no. 8, pp. 2431–2453, 1984.

[67] J. Watts and J. Castle, "The application of x-ray photoelectron spectroscopy to the study of polymer-to-metal adhesion," *Journal of materials science*, vol. 19, no. 7, pp. 2259–2272, 1984.

[68] J. Castle and P. Zhdan, "Characterization of surface topography by sem and sfm: Problems and solutions," *Journal of Physics D: Applied Physics*, vol. 30, no. 5, p. 722, 1997.

[69] P. A. Zhdan, "Nanoscale surface characterization of conducting and non-conducting materials with stm and contact sfm: Some problems and solutions," *Surface and Interface Analysis: An International Journal devoted to the development and application of techniques for the analysis of surfaces, interfaces and thin films*, vol. 33, no. 10-11, pp. 879–893, 2002.

[70] A. Kinloch, "Interfacial fracture mechanical aspects of adhesive bonded joints—a review," *Journal of Adhesion*, vol. 10, no. 3, pp. 193–219, 1979.

[71] R. Zheng, J.-p. Lin, P.-C. Wang, and Y.-R. Wu, "Effect of hot-humid exposure on static strength of adhesive-bonded aluminum alloys," *Defence Technology*, vol. 11, no. 3, pp. 220–228, 2015.

[72] D. Brewis, "Aluminium adherends," *Durability of structural adhesives; Appl. Science Publ*, pp. 215–254, 1983.

[73] M. Bowditch, "The durability of adhesive joints in the presence of water," *International Journal of Adhesion and Adhesives*, vol. 16, no. 2, pp. 73–79, 1996.

[74] J. Comyn, "The relationship between joint durability and water diffusion," *Developments in adhesives- 2.(A 82-28576 13-39) London, Applied Science Publishers, 1981,*, pp. 279–313, 1981.

[75] R. D. Adams, J. Comyn, and W. C. Wake, *Structural adhesive joints in engineering*. Springer Science & Business Media, 1997.

[76] A. Bethune, "Durability of bonded aluminum structure," *SAMPE Journal*, vol. 11, pp. 4–10, 1975.

[77] R. Butt and J. Cotter, "The effect of high humidity on the dynamic mechanical properties and thermal transitions of an epoxy-polyamide adhesive," *The Journal of Adhesion*, vol. 8, no. 1, pp. 11–19, 1976.

[78] M. Costa, G. Viana, L. da Silva, and R. Campilho, "Effect of humidity on the mechanical properties of adhesively bonded aluminium joints," *Proceedings of the Institution of Mechanical Engineers, Part L: Journal of Materials: Design and Applications*, vol. 232, no. 9, pp. 733–742, 2018.

[79] G. Viana, M. Costa, M. Banea, and L. da Silva, "Behaviour of environmentally degraded epoxy adhesives as a function of temperature," *The Journal of Adhesion*, vol. 93, no. 1-2, pp. 95–112, 2017.

[80] G. Viana, M. Costa, M. Banea, and L. da Silva, "A review on the temperature and moisture degradation of adhesive joints," *Proceedings of the Institution of Mechanical Engineers, Part L: Journal of Materials: Design and Applications*, vol. 231, no. 5, pp. 488–501, 2017.

[81] M. Abdel Wahab, "Fatigue in adhesively bonded joints: A review," *ISRN Materials Science*, vol. 2012, 2012.

[82] A. Crocombe and G. Richardson, "Assessing stress state and mean load effects on the fatigue response of adhesively bonded joints," *International Journal of Adhesion and Adhesives*, vol. 19, no. 1, pp. 19–27, 1999.

[83] S. De Barros, P. Kenedi, S. Ferreira, S. Budhe, A. Bernardino, and L. Souza, "Influence of mechanical surface treatment on fatigue life of bonded joints," *The Journal of Adhesion*, vol. 93, no. 8, pp. 599–612, 2017.

[84] S. Azari, M. Papini, and J. Spelt, "Effect of surface roughness on the performance of adhesive joints under static and cyclic loading," *The Journal of Adhesion*, vol. 86, no. 7, pp. 742–764, 2010.

[85] L. F. Da Silva, N. Ferreira, V. Richter-Trummer, and E. Marques, "Effect of grooves on the strength of adhesively bonded joints," *International Journal of Adhesion and Adhesives*, vol. 30, no. 8, pp. 735–743, 2010.

[86] D. J. Bland, A. J. Kinloch, and J. F. Watts, "The role of the surface pretreatment in the durability of aluminium-alloy structural adhesive joints: Mechanisms of failure," *The Journal of Adhesion*, vol. 89, no. 5, pp. 369–397, 2013.

[87] M. Costa, G. Viana, L. Da Silva, and R. Campilho, "Environmental effect on the fatigue degradation of adhesive joints: A review," *The Journal of Adhesion*, vol. 93, no. 1-2, pp. 127–146, 2017.

[88] M. Fernando, W. Harjoprayitno, and A. Kinloch, "A fracture mechanics study of the influence of moisture on the fatigue behaviour of adhesively bonded aluminium-alloy joints," *International journal of adhesion and adhesives*, vol. 16, no. 2, pp. 113–119, 1996.

[89] A. Kinloch, C. Korenberg, K. Tan, and J. Watts, "Crack growth in structural adhesive joints in aqueous environments," *Journal of materials science*, vol. 42, no. 15, pp. 6353–6370, 2007.

[90] M.-L. Abel, A. Adams, A. Kinloch, S. Shaw, and J. Watts, "The effects of surface pretreatment on the cyclic-fatigue characteristics of bonded aluminium-alloy joints," *International journal of adhesion and adhesives*, vol. 26, no. 1-2, pp. 50–61, 2006.

[91] K. Mizutani and T. Iwatsu, "Influence of external environments on fatigue crack growth in epoxy resin," *Polymer Engineering & Science*, vol. 23, no. 4, pp. 183–185, 1983.

[92] J. Ritter, J. Learned, G. Jacome, T. Russell, and T. Lardner, "Fatigue and durability of silane-bonded epoxy/glass interfaces," *The Journal of Adhesion*, vol. 76, no. 4, pp. 335–351, 2001.

[93] J. E. Ritter and A. Huseinovic, "Adhesion and reliability of epoxy/glass interfaces," *Journal of Electronic Packaging*, vol. 123, no. 4, pp. 401–404, 2001.

[94] G. G. Trantina, "Combined mode crack extension in adhesive joints," *Journal of Composite Materials*, vol. 6, no. 3, pp. 371–386, 1972.

[95] E. Andrews and A. J. Kinloch, "Mechanics of adhesive failure. ii," *Proc. R. Soc. Lond. A*, vol. 332, no. 1590, pp. 401–414, 1973.

[96] A. Gent and A. Kinloch, "Adhesion of viscoelastic materials to rigid substrates. iii. energy criterion for failure," *Journal of Polymer Science Part A-2: Polymer Physics*, vol. 9, no. 4, pp. 659–668, 1971.

[97] R. Gledhill, A. Kinloch, S. Yamini, and R. Young, "Relationship between mechanical properties of and crack progogation in epoxy resin adhesives," *Polymer*, vol. 19, no. 5, pp. 574–582, 1978.

[98] W. D. Bascom and R. L. Cottington, "Effect of temperature on the adhesive fracture behavior of an elastomer-epoxy resin," *The Journal of Adhesion*, vol. 7, no. 4, pp. 333–346, 1976.

[99] J. H. Oh, "Nonlinear analysis of adhesively bonded tubular single-lap joints for composites in torsion," *Composites science and technology*, vol. 67, no. 7-8, pp. 1320–1329, 2007.

[100] L. F. da Silva, F. De Magalhães, F. Chaves, and M. De Moura, "Mode ii fracture toughness of a brittle and a ductile adhesive as a function of the adhesive thickness," *The Journal of Adhesion*, vol. 86, no. 9, pp. 891–905, 2010.

[101] T. Wang, F. D. Blum, and L. R. Dharani, "Effect of interfacial mobility on flexural strength and fracture toughness of glass/epoxy laminates," *Journal of materials science*, vol. 34, no. 19, pp. 4873–4882, 1999.

[102] *ASTM D3433 - 99. Standard Test Method for Fracture Strength in Cleavage of Adhesives in Bonded Metal Joints*. 1999.

[103] A. Biel and U. Stigh, "An analysis of the evaluation of the fracture energy using the dcb-specimen," *Archives of Mechanics*, vol. 59, no. 4-5, pp. 311–327, 2007.

[104] J. Williams, "The fracture mechanics of delamination tests," *The Journal of strain analysis for engineering design*, vol. 24, no. 4, pp. 207–214, 1989.

[105] G. R. Irwin, P. C. Paris, and H. Tada, "The stress analysis of cracks handbook," *American Society of Mechanical Engineers. Three–Park Avenue, New York, NY*, vol. 10016, 2000.

[106] S. Krenk, "Energy release rate of symmetric adhesive joints," *Engineering Fracture Mechanics*, vol. 43, no. 4, pp. 549–559, 1992.

[107] N. Saleema and D. Gallant, "Atmospheric pressure plasma oxidation of aa6061-t6 aluminum alloy surface for strong and durable adhesive bonding applications," *Applied Surface Science*, vol. 282, pp. 98–104, 2013.

[108] D. Brewis, G. Critchlow, and C. Curtis, "Cryoblasting as a pretreatment to enhance adhesion to aluminium alloys: An initial study," *International journal of adhesion and adhesives*, vol. 19, no. 4, pp. 253–256, 1999.

[109] A. Bjørgum, F. Lapique, J. Walmsley, and K. Redford, "Anodising as pre-treatment for structural bonding," *International journal of adhesion and adhesives*, vol. 23, no. 5, pp. 401–412, 2003.

[110] G. W. Critchlow, K. A. Yendall, D. Bahrani, A. Quinn, and F. Andrews, "Strategies for the replacement of chromic acid anodising for the structural bonding of aluminium alloys," *International Journal of Adhesion and Adhesives*, vol. 26, no. 6, pp. 419–453, 2006.

[111] E. Baburaj, D. Starikov, J. Evans, G. Shafeev, and A. Bensaoula, "Enhancement of adhesive joint strength by laser surface modification," *International journal of adhesion and adhesives*, vol. 27, no. 4, pp. 268–276, 2007.

[112] P. Maressa, L. Anodio, A. Bernasconi, A. G. Demir, and B. Previtali, "Effect of surface texture on the adhesion performance of laser treated ti6al4v alloy," *The journal of adhesion*, vol. 91, no. 7, pp. 518–537, 2015.

[113] N. B. Dahotre and S. Harimkar, *Laser fabrication and machining of materials*. Springer Science & Business Media, Springer Science & Business Media, 2008.

[114] W. Duley, *Laser processing and analysis of materials*. Springer Science & Business Media, 1986.

[115] W. Koechner and M. Bass, *Solid-State Lasers: A Graduate Text*. Springer Science & Business Media, 2006.

[116] C. B. Hitz, J. J. Ewing, and J. Hecht, *Introduction to laser technology*. John Wiley & Sons, 2012.

[117] S. Pini, "Study, automation and planning of micromachining processes based on infrared pulsed fiber laser," PhD thesis, Università di Parma. Dipartimento di Ingegneria Industriale, 2011.

[118] R. Sen, M. Saha, S. D. Chowdury, N. Kumar, D. P. Shekhar, A. Ghosh, A. Dhar, A. Pal, and M. Pal, "High powder fiber lasers: Fundamentals to applications," *Science and culture*, 2015.

[119] W. M. Steen and J. Mazumder, *Laser material processing*. springer science & business media, Springer Science & Business Media, 2010.

[120] M. Fabian, E. Lewis, T. Newe, and S. Lochmann, "Optical fibre cavity for ring-down experiments with low coupling losses," *Measurement Science and Technology*, vol. 21, no. 9, 2010.

[121] J. Wilson and J. Hawkes, *Lasers, principles and applications*. Prentice Hall, 1987.

[122] D. Bäuerle, "Nanosecond-laser ablation," in *Laser Processing and Chemistry*, Springer, 2000, pp. 221–257.

[123] A. Vogel and V. Venugopalan, "Mechanisms of pulsed laser ablation of biological tissues," *Chemical reviews*, vol. 103, no. 2, pp. 577–644, 2003.

[124] X. Liu, D. Du, and G. Mourou, "Laser ablation and micromachining with ultrashort laser pulses," *IEEE journal of quantum electronics*, vol. 33, no. 10, pp. 1706–1716, 1997.

[125] P. Laurens, B. Sadras, F. Decobert, F. Arefi-Khonsari, and J. Amouroux, "Enhancement of the adhesive bonding properties of peek by excimer laser treatment," *International Journal of Adhesion and Adhesives*, vol. 18, no. 1, pp. 19–27, 1998.

[126] S. Preuss, A. Demchuk, and M. Stuke, "Sub-picosecond uv laser ablation of metals," *Applied physics A*, vol. 61, no. 1, pp. 33–37, 1995.

[127] U.-i. Kalsoom, S. Bashir, N. Ali, M. Akram, K. Mahmood, R. Ahmad, *et al.*, "Effect of ambient environment on excimer laser induced micro and nano-structuring of stainless steel," *Applied Surface Science*, vol. 261, pp. 101–109, 2012.

[128] J. Byskov-Nielsen and P. Balling, "Laser structuring of metal surfaces: Micro-mechanical interlocking," *Applied Surface Science*, vol. 255, no. 10, pp. 5591–5594, 2009.

[129] Q. Benard, M. Fois, M. Grisel, and P. Laurens, "Surface treatment of carbon/epoxy and glass/epoxy composites with an excimer laser beam," *International journal of adhesion and adhesives*, vol. 26, no. 7, pp. 543–549, 2006.

[130] *ISO 25178-2:2012. Geometrical product specifications (GPS) - Surface texture: Areal. Part 2: Terms, definitions and surface texture parameters*. 2012.

[131] F. Fischer, S. Kreling, and K. Dilger, "Surface structuring of cfrp by using modern excimer laser sources," *Physics procedia*, vol. 39, pp. 154–160, 2012.

[132] P. Molitor and T. Young, "Adhesives bonding of a titanium alloy to a glass fibre reinforced composite material," *International Journal of Adhesion and Adhesives*, vol. 22, no. 2, pp. 101–107, 2002.

[133] A. Demir, P. Maressa, and B. Previtali, "Fibre laser texturing for surface functionalization," *Physics Procedia*, vol. 41, pp. 759–768, 2013.

[134] R. Wong, A. Hoult, J. K. Kim, and T. Yu, "Improvement of adhesive bonding in aluminium alloys using a laser surface texturing process," *Journal of materials processing technology*, vol. 63, no. 1-3, pp. 579–584, 1997.

[135] A. Matsunawa and S. Katayama, "The changing frontier of laser materials processing," 1986.

[136] R. Higgins, "Engineering metallurgy part i–applied physical metallurgy," *Kent, Hodder & Stoughton*, pp. 246–254, 1991.

[137] M. Alfano, G. Lubineau, F. Furgiuele, and G. H. Paulino, "Study on the role of laser surface irradiation on damage and decohesion of al/epoxy joints," *International journal of Adhesion and Adhesives*, vol. 39, pp. 33–41, 2012.

[138] M. Alfano, S. Pini, G. Chiodo, M. Barberio, A. Pirondi, F. Furgiuele, and R. Groppetti, "Surface patterning of metal substrates through low power laser ablation for enhanced adhesive bonding," *The Journal of Adhesion*, vol. 90, no. 5-6, pp. 384–400, 2014.

[139] G. Chiodo, M. Alfano, S. Pini, A. Pirondi, F. Furgiuele, and R. Groppetti, "On the effect of pulsed laser ablation on shear strength and mode i fracture toughness of al/epoxy adhesive joints," *Journal of Adhesion Science and Technology*, vol. 29, no. 17, pp. 1820–1830, 2015.

[140] M. Alfano, F. Furgiuele, L. Pagnotta, and G. Paulino, "Analysis of fracture in aluminum joints bonded with a bi-component epoxy adhesive," *Journal of testing and Evaluation*, vol. 39, no. 2, pp. 296–303, 2010.

[141] R. Rechner, I. Jansen, and E. Beyer, "Optimization of the aluminum oxide properties for adhesive bonding by laser surface pretreatment," *Journal of Laser Applications*, vol. 24, no. 3, 2012.

[142] A. N. Rider, "The influence of porosity and morphology of hydrated oxide films on epoxy-aluminium bond durability," *Journal of adhesion science and technology*, vol. 15, no. 4, pp. 395–422, 2001.

[143] C. Mandolfino, E. Lertora, S. Genna, C. Leone, and C. Gambaro, "Effect of laser and plasma surface cleaning on mechanical properties of adhesive bonded joints," *Procedia Cirp*, vol. 33, pp. 458–463, 2015.

[144] A. Buchman, M. Rotel, and H. Dodiuk-Kenig, "Nd: Yag laser surface treatment of various materials to enhance adhesion," *Laser Surface Modification and Adhesion*, pp. 1–53, 2014.

[145] L. Galantucci, A. Gravina, G. Chita, and M. Cinquepalmi, "Surface treatment for adhesive-bonded joints by excimer laser," *Composites Part A: Applied Science and Manufacturing*, vol. 27, no. 11, pp. 1041–1049, 1996.

[146] D. Gilbert, M. Stoesslein, D. Axinte, P. Butler-Smith, and J. Kell, "A time based method for predicting the workpiece surface micro-topography under pulsed laser ablation," *Journal of Materials Processing Technology*, vol. 214, no. 12, pp. 3077–3088, 2014.

[147] R. Rechner, I. Jansen, and E. Beyer, "Influence on the strength and aging resistance of aluminium joints by laser pre-treatment and surface modification," *International Journal of Adhesion and Adhesives*, vol. 30, no. 7, pp. 595–601, 2010.

[148] Y. Wu, J. Lin, B. E. Carlson, P. Lu, M. P. Balogh, N. P. Irish, and Y. Mei, "Effect of laser ablation surface treatment on performance of adhesive-bonded aluminum alloys," *Surface and Coatings Technology*, vol. 304, pp. 340–347, 2016.

[149] F. Moroni, F. Musiari, and A. Pirondi, "Influence of laser ablation induced surface topology on the mechanical behavior of aluminum bonded joints," *Proceedings of the Institution of Mechanical Engineers, Part L: Journal of Materials: Design and applications*, vol. Special issue MDA 2018, accepted for publication, 2018.

[150] T. Childs, M. Berzins, G. Ryder, and A. Tontowi, "Selective laser sintering of an amorphous polymer—simulations and experiments," *Proceedings of the Institution of Mechanical Engineers, Part B: Journal of Engineering Manufacture*, vol. 213, no. 4, pp. 333–349, 1999.

[151] L. Romoli, F. Tantussi, and F. Fuso, "Laser milling of martensitic stainless steels using spiral trajectories," *Optics and Lasers in Engineering*, vol. 91, pp. 160–168, 2017.

[152] S. Du, H. Zhao, Y. Ge, Z. Yang, and X. Shi, "Laboratory investigation into the modification of transport properties of high-volume fly ash mortar by chemical admixtures," *Journal of Materials in Civil Engineering*, vol. 29, no. 10, p. 04 017 184, 2017.

[153] *ASTM E647: Standard Method for measurement of fatigue crack growth rates*. 1996.

[154] F. Moroni, F. Musiari, L. Romoli, and A. Pirondi, "Influence of laser treatment parameters on the mode i strain energy release rate of aluminum double cantilever beam joints," *International Journal of Adhesion and Adhesives*, vol. 85, pp. 208–218, 2018.

[155] L. Romoli, F. Moroni, and M. Khan, "A study on the influence of surface laser texturing on the adhesive strength of bonded joints in aluminium alloys," *CIRP Annals*, vol. 66, no. 1, pp. 237–240, 2017.

[156] F. Moroni, L. Romoli, and M. Khan, "Design of laser-textured surfaces to enhance the strength of adhesively bonded joints," *International Journal of Adhesion and Adhesives*, 2018.

[157] M. C. Kong, C. B. Miron, D. A. Axinte, S. Davies, and J. Kell, "On the relationship between the dynamics of the power density and workpiece surface texture in pulsed laser ablation," *CIRP Annals-Manufacturing Technology*, vol. 61, no. 1, pp. 203–206, 2012.

[158] F. Musiari, F. Moroni, C. Favi, and A. Pirondi, "Durability asssessment of laser treated aluminium bonded joints," *International Journal of Adhesion and Adhesives*, accepted for publication, 2018.

[159] P. Paris and F. Erdogan, "A critical analysis of crack propagation laws," *Journal of basic engineering*, vol. 85, no. 4, pp. 528–533, 1963.

[160] *DIN ISO 9142: Adhesives – Guide to the selection of standard laboratory ageing conditions for testing bonded joints*. 2003.

[161] C. Kothe, L. Rudolph, B. Weller, and J. Wünsch, "Investigations on the aging resistance of sealing materials for the protection of bonded point fixings," *Tagungsband Glass Performance Days*, pp. 278–280, 2015.

[162] J. Hildebrand and F. Werner, "Glass-plastic hybrid construction," in *Advances in Engineering Structures, Mechanics & Construction*, Springer, 2006, pp. 801–808.